Journal of South Carolina Water Resources

Volume 4, Issue 1 2017

A Publication of the

South Carolina Water Resources Conference

www.scwaterconference.org

Journal of South Carolina Water Resources

Published by Clemson University Press

Water Resources Research and Extension for South Carolina

JOURNAL MISSION STATEMENT

The Journal of South Carolina Water Resources (JSCWR) is an annual peer-reviewed journal dedicated to scientific research and policy on all aspects of water management to prepare for and meet the growing challenge of providing water resources for the sustainable growth of South Carolina's economy, while preserving its natural resources.

ISSN 2334-4962 (online)
ISSN 2334-4954 (print)

JSCWR MANAGING STAFF EDITOR

Dawn Anticole White, M.M.C., dawnw@clemson.edu
Clemson University Public Service and Agriculture (PSA)
South Carolina Water Resources Center
509 Westinghouse Road
Pendleton, South Carolina 29670
Phone: (864) 646-2145
http://www.clemson.edu/scwater

JSCWR EDITOR *(Term 2017-2019)*

Devendra M. Amatya, Ph.D., P.E.
USDA Forest Service
damatya@fs.fed.us

2017 JSCWR EDITORIAL COMMITTEE

2017 JSCWR GUEST REVIEWERS

We wish to express our sincere gratitude to our guest reviewers for this issue:

Francois Birgand, Ph.D., North Carolina State University
Paul Conrads, Ph.D. (1957-2017), U.S. Geological Survey
Anthony J. Gotvald, U.S. Geological Survey
Anand Jayakaran, Ph.D., Washington State University
Health Kelsey, Ph.D., University of Maryland
Venkat Lakshmi, Ph.D., University of South Carolina
David L. White, Ph.D., Clemson University

COVER PHOTOS:

(Top L-R) Goodale State Park, Camden - courtesy of Ruth Lackstrom, SC Master Naturalist;
(Bottom L-R) South Edisto River, Denmark - courtesy of Rebecca Berzinis, Atkins.

South Carolina Water Resources Conference (SCWRC)

The purpose of the SCWRC is to provide an integrated forum for discussion of water policies, research projects and water management in order to prepare for and meet the growing challenge of providing water resources to sustain and grow South Carolina's economy, while preserving our natural resources. The conference is a biennial event, held in even-numbered years. The Journal of South Carolina Water Resources was first published in 2014 with the support of a group of conference planning committee members who formed an editorial committee to extend the outreach efforts of the conference. (http://www.scwaterconference.org)

v020118

Journal of South Carolina Water Resources

Volume 4, Issue 1 2017

Contents

Foreword

Dawn Anticole White, M.M.C.

***Journal of South Carolina Water Resources* Managing Staff Editor**

For the better part of 2017, South Carolina saw an improvement in drought status for many of the state's 55 counties, with the SC Drought Response Committee reporting 28 of those in 'incipient' (first stage of drought) status and the remaining 17 in 'normal' status on November 27. With regard to major rain events, Tropical Storm Irma brought noteworthy levels of rainfall to much of the state in mid-September, as well as coastal flooding. Because of the ongoing significant weather events that continue to threaten water resources and related infrastructure, Clemson's SC Water Resources Center held its first Summit Series event entitled "Back to the Future of Drought" in April to begin bringing statewide water professionals together for issue specific forums during the 'off' years of the biennial SC Water Resources Conference (SCWRC). The presentations and discussions during the summit fostered new collaborations and shortly after, the SC State Climatology Office took the lead in coordinating a Drought and Water Shortage Tabletop Exercise in September at the SC Emergency Operations Center, drawing 80 participants from across the state. Included in this issue of the journal is a short communication paper about the exercise. Continuing to build on the benefits of statewide networking and collaboration, the SC State Climatology Office has also developed a 2017-18 Climate Connection Workshop series in collaboration with the Carolinas Integrated Sciences and Assessments (CISA) and the Clemson SC Water Resources Center. The first workshop was held in Greenville in December, and workshops are to be scheduled in Columbia and Charleston in early 2018. In addition, SCDNR in partnership with SCDHEC, USGS, Clemson SC Water Resources Center and USACE, held stakeholder meetings during the fall focused on the state's groundwater assessment. Events such as these, are filling the growing need to initiate collaborative efforts to positively impact water resources management, which in turn continue to grow the network of outreach.

Outreach efforts in the form of print mediums and their online versions have just as much value as personal interaction. The *Journal of South Carolina Water Resources* (JSCWR) was established in 2014. In an effort to further expand distribution of JSCWR, a new partnership was formed this past year with Clemson University Press to publish under the University trademark. This partnership is notable because it signifies that Clemson University Press recognizes that JSCWR is following best practices for journal management. JSCWR is archived in Clemson's TigerPrints digital repository at tigerprints.clemson.edu/jscwr. TigerPrints serves as the journal-publishing branch of Clemson University Press. The Call for Articles for the 2018 issue of the journal is now open, and the deadline to submit full articles is February 28.

Dr. Timothy Callahan with the College of Charleston wrapped up his three-year term as the JSCWR editor this past year and welcomed in the new current editor, Dr. Devendra Amatya with the USDA Forest Service. It is exciting to welcome Devendra into his term, as it was his encouragement for such a journal that opened up the discussion back in May of 2012 - which led to the formation of an editorial committee in April of 2013, with the publication of the first issue in 2014. Both Tim and Devendra are also long-time members of the SCWRC planning committee.

The 2018 SCWRC will be held October 17 and 18 at the Columbia Metropolitan Convention Center. The Call for Abstracts has been announced and the deadline to submit abstracts for oral presentation is April 16. Once again, over 300 participants will be expected to come together to communicate policy and management issues, new research methods and scientific knowledge to educate and disseminate information.

Over 1,020 people have attended the past five conferences, and there have been several dozen people who have attended every one. One of those persons was Paul Conrads, a surface-water specialist with USGS. Paul not only attended, but presented as well, oftentimes in both the oral and poster sessions. In the SCWRC archives, he is the author on five presentations and a co-author on 18 others. South Carolina has lost a passionate and brilliant water resources scientist, as Paul passed in early December. In memory of Paul and his dedication to water resources science and enthusiastic and memorable SCWRC participation, the student poster competition that is held during the South Carolina Water Resources Conference will be named after him. Students who are interested in participating in "The Paul A. Conrads Student Poster Competition" are encouraged to review Paul's SCWRC manuscripts and posters in the TigerPrints archives at https://tigerprints.clemson.edu/scwrc/ to get a glimpse of the remarkable work of a person who is a notable role model for those interested in pursuing educations and careers in water resources.

Polycyclic Aromatic Hydrocarbons and Suspended Materials in a Semi-urbanized Tidal Creek after an Historic Flood Event and Implications for Water Quality Monitoring

Barbara A. Beckingham[1,2*], Michael Shahin[1], Kathryn Ellis[2], and Timothy J. Callahan[1,2]

AUTHORS: [1]Department of Geology and Environmental Geosciences, College of Charleston, 66 George Street, Charleston, SC 29424 USA. [2] Master of Science in Environmental Studies Program, College of Charleston, 202 Calhoun Street, Charleston, SC 29401, USA. *beckinghamba@cofc.edu

Abstract. Tidal creeks transport both dissolved and particulate natural organic carbon materials and contaminants, connecting land-based activities with estuarine surface waters. It is important to characterize these materials in tidal creeks because it provides insights as to their origins and potential for ecosystem impacts. Surface water samples were collected from Bull Creek, Charleston, SC, a semi-urbanized tidal creek wetland, on five sampling dates from fall 2015 to spring 2016 to measure total suspended solids (TSS), turbidity, dissolved organic carbon (DOC), $SUVA_{254}$ (specific absorbance as an indicator of aromaticity of DOC), and total water concentrations of polycyclic aromatic hydrocarbons (PAHs), a ubiquitous class of hydrophobic organic contaminants of concern. Stream discharge was also measured to allow an estimation of material flux. One of the sampling dates captured these parameters following a historic rainfall related to Hurricane Joaquin in October 2015, and therefore the aim of the present study is to characterize the sources and to quantify the transport of carbonaceous materials and PAHs in Bull Creek, with a focus on the response to this storm event. The quality of suspended solids and DOC were different following the October storm event in comparison to the other sampling dates, and they were more terrestrially derived as shown by shifts in $SUVA_{254}$ and correlations between TSS and turbidity. Elevated levels of PAHs were detected in Bull Creek after the storm, and diagnostic ratios indicated that additional mixed sources were mobilized by the event. Combining the measures of both carbonaceous material quality and PAH profile contributed to a better understanding of the sources to the tidal creek. Shifts in PAH sources and suspended materials have implications for PAH toxicity to aquatic life, as well as for the appropriate approach to water quality monitoring. Future work should aim to develop relationships between discharge, suspended materials, and PAHs to facilitate more continuous monitoring of material transport in tidal creeks, especially during storm events, which have a strong influence on water quality.

INTRODUCTION

Tidal creeks are the capillaries that link land and sea in estuarine systems, where materials may be readily exchanged and processed. They can be highly productive ecosystems, with profound value as cultural, recreational, and economical resources. However, land use and land cover change are impacting the integrity of these unique systems by changing hydrology and point and non-point source pollution pressures (Holland et al., 2004; Sanger et al., 2015; Schueler, 2000). Urban land use can lead to release of a variety of pollutants of concern into the environment, including heavy metals, nutrients, fecal coliform bacteria, and organic chemicals. Contaminants released to air or on land may accumulate in soils and on roadways and buildings during dry periods and then be flushed into local waterways with stormwater (Krein & Schorer, 2000; Ngabe et al., 2000; Diamond et al., 2000).

Polycyclic aromatic hydrocarbons (PAHs) are one class of organic contaminants of concern and are a leading threat to aquatic life in urban environments (Van Metre and Mahler, 2005). Both natural and anthropogenic sources of PAHs are observed in the environment, including forest fires, fossil fuels, and coal tar sealants that leach from roofs and roadways (Van Metre and Mahler, 2010). A majority of PAH compounds are known or probable carcinogens, in addition to having other acute and chronic toxic effects to both human and ecological receptors (ATSDR, 1995). Sixteen US EPA priority PAHs are typically monitored in the environment and include compounds with structures containing two to

six fused aromatic carbon rings. This range in molecular size imparts differences in the physicochemical properties among PAH molecules; for instance, water solubility ranges over 3 orders of magnitude, from 30 mg/L for naphthalene to <1 µg/L for perylene (Schwartzenbach et al., 2003). Larger PAH compounds with lower water solubility are more hydrophobic and have a stronger tendency to sorb to lipid or organic-rich phases, such as sediments or dissolved organic carbon (DOC). Several studies have found direct associations between DOC or total suspended solids with transport of, for example, PAHs, mercury and other metals (Cai et al., 1999; Foster et al., 2000; Journey et al., 2012; Kirchner et al., 2011; Nasrabadi et al., 2016; Schwientek et al., 2013). High-flow events are major contributors to DOC and suspended sediment loads (Brown et al., 2014; Hinton et al., 1997) and to associated releases and transport of PAHs in rivers (Foster et al., 2000; Schwientek et al., 2013). Previous investigations have found sediments in stormwater ponds and tidal creeks in South Carolina to be impacted by PAHs, including Bull Creek, the location of the present study (Garner et al., 2009; Sanger et al., 1999; Weinstein et al., 2010).

Understanding the chemical properties of the suspended and dissolved material in streams can provide information about sources and system dynamics. For example, the aromaticity of the DOC matrix is indicative of its origin and biogeochemical activity (Weishaar et al., 2003). $SUVA_{254}$ is a simple surrogate indicator of the aromaticity of DOC. Allochthonous materials (with terrestrial origin) have been associated with higher $SUVA_{254}$ values relative to autochthonous material (with in-stream origin), such as algae, in streams (Weishaar et al., 2003). The organic matter content of particulate material may also indicate the source by providing a relative measure of organic and mineral composition. Further, analysis of the relative concentrations of PAH compounds in water samples is an approach used to fingerprint PAH sources (Yunker et al., 2002). Liu et al. (2013) used PAH distribution patterns and diagnostic ratios to differentiate ongoing point source contamination from diffuse background contamination in contrasting river catchments.

The objective of the present study is to characterize the loading of PAHs and carbonaceous matter in Bull Creek, a semi-urbanized tidal creek in Charleston, SC, with a specific look at changes after a historic flood event in October 2015. This flood event affected a large part of South Carolina after historic rainfall fell between October 1 and 5, 2015. Record discharges were recorded at river gages across the state (Feaster et al., 2015). The maximum stage of the Ashley River recorded at a gage site adjacent to Bull Creek (USGS 021720869) following the storm event was 4.3 m (~14 feet), which at that time was the second highest stage recorded at that site in its period of record since 1992. We collected data on PAHs, total suspended solids and their organic matter content, DOC and aromaticity, and stream discharge, in addition to general water quality characteristics, on four other sampling dates over the period September 2015 to April 2016 for comparison. We use the totality of the information provided by these measures to better understand sources to the tidal creek and to work toward improving water quality monitoring approaches.

METHODS

SITE DESCRIPTION

Bull Creek, a small tidal creek tributary watershed (~778 ha) of the Ashley River near Charleston, SC, was chosen as the study site. The Bull Creek watershed was digitized using United States Geological Survey (USGS) elevation derivatives for national applications (EDNAs) map information. NOAA 2010 Coastal Change Analysis Program (C-CAP) Land Cover Atlas data were used to determine the percent of land use distribution (e.g., developed, forested, and wetlands). Watershed location, delineation, and land use is illustrated in **Figure 1A, B**. The sampling location is also shown (star; 32°49′38″N, 80°01′44″W). Additionally, ArcGIS software tools were used to delineate the watershed upstream of the sampling location and to categorize land use (**Figure 1B**). The upstream watershed area of ~430 ha delineated by ArcGIS digital elevation modeling extends beyond the EDNA watershed boundaries, but upstream land use distribution followed the pattern of the entire watershed. The watershed is dominated by low- and medium-density development but also has some intact wetlands. Bull Creek watershed has a reported impervious cover of 38% (Sanger et al., 2015).

FIELD SAMPLING AND LABORATORY ANALYSES

Sampling dates and schedule are shown in **Table 1**. Sampling was conducted on five dates, with samples spaced over the course of the day between 9 a.m. and 5 p.m. and at different stages of the tidal cycle. Bull Creek exhibits a semi-diurnal tidal pattern, with two high tides and two low tides

Table 1. Sampling scheme and number of samples (N)

Date	Tidal Cycle Sampled	Sample Type and N	
		TSS/PAH	N, Ebb/Flood
9/22/15	Flood	TSS	8/0
		PAH	0/0
10/9/15	Ebb & Flood	TSS	3/1
		PAH	3/1
1/25/16	Ebb	TSS	4/0
		PAH	3/0
3/24/16	Ebb & Flood	TSS	3/1
		PAH	2/1
4/11/16	Ebb & Flood	TSS	4/3
		PAH	2/2

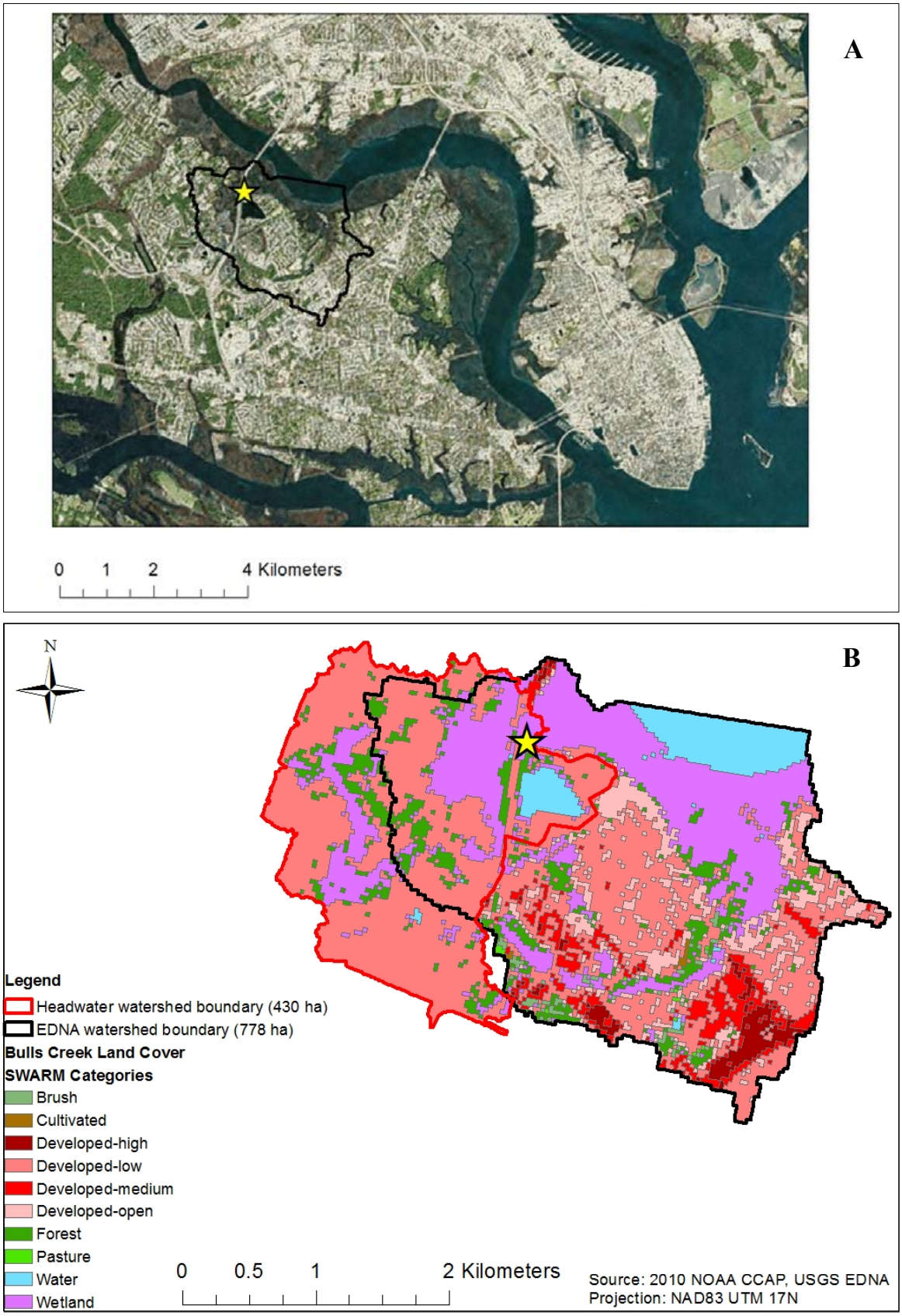

Figure 1. A. Location of the study site in Bull Creek adjacent to the Ashley River near Charleston, SC, with the USGS EDNA watershed shown in black outline. The sampling site within Bull Creek is shown with a star (32°49′38″N, 80°01′44″W). **B.** Watershed delineation and land use classification according to the USGS EDNA map system (black; area 778 ha), additionally with the watershed area delineated upstream of the sampling location by ArcGIS (red; area 430 ha).

over a lunar day (24 hours 50 minutes). The maximum depth of the channel transect over the tidal range was between 2.2 m and 4.0 m during the sampling dates. Antecedent precipitation data were acquired from the National Climate Data Center (ncdc.noaa.gov) at a local gage site (#US1SCCR0087).

Stream discharge, turbidity, and general water quality parameters were measured in the field. Discharge measurements were obtained every 30–60 minutes using a Teledyne RD Instruments acoustic Doppler current profiler (ADCP) (Ellis et al., this issue). The timing of these measurements was normalized to high tide slack (when discharge is negligible as the creek current switches direction between flood and ebb), which typically occurred about 40 minutes after high tide (the maximum stage of the creek). The ADCP was attached to the back of a kayak and pulled across the width of Bull Creek, collecting water velocity and depth data that are used to calculate average discharge. Two optical backscatter sensors were used to measure the turbidity (cloudiness) of the water: a Thermo-Scientific Orion Aquafast handheld portable turbidity meter and a YSI Multiparameter Water Quality Sonde (6600 V2). These two instruments measure turbidity at different angles of light scatter. The former detects light at a 180° angle with color compensation, while the later detects light at a 90° angle without color compensation. The handheld turbidity meter was used on sampling dates 9/22/15 and 10/9/15, and the sonde was used on 1/25/16, while both instruments were used to collect turbidity data on 3/24/16 and 4/11/16. A comparison of results for the turbidity meter and sonde on these two dates showed good agreement between the instruments, with the sonde generally indicating slightly higher turbidity but within 1 S.D. of the turbidity meter average (e.g., 3/24 11 am 8.09 ± 0.66 NTU vs. 8.7 NTU, and 4/11 4 pm 19.24 ± 0.89 NTU vs. 19.6 NTU). On the dates that both instruments were used, data from the handheld turbidity meter were reported. Temperature, pH, salinity, and conductivity were measured with the YSI.

Water samples were collected at elbow depth (~0.3 m) from a dock or kayak in coordination with discharge measurements to determine the PAH concentrations and to characterize the dissolved and suspended matter. A flow chart depicting the sample analysis is shown in **Figure 2**. Whole water samples collected in 1 L amber glass bottles were processed to quantify the total suspended solids, organic matter content of the solids, DOC concentration, and aromaticity of the DOC ($SUVA_{254}$). Total suspended solids were determined as the dry mass of the particulates captured on a GF/F glass fiber filter (0.7 µm pore size) after drying in an oven at 105°C to constant weight. The organic matter content of the solids was determined by loss on ignition after combusting the filter at 450°C for 4 hours (ASTM, 2014). The filtrate was acidified to pH 2–3 with 1 N HCl, purged in a sonication bath, and analyzed for DOC using a Shimadzu elemental analyzer (TOC-VPN) against calibration standards

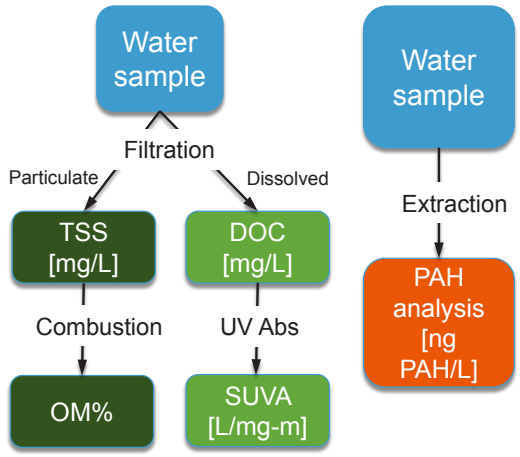

Figure 2. Sample analysis flowchart. Abbreviations: TSS = total suspended solids, OM = organic matter, DOC = DOC, $SUVA_{254}$ = specific UV absorbance, and PAHs = polycyclic aromatic hydrocarbons.

prepared with potassium hydrogen phthalate ($C_8H_5KO_4$). The specific UV absorbance at 254 nm wavelength ($SUVA_{254}$) was determined on an unacidified filtrate using a UV-Vis spectrophotometer (Thermo Scientific Evolution 220). $SUVA_{254}$ was determined as the absorbance of the sample normalized to its DOC content (Weishaar et al., 2003).

Whole water samples for PAH analysis were collected in 2 L glass bottles with Teflon-lined caps and kept refrigerated until sample processing. The samples for PAHs were collected on four of five sampling dates (**Table 1**). Liquid-liquid extraction was performed in the 2 L bottles by adding 15 mL of hexane and gently shaking on a horizontal shaker table for 24 hours (USEPA, 1996). The samples were allowed to settle for several hours to allow the layers to separate, as emulsions were common in the relatively high-DOC water matrix. Hexane was recovered by directly pipetting the top hexane layer off the bottle or with the aid of a separatory funnel. A second liquid-liquid extraction with hexane was performed by hand-shaking for 2 minutes. The recovered hexane layers were pooled for each sample, dried with sodium sulfate, and condensed to <350 µL. Blank DI water extractions were also performed to ensure no laboratory background or cross-contamination. PAHs were analyzed by an Agilent Technologies gas chromatograph with mass spectrometer detection in selective ion monitoring mode (GC-MS; model 7890A GC with directly coupled model 5975C MS). Separation was performed following injection and introduction of the sample in pulsed splitless mode onto an Agilent DB-XLB column (0.18 µm, 20 m x 0.180 mm I.D.), with He carrier gas (0.6 mL/min) and stepped oven temperature ramps from 55°C to 310°C during the 46 minute analytical run. Twelve PAHs were quantified against their ^{13}C-labelled internal standards by an isotope dilution method (Boden and Reiner, 2004), including: three-member ring compounds, acenaphthylene (ANY), acenaphthene (ACE), fluorene (FLN), phenanthrene (PHE), and anthracene (ANT);

four-member ring compounds, fluoranthene (FTH), pyrene (PYR), benzo(a)anthracene (BaA), and chrysene (CHR); and five-member ring compounds, benzo(b)fluoranthene (BbF), benzo(k)fluoranthene (BkF) and benzo(a)pyrene (BaP). The detection limit for each PAH was 1 ng L^{-1}.

CALCULATION OF PARTICLE AND PAH FLUXES

A full ebb tide was captured with periodic sampling on 10/9/15, 1/25/16, and 3/24/16. Discharge was measured at least hourly over the course of the ebb tide (PAHs two to three times and TSS three to four times). To calculate flux, TSS and PAH mass concentrations were averaged (C_{avg}, mass/L) and multiplied by the total water volume discharged past the sampling point in Bull Creek (V_{total}, L) divided by the duration (in hours) of the ebb cycle:

$$Flux\left[\frac{mass}{hr}\right] = \frac{C_{avg}V_{total}}{t},$$

where V_{total} was determined by integrating the discharge values measured over time. This approach is not flow-weighted and assumes that the surface water sample is representative of the stream cross section.

RESULTS

ENVIRONMENTAL CONDITIONS

Water temperature, pH, and conductivity, along with antecedent rainfall data for each of the sampling dates, are shown in **Table 2**. Of particular note is the dramatic reduction in conductivity in October, which reflects the high volume of freshwater runoff delivered to Bull Creek from the precipitation event related to Hurricane Joaquin (Oct 1–5). Water salinity is typically brackish at the site but was classified as freshwater in October 2015.

SUSPENDED MATTER: DISSOLVED AND PARTICULATE

The concentration and quality of particulate matter and DOC in water samples are shown in **Figure 3**. Samples collected on October 9, 2015, are plotted separately from the other sampling dates. Total concentration of suspended solids was generally lower in October but with similar organic matter content (**Figure 3A,B**). In contrast, although the DOC content was at a level consistent with other sampling dates, the $SUVA_{254}$ measurement was elevated (**Figure 3C,D**). The higher $SUVA_{254}$ values in October are indicative of a more aromatic, terrestrial source of DOC.

Although the organic matter content of suspended particulates was consistent across sampling dates (**Figure 3B**), the correlation between turbidity and TSS deviated in October (**Figure 4**). Turbidity is measured by optical light scattering, and the characteristics of the particles in solution that affect light scattering include the general type and, in particular, the particle size, geometry, density, and color (Gippel, 1995; Rügner et al., 2013). The offset correlation indicates that some fraction of the suspended material measured as TSS in the water samples following the October 2015 storm event scatters light differently and therefore has a different quality.

Table 2. Precipitation and water condition parameters for sampling dates (S.D. of average measures in parentheses)

Date	Antecedent precipitation		T	pH	Conductivity
	Period	(mm)	(ºC)		(mS/cm)
9/22/15	10 d	1.8	26.0 (0.8)	7.0 (0.1)	26.7 (3.8)
	5 d	0.0			
10/9/15	10 d	413.3	21.8 (0.9)	6.1 (0.2)	0.9 (0.5)
	5 d	42.4			
1/25/16	10 d	91.7	9.5 (0.8)	7.2 (0.2)	8.4 (5.1)
	5 d	39.7			
3/24/16	10 d	4.8	19.5 (0.7)	5.8 (0.8)	14.7 (1.2)
	5 d	2.3			
4/11/16	10 d	26.1	17.8 (1.4)	5.7 (0.6)	16.4 (3.1)
	5 d	1.0			

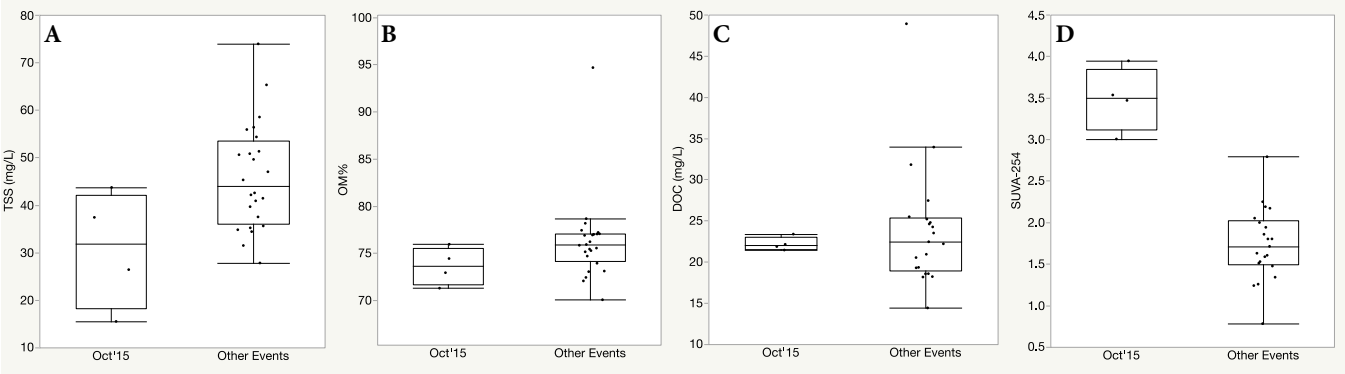

Figure 3. Box and whisker plots show data points, quartiles, and outliers for (A) total suspended solids (TSS), (B) suspended solids organic matter (OM) content, (C) dissolved organic carbon (DOC), and (D) specific absorbance of DOC ($SUVA_{254}$) in units of L $mg^{-1}m^{-1}$. Samples taken on 10/9/15 are plotted separately from the other dates.

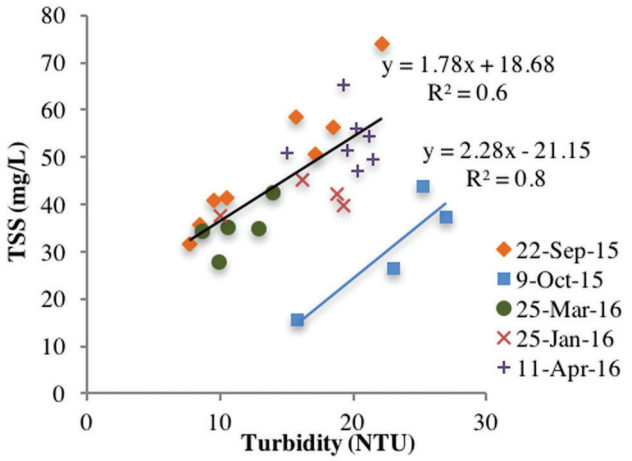

Figure 4. Total suspended solids (TSS) versus turbidity for water samples collected on 10/9/15, in contrast to the other sampling dates.

POLYCYCLIC AROMATIC HYDROCARBONS

The total concentration of 12 PAHs (PAH-12) in water was higher in October 2015 compared to the other sampling events (**Figure 5**). The concentrations of PAHs expressed on a particle mass basis indicated an even larger difference (data not shown), since the TSS concentration was lower in October. The distribution pattern of PAHs showed a larger contribution of lower molecular weight three-ring PAHs (ANY, ACE, FLN, PHE, ANT) in October 2015 (45% of the total PAH-12 concentration) compared to January, March, and April 2016 (0%, 0%, and 4% of the total PAH-12, respectively). The concentrations of PAHs in all samples analyzed were below the ecological risk assessment screening values for surface waters for the southeastern United States (US EPA, 2015).

Diagnostic ratios of PAH compounds were used to further distinguish sources as either petroleum or combustion derived, following Yunker et al. (2002) (**Figure 6**). The ratios of FTH/FTH+PYR and BaA/BaA+CHR were applied due to the robustness of these ratios and the consistent detection of these compounds in whole water samples in the present study. Further, since these PAHs are hydrophobic and are primarily associated with particles (octanol-water partition coefficient, $\log K_{OW} > 5$), it is more appropriate to apply the diagnostic ratios that are established for sediments and suspended particles. The diagnostic ratios cross-plot indicates a combination of biomass, coal, and petroleum combustion, with a stronger mixed-sources signal indicated by the lower BaA/BaA+CHR ratio for the October 2015 samples (**Figure 6**).

FLUXES OF PAHS AND CARBONACEOUS MATERIALS

The total cumulative discharge volume of the ~6 hour ebb tides captured on 10/9/15, 1/26/16, and 3/24/16 were 291,800 m^3, 287,200 m^3, and 137,100 m^3, respectively. The average flood and ebb discharge at this site is reported in Ellis et al. (this issue). The high discharge measured in January is attributed to the full moon on 1/25/16 and recent precipitation (5d antecedent precipitation was similar for January and October sampling dates, **Table 1**). The average hourly fluxes of PAHs, DOC, TSS and particulate organic matter (POM, calculated from TSS and OM%) estimated for these dates are shown in **Table 3**. The fluxes reported are for the ebb tide only at a midpoint within the Bull Creek watershed and therefore do not represent the entire net flux of suspended materials in this watershed.

The average hourly flux of TSS was highest in January, while for PAHs, it was highest in October. This is the direct

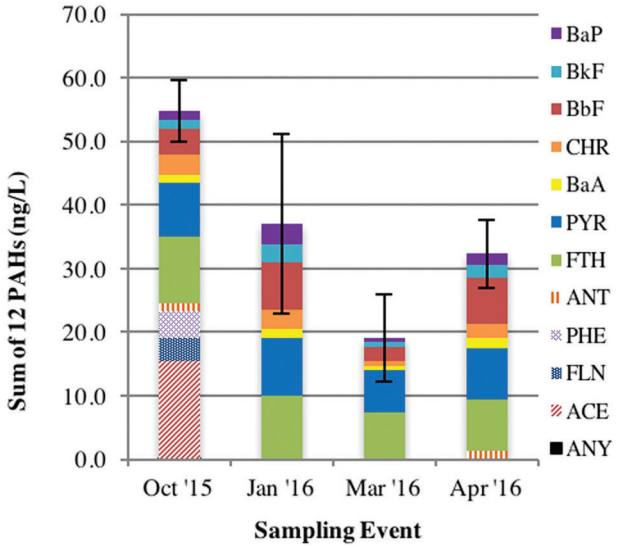

Figure 5. Concentration of 12 PAHs in whole water samples from Bull Creek, SC. Error bars show ±1 S.D. of the mean for the sum of PAHs.

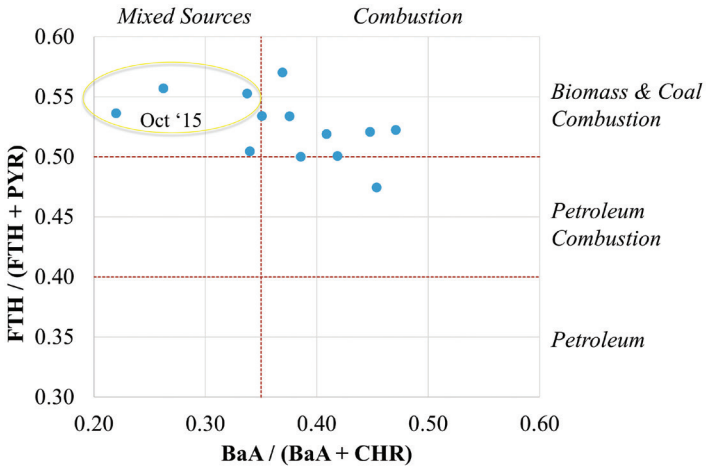

Figure 6. PAH diagnostic ratios can indicate sources of contamination, indicated in italics along the figure margins. Mixed sources include petroleum and combustion. Samples on 10/9/15 are encircled.

Table 3. Average hourly flux of materials calculated by grab samples and discharge measurements over an ebb tide in Bull Creek, SC.

Date	DOC (kg/hr)	TSS (kg/hr)	POM (kg/hr)	PAHs (g/hr)
10/9/15	1100	1525	1143	2.7
1/26/16	1200	1975	1520	1.8
3/24/16	838	800	610	0.5

result of higher concentrations of the materials measured on these respective dates when similarly high discharge was experienced. The range in calculated flux over these three sampling dates was greater for PAHs than TSS. The flux of PAHs measured in October was 1.5 times greater than in January, and six times greater than in March. The lowest flux was observed in March when there was slower mean water velocity and less antecedent precipitation.

DISCUSSION

Several different measures of water quality collected in the present study indicated a significant alteration of the Bull Creek system in response to the historic flood event in October 2015. In addition to a decrease in salinity from brackish to freshwater, the nature of the suspended particle and DOC load changed, and a different profile of PAHs was mobilized. The precipitation and flooding that followed in October 2015 delivered particulate and dissolved organic material that was likely of terrestrial origin that may not typically be mobilized during smaller rain events (e.g., January 2016) and that was carrying a relatively high load of PAHs.

The PAH distribution pattern in October 2015 shifted toward PAHs with lower molecular weight (**Figure 5**) and also indicated mixed sources (**Figure 6**). These lower molecular weight compounds are relatively more mobile and bioaccessible due to higher water solubility and are capable of exerting an acute narcosis toxicity risk to aquatic organisms (Di Toro and McGrath, 2000). While the mixed-sources signal in October may have included both petroleum and combustion sources and is difficult to interpret, the shift suggests a contribution of petroleum combustion products in the water samples, possibly from diesel burning since this variable source falls into the ranges observed for both diagnostic ratios examined (Yunker et al., 2002). A number of major roadways are in the vicinity, including a highway bridge upstream of the study site. The predominance of three-ring PAHs in October may also suggest that less-weathered sources were mobilized by the flood waters (Vulava et al., 2016). The influx of fresh water to a system can drive the dissolution of low-molecular weight PAHs. In another study in coastal South Carolina, PAHs in runoff and in tidal creeks were also found to be combustion derived and more similar to atmospheric deposition end members than oils (Ngabe et al., 2000). A previous investigation of sediments also concluded that pyrogenic sources predominate in the Bull Creek watershed (Garner et al., 2009). However, the present study highlights the potential for specific combustion source profiles of PAHs to Bull Creek to change depending on the storm event, likely depending on the hydrologic connectivity of the watershed, wetland system, and time of year. Additional characterization of soil, sediment, and atmospheric deposition matrices in the watershed and expansion of the PAH compounds analyzed, including alkylated PAHs, could provide further insight into sources in the watershed.

Sediments accumulate contamination that may be redistributed during storm events, and suspended material reflect the character of the existing in-stream sediment and the overland-derived particulate and dissolved material. The sampling date of 10/9/15 was a week after Hurricane Joaquin, and therefore the state of the system when it was experiencing the greatest flows and inputs following the storm were not captured. Lower TSS concentrations in October than in January may indicate that much of the mobile material in Bull Creek had already been flushed downstream, leaving a post-storm signature that we captured on 10/9. Also, DOC is often correlated with discharge during storm events (Hinton et al., 1997), and therefore the DOC we measured on 10/9 was likely on the falling limb of DOC export. The $SUVA_{254}$ characterization of DOC indicated a difference in the quality of DOC following the October 2015 storm, and changes in the nature of DOC in streams due to storms has been reported in other systems (e.g., Dalzell et al., 2005). More time-discretized monitoring and modeling is required to capture material transport during storm events.

Turbidity monitoring using *in situ* sensors has been advanced as an important proxy of suspended solids and particle-associated contaminants for the continuous monitoring of water quality, since grab samples cannot fully capture a dynamic system (e.g., Schweintek et al., 2013). However, the use of turbidity as a proxy relies on stability in the correlations, which can shift due to changes in suspended loads following storms (Downing, 2006), as observed in the present study. Interestingly, the OM content of particles does not help describe the differences in suspended matter that would lead to a different turbidity versus TSS correlation. Particle size analysis and coloration are two additional measures that may contribute to a better understanding of changes in backscatter in water samples and that may aid the development of multi-parameter or flow regime-dependent correlations for a system. The storm event in October 2015 may have been an outlier in the TSS versus the turbidity correlation due to sampling timing several days after the storm, following the loss of sediment and contaminant storage from within the tidal creek channel (Schwientek

et al., 2017). However, this level of understanding (e.g., outlier determination, or multi-parameter correlations) would require a longer data record and more extensive parameterization than are presently available for Bull Creek. Additional sampling and characterization may also uncover seasonal patterns that need to be accounted for, such as changes in terrestrial carbon and PAH sources and primary in-stream productivity and plankton assemblages (Osburn et al., 2015; Reed et al., 2015). While TSS versus turbidity correlations have been established for tidal creek salt marsh systems in other studies (Suk et al., 1998), it is possible that the impact of urbanization and stormwater complicates this approach, especially in smaller watersheds. This presents an opportunity for further study.

In conclusion, changes in both carbonaceous matter and PAH profile during storm events present a challenge for water quality monitoring in tidal creeks since the dynamics are difficult to capture with routine sampling approaches. These changes are important to understand due to the potential concomitant alteration of contaminant bioavailability and toxicity. Hydrology data collected in these systems, coupled with water quality monitoring results, will provide better data to guide management and regulatory decisions. Discharge conditions for ebb and flood tides in tidal creeks have been shown to be asymmetric (e.g., Ellis et al, this issue), and therefore both the duration and relative discharge of ebb and flood tides need to be accounted for to determine the net flux of materials. An additional aspect to consider is the accuracy of loading models, such as those for total maximum daily load (TMDL) predictions. Future work should aim to explore the parameterization needed to establish rating curves for tracking changes in water quality and contaminant transport in tidal creeks.

ACKNOWLEDGEMENTS

This study was supported by startup funding for B. Beckingham from the College of Charleston (CofC). South Carolina Department of Natural Resources is thanked for the use of the ADCP, and several CofC student research participants are acknowledged for their contributions to data collection (Emily Townsend, William Vesely, Jessica Woodruff, Austin Morrison, Kimberly Sitta, Hayley Bell, Devon Rutledge, and Mikala Randich). We would also like to thank Vijay Vulava and anonymous reviewers for comments on the manuscript.

LITERATURE CITED

ASTM D2974-14, Standard Test Methods for Moisture, Ash, and Organic Matter of Peat and Other Organic Soils, ASTM International, West Conshohocken, PA. 2014, www.astm.org.

ATSDR 1995. Toxicological Profile For Polycyclic Aromatic Hydrocarbons. U.S. Department of Health and Human Services, Agency for Toxic Substances and Disease Registry, Atlanta, GA. August 1995.

Boden, A.R. and Reiner, E.J., 2004. Development of an isotope-dilution gas chromatographic-mass spectrometric method for the analysis of polycyclic aromatic compounds in environmental matrices. *Polycycl. Aromat. Comp.* 24, 309–323.

Brown, M.M., Mulligan, R.P., and Miller, R.L., 2014. Modeling the transport of freshwater and dissolved organic carbon in the Neuse River Estuary, NC, USA following Hurricane Irene (2011). *J. Estuar. Coast. Shelf Sci.* 139:148–158.

Cai, Y., Jaffe, R. and Jones, R., 1999. Interactions between dissolved organic carbon and mercury species in surface waters of the Florida Everglades. *Appl. Geochem.* 14:395–407.

Dalzell, B.J., Filley, T.R., and Harbor, J.M. 2005. Flood pulse influences on terrestrial organic matter export from an agricultural watershed. *J. Geophys. Res.* 110:1–14.

Diamond, M.L., Gingrich, S.E., Fertuck, K., McCarry, B.E., Stern, G.A., Billeck, B., Grift, B., Brooker, D., and Yager, T.D. 2000. Evidence for organic film on an impervious surface: characterization and potential teratogenic effects. *Environ. Sci. Technol.* 34:2900–2908.

Di Toro, D.M. and McGrath, J.A. 2000. Technical basis for narcotic chemicals and polycyclic aromatic hydrocarbon criteria. II. Mixtures and sediments. *Environ. Toxicol. Chem.* 19:1971–1982.

Downing, J. 2006. Twenty-five years with OBS sensors: The good, the bad, and the ugly. *Cont. Shelf. Res.* 26:2299–2318.

Ellis, K.K., Callahan, T., Greenfield, D.I., Sanger, D., and Robinson, J. *In review, this issue.* Hydrologic assessments of tidal creeks to inform nutrient management recommendations. *J. SC Water Res.*

Feaster, T.D., Shelton, J.M., and Robbins, J.C. 2015. Preliminary peak stage and streamflow data at selected USGS streamgaging stations for the South Carolina flood of October 2015 (ver. 1.1, November 2015): U.S. Geological Survey Open-File Report 2015-1201, 19 p., https://dx.doi.org/10.3133/ofr20151201.

Foster, G.D., Roberts, E.C., Gruessner, B., and Velinksy, J. 2000. Hydrogeochemistry and transport of organic contaminants in an urban watershed of Chesapeake Bay (USA). *Appl. Geochem.* 15:901–915.

Garner, T.R., Weinstein, J.E., and Sanger, D.M. 2009. Polycyclic aromatic hydrocarbon contamination in South Carolina salt marsh-tidal creek systems: Relationships among sediments, biota, and watershed land use. *Arch. Environ. Contam. Toxicol.* 57:103–115.

Gippel, C.J. 1995. Potential of turbidity monitoring for measuring the transport of suspended solids in streams. *Hydrol. Process.* 9:83–97.

Hinton, M.J., Schiff, S.L., and English, M.C. 1997. The significance of storms for the concentration and export of

dissolved organic carbon from two Precambrian Shield sediments. *Biogeochem.* 36:67–88.

Holland, A.F., Sanger, D.M., Gawle, C.P., Lerberg, S.B., Santiago, M.S., Riekerk, G.H., Zimmerman, L.E., and Scott, G.I. 2004. Linkages between tidal creek ecosystem and the landscape and demographic attributes of their watersheds. *J. Exp. Mar. Bio. Ecol.* 298:151–178.

Journey, C.A., Burns, D.A., Riva-Murray, K., Brigham, M.E., Button, D.T., Feaster, T.D., Petkewich, M.D., and Bradley, P.M. 2012. Fluvial transport of mercury, organic carbon, suspended sediment, and selected major ions in contrasting stream basins in South Carolina and New York, October 2004 to September 2009: U.S. Geological Survey Scientific Investigations Report 2012-5173, 125 p.

Kirchner, J.W., Austin, C.M., Myers, A., and Whyte, D.C. 2011. Quantifying remediation effectiveness under variable external forcing using contaminant rating curves. *Environ. Sci. Technol.* 45:7874–7881.

Krein, A., Schorer, M. 2000. Road runoff pollution by polycyclic aromatic hydrocarbons and its contribution to river sediments. *Wat. Res.* 34:4110–4115.

Liu, Y., Beckingham, B., Rügner, H., Li, Z., Ma, L., Schwientek, M., Xie, H., Zhao, J., and Grathwohl, P. 2013. Comparison of sedimentary PAHs in the rivers Ammer (Germany) and Liangtan (China): Differences between early- and newly-industrialized countries. *Environ. Sci. Technol.* 47:701–709.

Nasrabadi, T., Ruegner, H., Sirdari, Z.Z., Schwientek, and M., Grathwohl, P. 2016. Using total suspended solids (TSS) and turbidity as proxies for evaluation of metal transport in river water. *Appl. Geochem.* 68:1–9.

Ngabe, B., Bidleman, T.F., Scott, and G.I. 2000. Polycyclic aromatic hydrocarbons in storm runoff from urban and coastal South Carolina. *Sci. Tot. Environ.* 225:1–9.

Osburn, C.L., Mikan, M.P., Etheridge, J.R., Burchell, M.R., and Birgand, F. 2015. Seasonal variation in the quality of dissolved and particulate organic matter exchanged between a salt marsh and its adjacent estuary. *J. Geophys. Res.* 120:1430–1449.

Reed, M.L., DiTullio, G.R., Kacenas, and S.E., Greenfield, D.I. 2015. Effects of nitrogen and dissolved organic carbon on microplankton abundances in four coastal South Carolina (USA) systems. *J. Aq. Micro. Ecol.* 78:1–14.

Rügner, H., Schientek, M., Beckingham, B., Kuck, B., and Grathwohl, P. 2013. Turbidity as a proxy for total suspended solids (TSS) and particle facilitated pollutant transport in catchments. *Environ. Earth Sci.* 69:373–380.

Sanger, D.M., Holland, A.F., and Scott, G.I. 1999. Tidal creek and salt marsh sediments in South Carolina coastal estuaries: II. Distribution of organic contaminants. *Arch. Environ. Contam. Toxicol.* 37:458-471.

Sanger, D., Blair, A., DiDonato, G., Washburn, T., Jones, S., Riekerk, G., Wirth, E., Stewart, J., White, D., Vandiver, L., and Holland, A.F. 2015. Impacts of coastal development on the ecology of tidal creek ecosystems of the US Southeast including consequences to humans. *Estuaries and Coasts*. 38(Suppl 1):S49–S66.

Schueler, T. 2000. The importance of imperviousness. *Watershed Protection Techniques* 1(3):100–111.

Schwartzenbach, R.P., Gschwend, P.M., and Imboden, D.M. 2003. Environmental Organic Chemistry, 2nd Edition. Wiley-Interscience: Hoboken, NJ USA.

Schweintek, M., Rügner, H., Beckingham, B., Kuck, B., and Grathwohl, P. 2013. Integrated monitoring of particle associated transport of PAHs in contrasting catchments. *Environ. Poll.* 172:155–162.

Schwientek, M., Rügner, H., Scherer, U., Rode, M., Grathwohl, P. 2017. A parsimonious approach to estimate PAH concentrations in river sediments of anthropogenically impacted watersheds. *Sci. Tot. Environ.* 601–602:636–645.

Suk, N.S., Guo, Q., Psuty, N.P. 1998. Feasibility of using a turbidimeter to quantify suspended solids concentration in a tidal saltmarsh creek. *Estuar. Coast. Shelf Sci.* 46:383–391.

US EPA, 1996. Method 3510C Separatory Funnel Liquid-Liquid Extraction. Revision 3. December 1996.

US EPA, 2015. Region 4 Ecological Risk Assessment Supplemental Guidance, Interim Draft. United States Environmental Protection Agency, Superfund Division. Accessed online 7 Sept. 2016. https://www.epa.gov/sites/production/files/2015-09/documents/r4_era_guidance_document_draft_final_8-25-2015.pdf

Van Metre, P.C., Mahler, B. 2005. Trends in hydrophobic organic contaminants in urban and reference lake sediments across the United States, 1970-2001. *Environ. Sci. Technol.* 39: 5567–5574.

Van Metre, P.C., Mayler, B. 2010. Contribution of PAHs from coal-tar pavement sealcoat and other sources to 40 U.S. lakes. *Sci Tot. Environ.* 409:334–344.

Vulava, V.M., Vaughn, D.S., McKay, L.D., Driese, S.G., Cooper, L.W., Menn, F-M., Levine, N.S., Sayler, G.S. 2017. Flood-induced transport of PAHs from streambed coal tar deposits. *Sci. Tot. Environ.* 575:247–257.

Weinstein, J.E., Crawford, K.D., Garner, T.R., Flemming, A.J. 2010. Screening-level ecological and human health risk assessment of polycyclic aromatic hydrocarbons in stormwater detention pond sediments of coastal South Carolina, USA. *J. Haz. Mat.* 178:906–916.

Weishaar, J.L., Aiken, G.R., Bergamaschi, B.A., Fram, M.S., Fuji, R., and Mopper, K. 2003. Evaluation of specific ultraviolet absorbance as an indicator of the chemical composition and reactivity of dissolved organic carbon. *Environ. Sci. Technol.* 37:4702–4708.

Yunker, M.B., Macdonald, R.W., Vingarzan, R., Mitchell, R.H., Goyette, D., Sylvestre, S. 2002. PAHs in the Fraser River basin: a critical appraisal of PAH ratios as indicators of PAH source and composition. *Org. Geochem.* 33:489–515

Long-term and Two-period Analysis of Hydrologic Conditions of the South Edisto River

Rebecca W. Berzinis[1]

AUTHORS: [1] Senior Scientist, Atkins, 5600 Seventy Seven Center Drive, STE 340, Charlotte, NC, 28217, USA.

Abstract. The U.S. Geological Survey (USGS) long-term daily streamflow record at station 02173000 in Bamberg County, South Carolina on the South Fork Edisto River (Latitude 33°23'35", Longitude 81°08'00" NAD27) spans from 1932 to 2015 and was used for this study. The Nature Conservancy's Indicators of Hydrologic Alteration (IHA) software was used to analyze the entire record of hydrologic data as ecologically relevant parameters and to categorize the flows. A two-period analysis was conducted to evaluate whether a significant difference could be observed in historic flow data from 1932–1985 (period one) compared to 1986–2015 (period two). An extreme low flow was defined as an initial low flow below 10% of daily flows for the period. Over the entire 76-year period of record, 51 years had at least one occurrence of extreme low flows. A median of 4 days per year had occurrences of extreme flows in period one in contrast to a median of 60 days per year during period two. Annual precipitation totals were not correlated with the number of days per year with extreme low flows. The two-period analysis showed significant differences between period one and period two for monthly mean flow for February, April, May, and August, as well as for 1-day and 30-day minima and maxima values. The analysis calculated the 7Q10 (the lowest stream flow for seven consecutive days that would be expected to occur once in ten years) at 4.4 cubic meters per second (cms), which was -10.9% different from the most recently published estimate. Results presented in this study have shown that spring and summer flows in the South Fork Edisto are statistically significantly lower in period two compared to period one.

INTRODUCTION

The South Fork Edisto River and the Edisto River provide valuable recreational opportunities for the public and economic opportunities for industry; however, this valued resource may be in decline. To effectively manage water resources and understand whether current policies are preserving the resource for public, industrial, and ecological uses, decision and policy makers must have information on historic streamflow conditions to compare to existing conditions, especially during periods of low flow. Therefore, the USGS long-term daily streamflow record at station 02173000 (South Fork Edisto River at the Highway 321 bridge near Denmark, South Carolina) was used to conduct a two-period analysis to evaluate whether a significant difference in historic flow data could be observed in period one as compared to period two. Accounting for historic conditions and departures from normal flows is critical to decision making with regards to water withdrawal policy.

PROJECT DESCRIPTION

BACKGROUND

The Edisto River is the longest (approximately 400 kilometers [Marcy and O'Brien-White, 1995]) free-flowing blackwater river system in the United States. The basin is located in the Coastal Plain Physiographic Province of South Carolina (SC). The South Fork Edisto River begins in the upper Coastal Plain Physiographic Province east of Edgefield, SC, and converges with the North Fork Edisto River near the town of Branchville, SC, to form the Edisto River. The river continues south and east through the lower Coastal Plain Physiographic Province and joins the Atlantic Ocean at Edisto Island, south of Charleston, SC (Feaster and Guimaraes, 2012).

This river, combined with the Ashepoo and Combahee, is referred to as the "ACE" basin and was considered one of the most pristine coastal plain watersheds in the southeastern United States in the late 1990s (NMFS, 1998). Extensive adjacent wetlands and large tracts of forestland within the river

basin have kept water quality relatively high, supporting an abundance of aquatic life. According to respondents in a 1995 State survey, the Edisto River was ranked as the number one river fished with an economic worth of over 1 million dollars annually (Marcy and O'Brien-White, 1995). The economic worth in today's dollars would be 1.6 million (Bureau of Labor Statistics, 2016). The Edisto fishery is diverse, with a high percentage of indigenous species (SCDNR, 1996). SC's State Wildlife Action Plan (2015 revision) identified 16 freshwater fish and 13 mussels of highest conservation priority. Of the state's highest conservation priority species, eight fish species inhabit the Edisto basin (SCDNR, 2015; Marcy and O'Brien-White, 1995) and three mussel species inhabit the ACE basin (SCDNR, 2015). The federally listed aquatic species occurring in the Edisto basin include the endangered Atlantic sturgeon and shortnose sturgeon (USFWS, 2016).

In 2014, American Rivers included the South Fork Edisto River on its annual Most Endangered Rivers list (American Rivers, 2016). In 2015, this listing was extended to the entire Edisto River. American Rivers identified excessive water withdrawals as the main threat to fish and wildlife habitat, recreation, and water quality (American Rivers, 2015). Anecdotal accounts from recreational users of the South Fork Edisto have suggested that over their lifetimes, the once completely fishable, swimmable, and navigable river is now characterized by greatly diminished recreational opportunities for boating, fishing, and swimming.

RELATED WORK

Differing approaches are used to evaluate changes in hydrologic conditions. Many of these approaches are evaluated and discussed by Gao et al. (2009). Shiau and Wu (2004) compared flow conditions before and after weir construction using the parameters generated by the Indicators of Hydrologic Alteration (IHA), with an approach developed by The Nature Conservancy (Richter et. al., 1996; Richter, Baumgartner, Wigington, and Braun, 1997; Richter, Baumgartner, Braun, and Powell, 1998). Poff, et al. (2009) developed an alternate method called the ecological limits of hydrologic alteration (ELOHA) as a framework for developing regional environmental flow standards and detecting hydrologic alteration. Finally, others, such as Sun and Feng (2012), have used a combination of statistical methods and multistage hydrologic analysis to identify temporal variability in the flow regimes of the Yellow River in China.

In the southeast, one study on the Satilla River, in Georgia (Elkins, 2001) and a study on the Trinity River basin in Texas (Kiesling, 2003) utilized the IHA to investigate the potential of human-altered flow regimes. Two studies have investigated the hydrology of the South Fork Edisto at USGS station 02173000. Marshall (1993) completed an analysis of the single-mass curves of precipitation and streamflow for USGS station 02173000 during the period 1939 to 1990, indicating that changes in streamflow were the result of changes in precipitation. Feaster and Guimaraes (2012) compiled previously published values for low-flow frequency and flow duration for continuous-record stream gaging stations including USGS station 02173000 and other stations in the Saluda, Congaree, and Edisto River basins. The annual minimum 7-day average streamflow with a 10-year recurrence interval (7Q10) for station 02173000 was found to decrease during the 1970–2012 period from 6.0 cms (Bloxham, 1979) to 5.7 cms (Zalants, 1991) and finally to 5.0 cms (Feaster and Guimaraes, 2012).

EXPERIMENTAL DESIGN

The USGS long-term daily streamflow record at station 02173000 (South Fork Edisto River at the Highway 321 bridge near Denmark, South Carolina) was used to conduct a two-period analysis to evaluate whether a significant difference in historic flow data could be observed from period one compared to period two. For this analysis, values $\leq$0.05 indicate that the difference between periods is highly significant; the significance count can be interpreted similarly to a p-value in parametric statistics (TNC, 2009). Therefore, the difference in the 12 monthly means/medians and 1-day and 30-day minima and maxima between periods were significant if the significance counts were $\leq$0.05.

METHODS

The USGS long-term daily streamflow record of the South Fork Edisto River (Latitude 33°23'35", Longitude 81°08'00" NAD27) at station 02173000 in Bamberg County, South Carolina, spans from 1932 through 2015 (with a data gap from 1972–1980 due to equipment failure). This streamflow record was used to evaluate the flow alterations associated with human perturbations, such as water withdrawals or global climate change. Station 02173000 is in hydrologic unit code 03050204, the gage datum is 47.45 meters above NGVD29, and the drainage area is 1,865 km^2 (Feaster and Guimaraes, 2012). The IHA software was used to analyze the entire record of hydrologic data as ecologically relevant parameters and to categorize flows as large floods, small floods, high flow pulses, low flows, or extreme low flows (TNC, 2009). According to the IHA recommendation (based on Richter et al., 1997), at least 20 years of daily records should be used to analyze hydrologic alterations for each period of interest. Also, the USGS characterizes stream gages as long term when the period of record is 30 years or greater (USGS, 2016a). The highest land use/land cover in watershed 03050204-03 is agricultural land (40.2%) (SCDHEC, 2012). In the past 30 years, the population and number of hectares under irrigation in the southeast has grown considerably (Mullen, 2009).

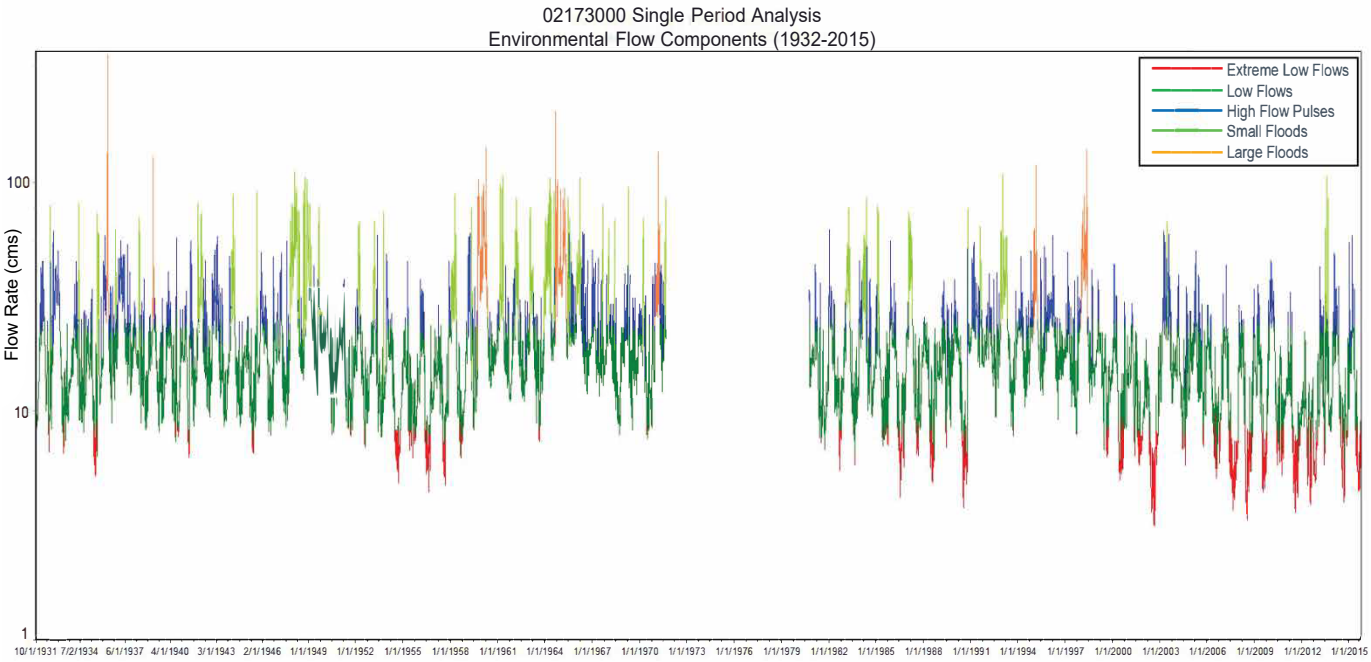

Figure 1. Environmental flow components analysis.

LONG-TERM HYDROLOGIC RECORD ANALYSIS

Basic statistics (count, mean, median, minimum, and maximum) for the long-term hydrologic record were calculated for the 12 monthly means/medians and 1-day and 30-day minima and maxima. The monthly means/medians capture one aspect of flow variability (seasonal flow distribution) and reflect the timing of flow events and magnitude. To capture the variability of flows at top and low ends of the flow range, 1-day and 30-day minima and maxima are presented. Low and high flows represent the smallest/largest values of mean discharge computed over any 1 or 30 consecutive days during the period.

Five different types of environment flow components (EFCs) are calculated by the IHA: low flows, extreme low flows, high flow pulses, small floods, and large floods. These EFCs are ecologically relevant hydrologic patterns that must be present in a system to sustain ecological integrity. For example, extreme low flows may be critical for species such as bald cypress that need dried out floodplains to regenerate, while large floods are necessary to promote the diversity of the physical structure of a river and its floodplain (TNC, 2009). All flows that exceeded 75% of daily flows for the period were classified as high flows. All flows below this level were classified as low flows. A small flood event was defined as an initial high flow with a peak flow greater than the 2-year return interval event (i.e., 50 percent chance of occurrence in any given year, per USGS, 2016b). A large flood event was defined as an initial high flow with a peak flow greater than the 10-year return interval event (i.e., 10 percent chance of occurrence in any given year, per USGS, 2016b). All initial high flows not classified as small flood or large floods were classified as high-flow pulses. Finally, an extreme low flow was defined as an initial low flow below 10% of daily flows for the period (TNC, 2009).

TWO-PERIOD ANALYSIS

In the two-period analysis, the median (i.e., the 50th percentile), coefficients of variation, deviation factors, and significance counts for the deviation values were calculated. The significance count can be interpreted as being similarly to a p-value in parametric statistics (TNC, 2009). These statistics were calculated for the 12 monthly means/medians and 1-day and 30-day minima and maxima.

PRECIPITATION DATA ANALYSIS

Annual precipitation totals summarized by year (January 1–December 31) were obtained from the U.S. Historical Climatology Network (Menne, Williams, and Vose, 2015) for station number 380764 in Blackville, South Carolina (Latitude 33.3631, Longitude -81.3292). The station is approximately 19 kilometers southeast of USGS station 02173000. Basic statistics (mean, median, minimum, and maximum) were calculated for period one (1932–1985) and period two (1986–2014). Annual precipitation totals (1932–2014) were plotted with annual days with extreme low flows (1932–2014, minus data from 1972–1980 due to equipment failure). Pearson correlations were calculated for annual precipitation and annual days with extreme low flows for period one and two.

RESULTS

LONG-TERM HYDROLOGIC RECORD ANALYSIS

The mean annual flow was 20.4 cms for the 75-year period of record. The monthly median flows increased from October (12.5 cms) to a peak in March (26.5 cms), and then flow sharply declined in April (20.7 cms) and May before steadily decreasing into the growing season months of June (13.5 cms) through September (12.0 cms). The median 1-day minimum and 30-day minimum flows were 7.0 cms and 9.1 cms, respectively, while the median 1-day maximum and 30-day maximum flows were 62.0 cms and 35.6 cms, respectively (Table 1). These low and high flows represent the smallest/largest values of median discharge computed over any 1 or 30 consecutive days during the period. The 7Q10 (the annual 7-day minimum flow with a 10-year recurrence interval or non-exceedance probability of 10 percent) was 4.4 cms. The highest recorded flow in the period of record (4/11/1936, 359.6 cms or 10.91 stage) was verified by the USGS (2016c).

Table 1. Basic statistics for long-term hydrologic record.

Month	Count	Mean	Median	Minimum	Maximum
October	2356	15.8	12.5	4.6	105.1
November	2280	17.6	15.0	4.8	102.2
December	2355	22.0	18.4	6.9	93.7
January	2325	25.9	22.2	8.5	103.4
February	2118	28.5	25.0	8.5	115.2
March	2325	30.6	26.5	10.0	134.8
April	2250	26.7	20.7	5.8	359.6
May	2325	17.7	15.6	4.7	115.0
June	2250	15.3	13.5	3.6	85.2
July	2325	14.4	12.3	3.3	93.2
August	2353	15.5	12.4	3.1	198.2
September	2252	14.7	12.0	3.6	203.3
1-day minimum		7.4	7.0		
30-day minimum		9.8	9.1		
1-day maximum		72.3	62.0		
30-day maximum		39.4	35.6		

The EFCs were calculated, and the flows were categorized as large floods, small floods, high flow pulses, low flows, or extreme low flows. Evaluating the visual representation of this data (Figure 1) from the 1930s to roughly 1970, very few extreme low flows occurred. In contrast, from 2000 to the present, many have taken place. Also, from 1980 to the present, a lower frequency of small and large floods can be observed. Over the entire 76-year period of record, 51 years had at least one occurrence of extreme low flows. A median of 4 days per year had occurrences of extreme low flows in period one in contrast to a median of 60 days per year during period two (Figure 2).

TWO-PERIOD ANALYSIS

The mean annual flow for period one was 22.1 cms compared to 17.7 cms for period two (median). The median monthly flows also differed greatly between time periods (Figure 3). For example, the median monthly flow for February was 28.9 cms in period one compared to 21.2 cms in period two, while the values for August were 13.5 cms in period one compared to 10.1 cms in period two. The significance count for differences in the median monthly flow for February was 0.04, and August was 0.05 (Table 2). Values $\leq$0.05 indicate that the difference between periods is significant. The significance count for differences between annual minima and annual maxima 1-day and 30-day means for period one and period two were highly significant (between 0.00 and 0.001).

In conclusion, the two-period analysis showed significant differences between 1932–1985 (period one) and 1986–2015 (period two) for monthly mean flow for February, April, May, and August, as well as for 1-day and 30-day minima and maxima values.

Table 2. Basic statistics for two-period analysis.

	Medians		Significance Count	
	Period 1	Period 2	Medians	C.D.
October	12.6	11.3	0.33	0.11
November	15.0	13.4	0.25	0.04
December	19.2	18.2	0.42	0.80
January	24.7	20.8	0.07	0.57
February	28.9	21.2	0.04	0.94
March	28.1	23.1	0.08	0.65
April	25.1	18.0	0.03	0.43
May	16.8	13.2	0.04	0.64
June	14.0	11.5	0.07	0.00
July	13.1	11.1	0.19	0.02
August	13.5	10.1	0.05	0.00
September	12.2	9.9	0.08	0.01
1-day min	7.9	5.3	0.00	0.03
30-day min	9.8	7.1	0.00	0.01
1-day max	76.7	44.5	0.00	0.39
30-day max	41.8	30.0	0.00	0.86

PRECIPITATION DATA ANALYSIS

Basic statistics for the long-term precipitation record are included in Table 3. Annual precipitation totals for the period of record were sorted in order from lowest total precipitation to highest. These values were plotted for annual days with extreme low flows (Figure 4). A Pearson correlation was calculated as -0.48 for annual precipitation and annual days with extreme low flows for the entire period of record (1932–2014).

Table 3. Basic statistics for long-term precipitation (mm) record.

	Period 1	Period 2
Count	46	29
Mean	1149	1127
Median	1103	1040
Minimum	777	800
Maximum	1888	1731
Pearson	-0.39	-0.65

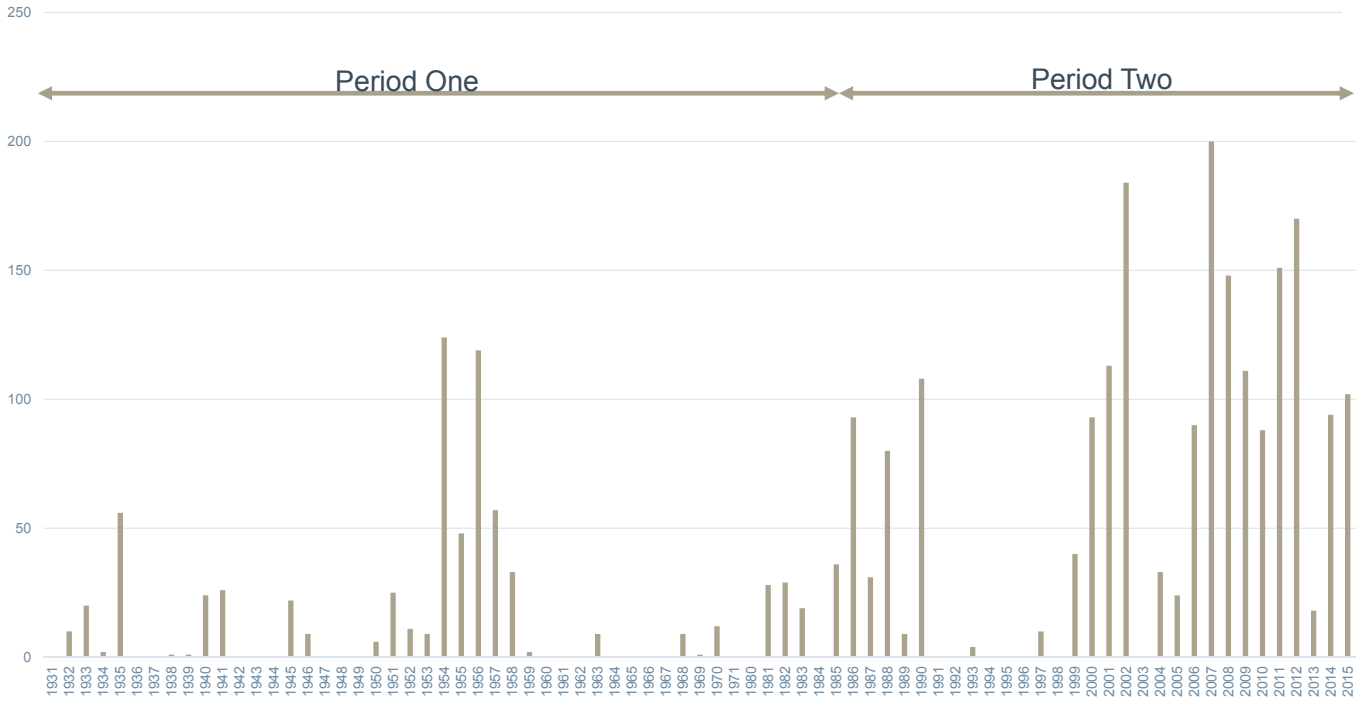

Figure 2. Number of days with extreme low flow conditions.

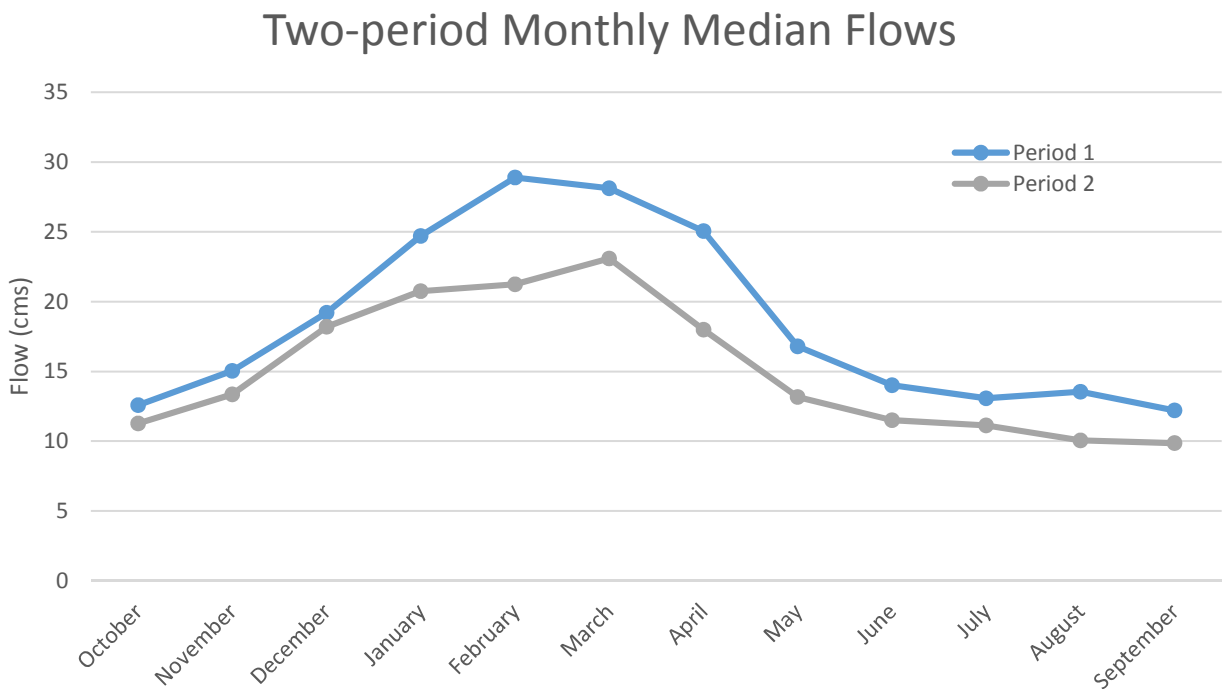

Figure 3. Two-period analysis of monthly median flows (cms).

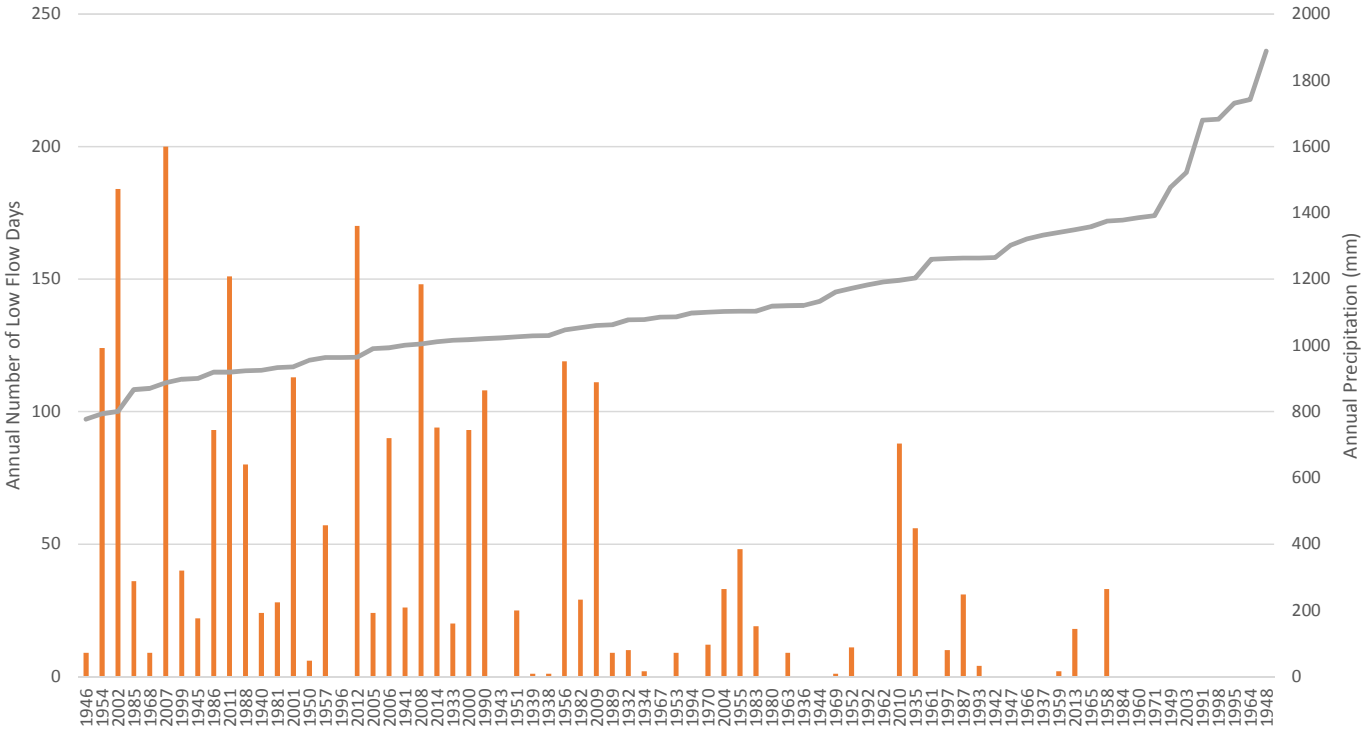

Figure 4. Annual precipitation (mm) and annual days with extreme low flows (1936–2014).

DISCUSSION

The annual minimum 7-day average streamflow with a 10-year recurrence interval (7Q10) for station 02173000 was found to decline from 6.0 cms (Bloxham, 1979) to 5.7 cms (Zalants, 1991) and finally to 5.0 cms (Feaster and Guimaraes, 2012). The analysis presented above calculated the 7Q10 at 4.4 cms, which was -10.9% different from the most recent estimate. This declining trend is concerning, considering that extremely low stream flows also can correspond with low dissolved oxygen values and organic channel bottoms (Ice and Sugden, 2003). Dissolved oxygen is one of the four primary factors controlling river fauna (Hynes, 1966): 1) dissolved salts, 2) current, 3) temperature, and 4) dissolved oxygen. Also, Allan (1995) indicated that the biota of flowing waters is highly dependent on the availability of oxygen. Hydrologic disturbances, such as flood and drought, can affect biota because the frequency, duration, and intensity of such disturbances influence the response and recovery time of communities (Gomi et al., 2002).

The results presented in this study have shown that spring and summer flows in the South Fork Edisto are statistically significantly different. Atlantic sturgeon is federally listed by the NMFS as an endangered species (NMFS, 2012). Spawning has been documented in both the fall and spring in the Edisto (SCDNR, 2016a), and the population size is thought to be similar to the better known populations in the Altamaha and the Savannah Rivers (personal communication, Bill Post). Spawning behavior has been documented in the South Edisto approximately 30 miles downstream of station 02173000. Most presumed spawning movements for Atlantic sturgeon begin near the end of July through the beginning of August. The diadromous fish were detected on the spawning grounds through October in each year of the study period (Post et al., 2014). It is unclear whether the current hydrologic conditions in the South Fork Edisto are impacting Atlantic sturgeon populations; however, this is a topic for further research. Floodplain inundation is important for the state's other diadromous species of concern that spawn in the spring, such as blueback herring, hickory shad, and American shad, which are known to occur in the South Fork Edisto (SCDNR, 2015, 2016b, 2016c, 2016d). If spring flows are inadequate for spawning, other species of concern in the state could be impacted.

The finding of significant differences between 1932–1985 (period one) and 1986–2015 (period two) for monthly mean flow for February, April, May, and August, as well as for 1-day and 30-day minima and maxima values, indicates that changes occurred in the hydrologic system between time periods. Annual rainfall over the two periods is similar; the mean precipitation was 1,149 mm for period one and 1,127 mm for period two. However, an examination of the relationship between annual precipitation and annual days with extreme low flows (Figure 4) shows that similar precipitation in period one versus period two results in a different number of annual days with extreme low flows. For example, annual precipitation was 793 mm in 1954, with 124 extreme low flow days, while annual precipitation

was 800 mm with 184 extreme low flow days in 2002. The relationship between precipitation and runoff is influenced by the amount of precipitation that fell in the previous year (Searcy and Hardison, 1960, as cited in Marshall, 1993), and future research should explore methods to account for this variability. The Pearson correlation was -0.39 for period one and -0.65 for period two, which indicates a stronger negative relationship between annual precipitation and annual days with extreme low flows for period two. Future research should further evaluate climate data, water withdrawal information, and flow data for a similar river system to explore the potential causes for the departure from historic flows in the South Edisto River.

ACKNOWLEDGEMENTS

Thanks to Cheryl W. Propst, CSE, who reviewed drafts of this manuscript and provided valuable editorial comments and insights. Bill Post provided data on Atlantic sturgeon, which gave the information presented in the paper important context.

LITERATURE CITED

Allan, J.D., *Stream Ecology Structure and Function of Running Waters*. Dordrecht, the Netherlands: Kluwer Academic Publishers, 1995.

American Rivers. 2016. America's Most Endangered Rivers for 2014: South Fork of the Edisto River. http://www.americanrivers.org/endangered-rivers/2014-report/edisto/. Accessed: 4/16/2016.

American Rivers. 2015. America's Most Endangered Rivers for 2015: Edisto River. http://www.americanrivers.org/endangered-rivers/2015-report/edisto-river/. Accessed: 12/31/2015.

Bloxham, W.M., 1979. Low-flow frequency and flow duration of South Carolina streams: South Carolina Water Resources Commission Report No. 11, 90 p.

Bureau of Labor Statistics. 2016. CPI Inflation Calculator. http://www.bls.gov/data/inflation_calculator.htm. Accessed: 9/11/2016.

Elkins, Duncan. 2001. An Analysis of Historic Flows in the Satilla River Using Two Statistical Methods. *Proceedings of the 2001 Georgia Water Resources Conference*. March 26-27, 2001. Kathryn J. Hatcher, Ed. Institute Ecology, the University of Georgia. Available online: https://smartech.gatech.edu/bitstream/handle/1853/44457/ElkinsD-01.pdf.

Feaster, T.D., and Guimaraes, W.B., 2012. Low-flow frequency and flow duration of selected South Carolina streams in the Saluda, Congaree, and Edisto River basins through March 2009: U.S. Geological Survey Open-File Report 2012–1253, 53 p. Gao, Yongxuan, Richard M. Vogel, Charles N. Kroll, N. LeRoy Poff, and Julian D. Olden. Development of representative indicators of hydrologic alteration. *Journal of Hydrology*. v. 374, no. 2009, p. 136–147.

Gomi, T., R.C. Sidle, and J.S. Richardson. 2002. Understanding processes and downstream linkages of headwater systems. *BioScience*, v. 52, no. 10, p. 905–916.

Hynes H.B.N. 1966. *The Biology of Polluted Waters*. Liverpool, England: Liverpool University Press. 202 pp.

Ice, G., and Sugden, B. 2003, Summer dissolved oxygen concentrations in forested streams of Northern Louisiana. *Southern Journal of Applied Forestry*, v. 27, no. 2, p. 92–99(8).

Kiesling, Richard L. 2003. Applying Indicators of Hydrologic Alteration to Texas Streams-Overview of Methods with Examples from the Trinity River Basin. US Geological Survey Fact Sheet 128-03. Available online: https://pubs.usgs.gov/fs/fs12803/pdf/FS_128-03.pdf

Marcy, B.C., and O'Brien-White, S.K. 1995. Fishes of the Edisto River Basin: Bibliography, Historical Sampling, and Locations Species Occurrence. Report 6. Fisheries Habitat Committee, Edisto River Basin Project, S.C. Department of Natural Resources, Water Resources Division. Columbia, South Carolina. March 1995.

Marshall, W.D. 1993. Assessing Change in the Edisto River Basin: An Ecological Characterization. South Carolina Water Resources Commission. Columbia, South Carolina. Report No. 177. October 1993.

Menne M. J., C. N. Williams, Jr., and R. S. Vose, 2015. United States Historical Climatology Network Daily Temperature, Precipitation, and Snow Data. Carbon Dioxide Information Analysis Center, Oak Ridge National Laboratory, Oak Ridge, Tennessee. Available on-line: (http://cdiac.ornl.gov/epubs/ndp/ushcn/ushcn.html) from the Carbon Dioxide Information Analysis Center, Oak Ridge National Laboratory, Oak Ridge, Tennessee.

Mullen, J. D., Y. Yua, G. Hoogenboomb. 2009. Estimating the demand for irrigation water in a humid climate: A case study from the southeastern United States. *Agricultural Water Management*, v. 96, no., 10, p. 1421–1428.

National Marine Fisheries Service (NMFS). 1998. Recovery Plan for the Shortnose Sturgeon (*Acipenser brevirostrum*). Prepared by the Shortnose Sturgeon Recovery Team for the National Marine Fisheries Service, Silver Spring, Maryland. 104 pages.

NMFS. 2012. Final listing determinations for two distinct population segments of Atlantic Sturgeon (*Acipenser oxyrinchus oxyrinchus*). Federal Register. v. 77, no. 24.

Poff, N. Leroy, Brian D. Richter, Angela H. Arthington, Stuart E. Bunn, Robert J . Naiman, Eloise Kendy, Mike Acreman, Colin Apse, Brian P. Bledsoe, Mary C. Freeman, James Henriksen, Robert B. Jacobson, Jonathan G. Kennen, David M. Merritt, Jay H. O'keeffe, Julian D. Olden, Kevin Rogers, Rebecca E. Tharme, and Andrew Warner. 2009. The ecological limits of hydrologic alteration (ELOHA): a new framework for developing regional environmental flow standards. *Freshwater Biology*. doi:10.1111/j.1365-2427.2009.02204.x.

Post, B., T. Darden, D. L. Peterson, M. Loeffler, and C. Collier. 2014. Research and Management of Endangered and Threatened Species in the Southeast: Riverine Movements of Shortnose and Atlantic sturgeon, South Carolina Department of Natural Resources: 274.

Richter, B.D., Baumgartner, J.V., Powell, J., and Braun, D.P. 1996. A method for assessing hydrologic alteration within ecosystems. *Conservation Biology*, v. 10, no. 4, p. 1163–1174.

Richter, B.D, J.V. Baumgartner, R. Wigington, and D.P. Braun. 1997. "How much water does a river need?" *Freshwater Biology*, v. 37, p. 231–249.

Richter, B.D., Baumgartner, J.V., Braun, D.P., and Powell, J. 1998. A spatial assessment of hydrologic alteration within a river network. *Regulated Rivers: Research & Management*, 14, p. 329–340.

Shiau, Jenq-Tzong and Fu-Chun Wu. 2004. Assessment of hydrologic alterations caused by Chi-Chi diversion weir in Chou-Shui Creek, Taiwan: opportunities for restoring natural flow conditions. River Research and Applications. v. 20, no. 4. p. 401–412.

South Carolina Department of Health and Environmental Control (SCDHEC). 2012. Watershed Water Quality Assessment: Edisto River Basin. Bureau of Water. Columbia, South Carolina. http://www.scdhec.gov/HomeAndEnvironment/Docs/ed-005-12.pdf. Accessed: December 31, 2015.

South Carolina Department of Natural Resources (SCDNR) Water Resources Division. 1996. Managing Resources for a Sustainable Future: The Edisto River Basin Project Report. Report 12. Columbia, South Carolina. 226 pages.

SCDNR. 2015. SC's State Wildlife Action Plan. http://www.dnr.sc.gov/swap/index.html. Accessed 9/11/16.

SCDNR 2016a. Freshwater Fish – Species: Atlantic sturgeon (*Acipenser oxyrinchus*). http://portal.dnr.sc.gov/fish/species/atlanticsturgeon.html Accessed 9/14/16.

SCDNR 2016b. Freshwater Fish – Species: American shad (*Alosa sapidissima*) – Native. http://portal.dnr.sc.gov/fish/species/americanshad.html Accessed 9/14/16.SCDNR 2016c. Freshwater Fish – Species: Blueback herring (*Alosa aestivalis*) - Native. http://portal.dnr.sc.gov/fish/species/bluebackherring.html Accessed 9/14/16.

SCDNR 2016d. Freshwater Fish – Species: Hickory shad (*Alosa mediocris*). http://portal.dnr.sc.gov/fish/species/hickoryshad.html Accessed 9/14/16.

Sun, T. and M. L. Feng. 2012. Multistage analysis of hydrologic alterations in the Yellow River, China. *River Research and Applications*. v. 29, no. 8, p. 991–1003.

The Nature Conservancy (TNC). 2009. Indicators of Hydrologic Alteration. Version 7.1 User's Manual.

U.S. Fish & Wildlife Service (USFWS). 2016. IPaC - Information for Planning and Conservation (https://ecos.fws.gov/ipac/) Trust Resources Report. Generated April 16, 2016 06:57 AM MDT, IPaC v3.0.2.

U.S. Geological Survey (USGS). 2016a. National Streamflow Information Program (NSIP): Accessed September 11, 2016, at http://water.usgs.gov/nsip/history1.html.

USGS. 2016b. Floods: Recurrence intervals and 100-year floods (USGS). https://water.usgs.gov/edu/100yearflood.html Accessed July 21, 2017.

USGS. 2016c. Map of real-time streamflow compared to historical streamflow for the day of the year (South Carolina). http://waterwatch.usgs.gov/?m=real&r=sc Accessed August 13, 2016.

Zalants, M.G., 1991. Low-flow frequency and flow duration of selected South Carolina streams through 1987: U.S. Geological Survey Water-Resources Investigations Report 91-4170, 87 p.

Measuring and Modeling Flow Rates in Tidal Creeks: A Case Study from the Central Coast of South Carolina

Kathryn K. Ellis[1], Timothy Callahan[2*], Dianne I. Greenfield[3,4§], Denise Sanger[5], Joshua Robinson[6], and Martin Jones[7]

AUTHORS: [1]M.S. in Environmental Studies Program, College of Charleston, 66 George Street, Charleston, SC 29424. [2]Department of Geology and Environmental Geosciences, College of Charleston, 66 George Street, Charleston, SC 29424. [3]Belle W. Baruch Institute for Marine and Coastal Sciences, University of South Carolina, 331 Fort Johnson Road, Charleston, SC 29412. [4]Marine Resources Research Institute, South Carolina Department of Natural Resources, 217 Fort Johnson Road, Charleston, SC. [5]ACE Basin National Estuarine Research Reserve, Marine Resources Research Institute, South Carolina Department of Natural Resources, 217 Fort Johnson Road, Charleston, SC 29412. [6]Robinson Design Engineers, 1630-2 Meeting Street Road, Charleston, SC 29405. [7]Department of Mathematics, College of Charleston, 66 George Street, Charleston, SC 29424

*Contact author: 843-953-8278, callahant@cofc.edu §Current address: Advanced Science Research Center at the Graduate School, City University of New York, 85 Saint Nicholas Terrace, New York, NY 10031

Abstract. The purpose of this study was to collect site- and condition-specific hydrology data to better understand the water flow dynamics of tidal creeks and terrestrial runoff from surrounding watersheds. In this paper, we developed mathematical models of tidal creek flow (discharge) in relation to time during a tidal cycle and also estimated terrestrial runoff volume from design storms to compare to tidal creek volumes. Currently, limited data are available about how discharge in tidal creeks behaves as a function of stage or the time of tide (i.e., rising or falling tide) for estuaries in the southeastern United States, so this information fills an existing knowledge gap. Ultimately, findings from this study will be used to inform managers about numeric nutrient criteria (nitrogen-N and phosphorus-P) when it is combined with biological response (e.g., phytoplankton assemblages) data from a concurrent study.

We studied four tidal creek sites, two in the Ashepoo-Combahee-Edisto (ACE) Basin and two in the Charleston Harbor system. We used ArcGIS to delineate two different watersheds for each study site, to classify the surrounding land cover using the NOAA Coastal Change Analysis Program (C-CAP) data, and to analyze the soils using the NRCS Soil Survey Geographic database (SSURGO). The size of the U.S. Geological Survey's Elevation Derivatives for National Application (EDNA) watersheds varied from 778 to 2,582 ha; smaller geographic watersheds were delineated for all sites (except Wimbee) for stormwater modeling purposes. The two sites in Charleston Harbor were within the first-order Horlbeck Creek and the second-order Bulls Creek areas. The ACE Basin sites were within the third-order Big Bay Creek and the fourth-order Wimbee Creek areas. We measured the stage and discharge in each creek with an acoustic Doppler current profiler (ADCP) unit for multiple tide conditions over a 2-year period (2015–2016) with the goal of encompassing as large of a range of tide stage and discharge data measurements as possible. The Stormwater Runoff Modeling System (SWARM) was also used to estimate the potential water entering the creeks from the land surface; this volume was very small relative to the tide water volume except for the more-developed Bulls Creek watershed.

The results show that the peak discharge occurred on the ebb tide and that the duration of the flood tide spanned a longer period of time; both of these observations are consistent with traits associated with an ebb-dominated tidal creek system. The tidal inflow and outflow (flood and ebb tides, respectively) showed an asymmetrical pattern with respect to stage and discharge; peak discharge during the flood (rising) tide occurred at a higher stage than for the peak discharge during the ebb (falling) tide. This is not an unexpected result, as the water on an ebb tide is moving down gradient funneled through the creek channel toward the coast. Furthermore, water moving with the rising flood tide must overcome frictional losses due to the marsh bank and vegetation; i.e., the peak discharge can only happen when the water has risen above these impediments. We infer from the flow dynamics data that faster water velocities during ebb tide imply that more erosive energy could transport a larger mass of suspended solids and associated nutrients (e.g., orthophosphate) from the estuary to the coastal ocean. However, the discharge and

runoff modeling indicate that land-based flux was important in the developed Bulls Creek watershed, but not at the larger and less-developed Big Bay Creek watershed. At Big Bay Creek, the relatively large tidal discharge volume compared to the smaller potential runoff generated within the watershed indicates that the creek could potentially dilute terrestrial runoff contaminants. Smaller, more-urbanized tidal wetland systems may not benefit from such dilution effects and thus are vulnerable to increased runoff from adjacent developed landscapes.

INTRODUCTION

Tidal creeks are common landscape features in southeastern US coastal areas. They act as a primary hydrologic link between estuaries and the terrestrial environment, and they also provide feeding grounds, spawning areas, and nursery habitats for shellfish, fish, birds, and mammals (Sanger et al., 2015). In South Carolina, the estuaries exhibit a semidiurnal tidal pattern (two high tides and two low tides daily) and are classified as mesotidal systems with an average tidal range of 1.4–2.6 meters (Barwis, 1977). These creeks are between 5 and 100 meters in width and 0 to 15 meters in depth (Blanton et al., 2006). Along the South Carolina coast, the SC Estuarine and Coastal Assessment Program (SCECAP) estimated that 17% of the estuarine water area is tidal creek habitat. This generally includes creeks that are approximately 10–100 m wide (Van Dolah et al., 2002).

The hydrology of the bidirectional-flow in tidal creeks is unique when compared to unidirectional nontidal systems. The bidirectional nature of flow means that water-borne constituents have the ability to enter the system from both the coastal ocean (downstream) and terrestrial (upstream) sources. Furthermore, the flow characteristics (i.e., the relationship between stage/water depth and discharge/flow rate) of tidal creeks cannot be interpreted using a typical rating curve approach where increasing water depth corresponds to increasing discharge, such as what occurs following a storm event. In tidal creek systems, the maximum discharge occurs at an intermediate stage between high and low tides. In many cases, the discharge is not symmetric on the flood (rising tide) and ebb (falling tide) cycles.

Although stage varies with time in a smooth sinusoidal manner (Leopold et al., 1993), this is not true for velocity or discharge. Previous studies in South Carolina marsh creek systems have shown that the ebb-dominant estuaries are common south of Cape Romain, South Carolina (Barwis, 1977). Ebb-dominant systems usually have longer lag times at high water than low water, longer-duration rising tide periods, and stronger ebb than flood currents, and they tend to be deeper with extensive regions of flats and marshes (Speer et al., 1991). These systems experience inefficient water exchange between the extensive intertidal marshes and the deep channels near the time of high water (Blanton et al., 2006). This tidal distortion is the result of nonlinear interaction of the oceanic tide (or the semidiurnal lunar tide, M2) with shallow water in the estuary, which produces harmonic and compound tides, such as the M4 lunar quarter-diurnal tide and the M6 sexta-diurnal lunar tide (Dronkers, 1986; Blanton et al., 2002; Huang et al., 2008).

The objective of this study was to describe a new methodology to measure tidal creek discharge with respect to time and stage. The motivation for this study was to provide the site- and timing-specific data needed to inform management decisions for coastal wetlands, specifically whether hydrodynamic data can help inform nutrient (nitrogen and phosphorus) thresholds in South Carolina coastal systems. Four tidal creek sites were used here: two are in the Ashepoo-Combahee-Edisto (ACE) Basin estuary, and two are in the Charleston Harbor estuary (Figure 1). The two sites in Charleston Harbor were located within the first-order Horlbeck Creek and the second-order Bulls Creek areas. The ACE Basin sites were within the third-order Big Bay Creek and the fourth-order Wimbee Creek areas. All four creeks are classified as blackwater systems, meaning that the streams originate in the Coastal Plain (and not in the Piedmont), have a moderate freshwater surface inflow, may have substantial fresh groundwater inflow, and receive dissolved organic matter inputs from terrestrial vegetation (Chow et al., 2013; Alber et al., 2015), though considerable dissolved organic carbon (DOC) may also be internally regenerated (Reed et al., 2015). Previous studies have shown that South Carolina blackwater systems, including creeks used herein, are primarily nitrogen limited. Developed areas in particular may be susceptible to increases in phytoplankton growth, particularly in response to elevated concentrations of reduced nitrogen, especially dissolved organic N (as urea), as determined experimentally (Reed et al., 2015; Reed et al., 2016). DOC concentrations have also been shown to be higher in undeveloped watersheds than developed ones, with urea stimulating a greater contribution of phytoplankton-derived DOC in developed watersheds, suggesting that N-inputs may affect the biogeochemical cycling of carbon in these systems (Reed et al., 2015). We also hypothesized that more developed and populated watersheds would generate more stormwater runoff as a result of increased impervious surfaces from roads, homes, and soil compaction. This was tested using a stormwater runoff model calibrated for coastal systems.

METHODS

STAGE-DISCHARGE DATA COLLECTION AND INTERPRETATION

Four tidal creeks in South Carolina were studied over the course of 2 years to understand the relationship between tide stages (water depth) and discharge (volumetric flow rate). Two of the creeks (Wimbee and Big Bay) were in the relatively undeveloped ACE Basin and two in the more urbanized Charleston Harbor (Horlbeck and Bulls), as shown in Figure 1. Within each drainage system, one creek was classified as more disturbed or developed than the other; thus, in order of degree of impact from least to greatest, the creeks are Wimbee (WC), Big Bay (BBC), Horlbeck (HC), and Bulls (BC). The degree of development in each watershed was quantified using 2010 NOAA Coastal Change Analysis Program (C-CAP) GIS data. We selected the USGS Elevation Derivatives for National Application (EDNA) data to establish the watershed units for land cover analysis and comparison.

For the Atlantic coast of the United States, tides are classified as semidiurnal, meaning that two high tides and two low tides typically occur in a lunar day (24 hours, 50 minutes). For an ideal symmetric semidiurnal tidal system, high tides occurs 12 hours and 25 minutes apart, with 6 hours and 12.5 minutes between high and low tide (NOS 2008). In our study, the time of the discharge measurements was normalized to high water slack (HWS) for each day's effort. In this way, we can compare many different days' efforts relative to time in the tidal cycle. Additionally, by plotting discharge as a function of time, we were able to integrate the area under each curve to determine the total volume of water for any period of the tidal cycle (Boon, 1975; Blanton et al., 2006).

Discharge measurements were recorded using a Teledyne RD Instruments acoustic Doppler current profiler (ADCP) WorkHorse Monitor 1,200 kHz model (Teledyne RD Instruments 2011, 2014). This equipment uses sonar pings to measure water velocity within a consistent-sized subarea all along the transect cross section. The equipment calculated the discharge for each width-depth increment across the creek and then summed the increments to provide a total discharge for the entire cross section at a specific time. To differentiate between the flood and ebb data, we noted the flow direction as a positive discharge for ebb tide flow (toward the mouth of the creek), and a negative discharge was considered flood tide flow (toward the headwaters of the creek). At each study site, we designated a single transect location (a perpendicular cross section to the flow in the

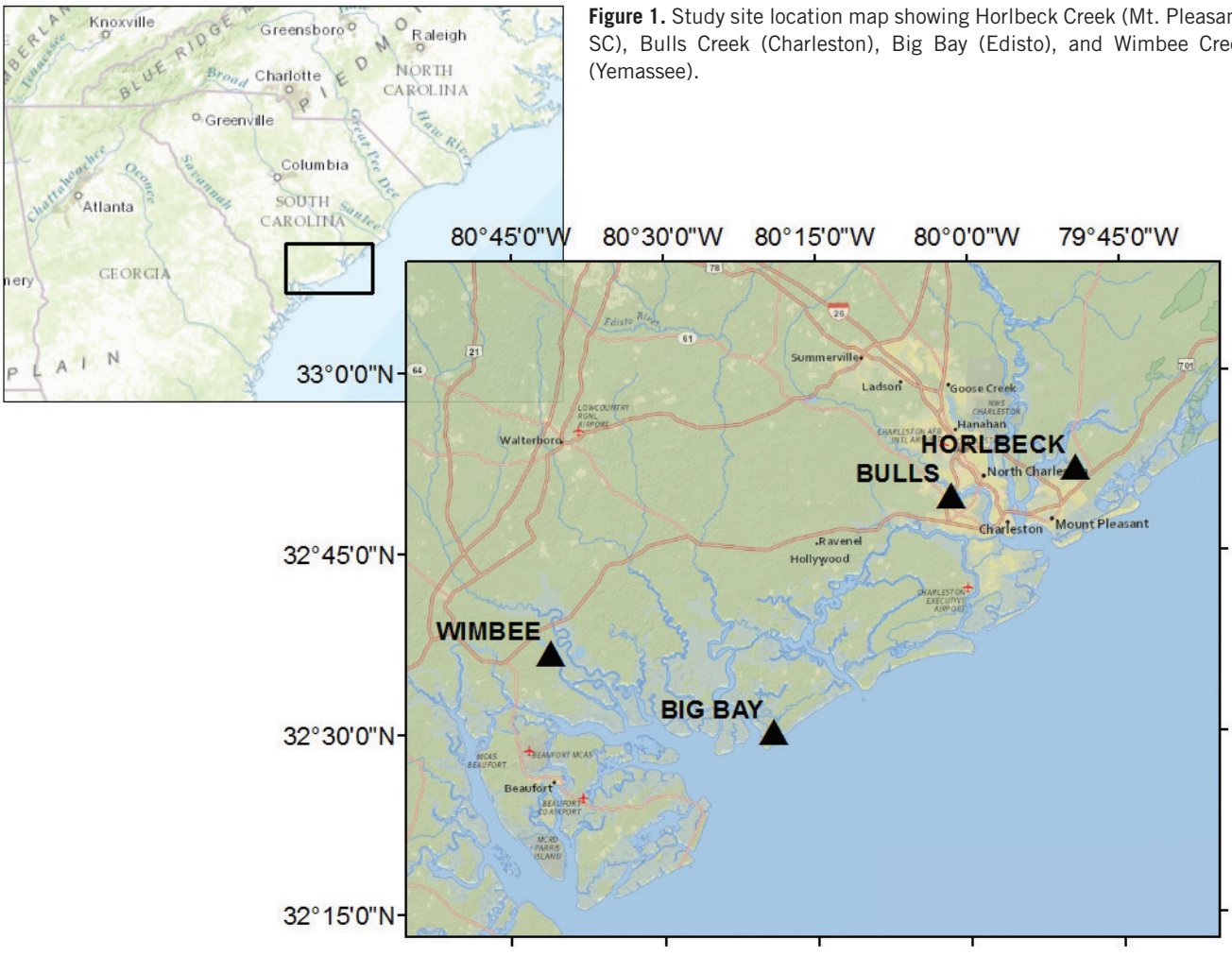

Figure 1. Study site location map showing Horlbeck Creek (Mt. Pleasant, SC), Bulls Creek (Charleston), Big Bay (Edisto), and Wimbee Creek (Yemassee).

creek). To assure consistency in discharge measurements, we performed three to four measurements along the same transect. These groups of measurements were spaced at intervals of 30–40 minutes throughout a day's monitoring effort, with the goal of capturing as much of a tidal cycle as possible (usually about 8–10 hours of data). We followed the Teledyne RDI methodology for rejecting any measurements that produced a transect measurement with more than 25% Bad Bins (Teledyne RD Instruments 2007). The field monitoring efforts were planned during the 2015–2016 period to observe as many different tidal conditions (flood, ebb, spring tide, and neap tide) as possible for each study site to account for variability in creek stages and velocities.

The data for each field campaign at each site were inspected separately as flood and ebb tide conditions (Figure 2). Several nonlinear regression models (sine functions and polynomial functions) were developed using RStudio software (RStudio Team 2016), which is a free and robust mathematical and statistical software package. The resulting regression equations were plotted using a graphing calculator to determine 1) the duration of the tidal cycle, 2) the time and value for the peak discharge, and 3) total volume for each tidal cycle. The duration of the flood tide is the time from low water slack (LWS) to HWS. For the purpose of this study, HWS is defined as time = 0 when discharge = 0. Similarly, the length of the ebb cycle is the time from HWS to LWS. The length of the tidal cycle was determined by using built-in functions in the graphing calculator to determine the x-intercept of the equation to find the point of LWS (e.g., the point where the best fit line crosses the x-axis at discharge = 0). If the best fit line did not cross the x-axis, the time of LWS was assumed to be the minimum (for ebb) or maximum (for flood) point of the curve. Finally, the equations for discharge versus time were integrated to obtain the total discharge (or tidal prism) for the flood and ebb, respectively (Boon, 1975).

GIS ANALYSIS OF LAND COVER AND POPULATION

Two different watershed types were utilized during this study (Figure 3). The USGS EDNA watersheds were utilized in lieu of a generic buffer distance around each study site as a way to quantify population density and land use/land cover differences. We assumed that the EDNA served as a "hydrologic buffer" rather than one based on an arbitrary distance. Please note that the study site location could fall anywhere in the EDNA watershed, so it was not necessarily a consistent landmark in each EDNA watershed (such as the outlet). Land cover data were obtained from the 2010 NOAA Coastal Change Analysis Program (C-CAP) files, and population density was calculated using 2010 US Census block data.

The second watershed type was a manual delineation of the watersheds upstream of our transect and nutrient sampling locations; this provided us with the ability to assess the area expected to drain past the sampling location (compared to the EDNA). The geographic watershed was not able to be delineated for the Wimbee Creek study site due to the complicated systems of impoundments (managed for waterfowl) and braided creek channels. Land cover data were obtained from the 2010 NOAA C-CAP files, and soil

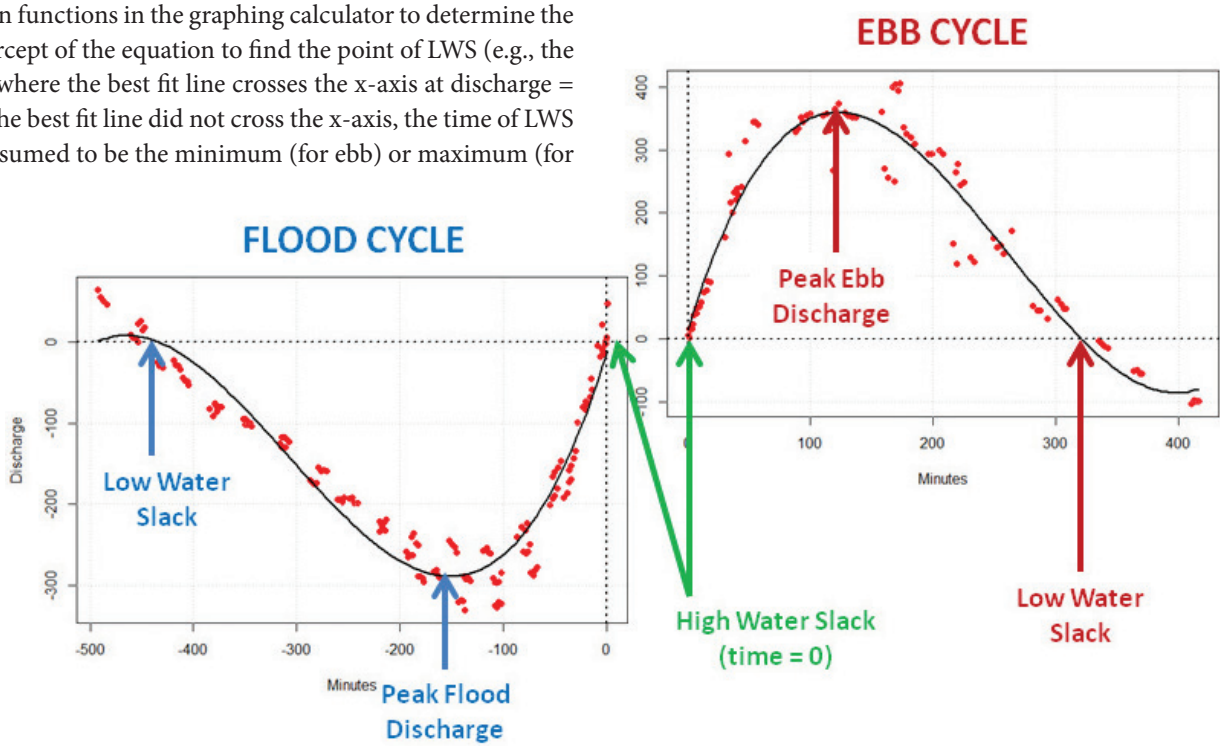

Figure 2. Tidal creek discharge example data (symbols) showing the endpoints and peak discharge for flood (left) and ebb (right). Flood tide onset and end were defined as low water slack (LWS) tide stage and high water slack (HWS; time = 0, discharge = 0), respectively. Conversely, ebb tide onset and end were defined as HWS and LWS, respectively. The solid curves represent a polynomial function best-fit curve to the data, interpreted separately as flood tide data and ebb tide data. Note the longer period for flood tide relative to ebb tide, due to the larger rate of ebb tide discharge (i.e., larger average water velocity during ebb).

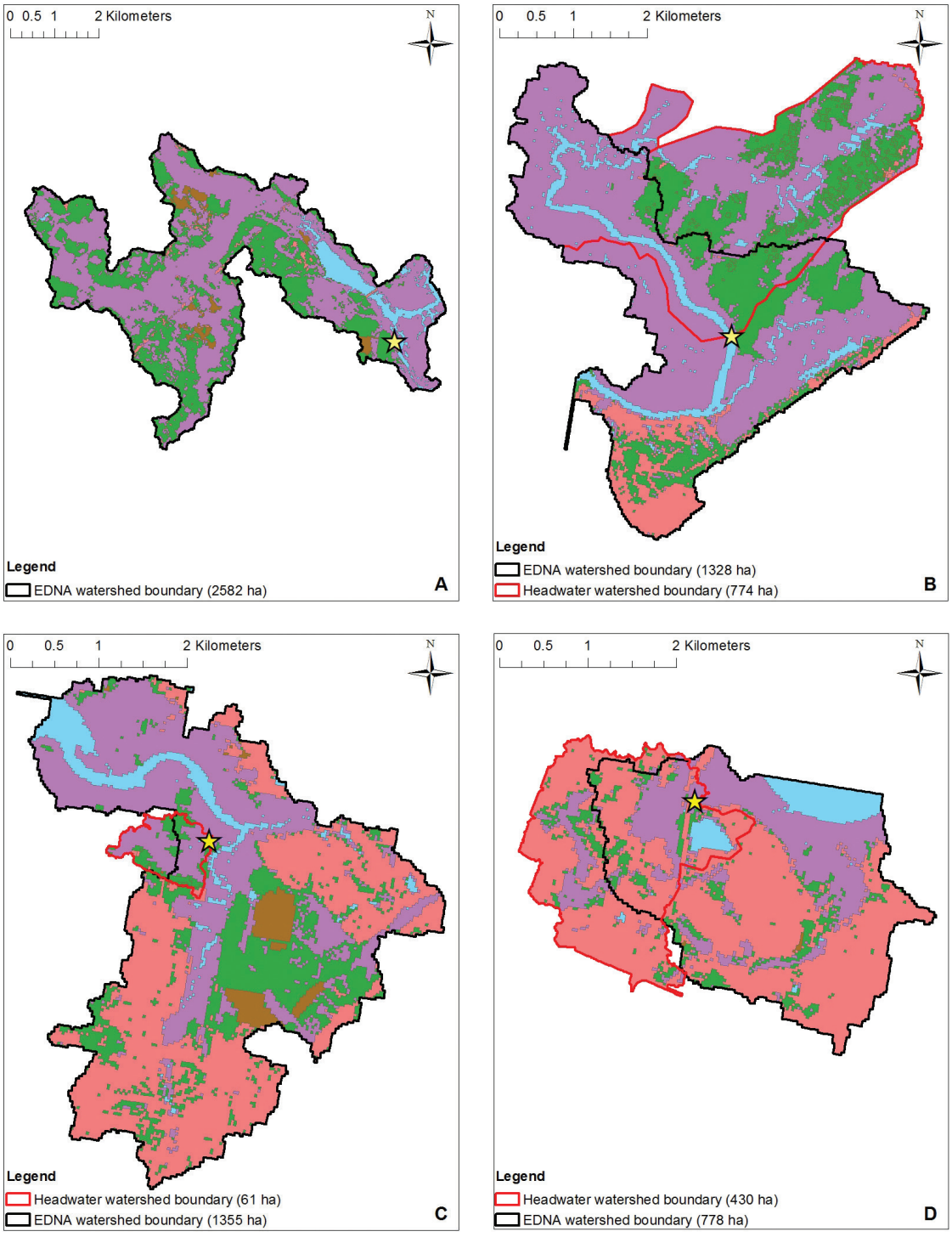

Figure 3. Comparison of land cover for the geographic (headwater) and EDNA watersheds for the sites. From top left Wimbee Creek (A), Big Bay Creek (B), Horlbeck Creek (C), and Bulls Creek (D). The headwater watershed for Big Bay was calculated as a proportion of two smaller units, for a total of 774 ha. A headwater watershed was not delineated for Wimbee, and this creek was not included in stormwater modeling.

data was obtained from the NRCS Soil Survey Geographic database (SSURGO). The results from this geographic watershed analysis were input directly into the stormwater runoff model described below.

STORMWATER RUNOFF MODELING

Land-based runoff was estimated for three of the four study sites by the Stormwater Runoff Modeling System (SWARM). Wimbee was not included in this analysis because a geographic watershed could not be delineated. SWARM has been calibrated to reflect stormwater runoff generated in the shallow slopes and poorly drained soils of the South Carolina coastal plain (Blair et al. 2014a; Blair et al. 2014b). We calculated runoff volumes for several design storm scenarios at the three sites. The discharge volume calculated for each of the creeks was compared to potential stormwater runoff calculated by SWARM.

RESULTS AND DISCUSSION

GIS ANALYSIS OF LAND COVER AND POPULATION

The EDNA land cover analysis for each watershed supported the initial classification of the ACE Basin sites as relatively undisturbed "reference" watersheds in contrast to the more developed Charleston Harbor watersheds (Figure 3). Wetland land cover comprised the largest percentage for all sites except for Bulls watershed, for which wetland was second to developed land cover classes. The ACE Basin creeks were less developed than the two Charleston Harbor system creeks. The two in the ACE Basin were predominantly forest and wetland land types, making up nearly 80% of the watershed land cover. Development of any kind made up a very small percentage of the land cover in the ACE Basin creeks (11% in Big Bay and 2% in Wimbee). Conversely, the largest land use component (32%) in the Bulls Creek watershed was "developed-low," and total development land classes for that watershed made up more than half of the land (56%). The total of all development classes made up about 40% of the land cover in Horlbeck Creek, with wetlands (55%) and forests (18%) making up the other significant classifications. These findings supported Reed et al. (2016), who used a 2000 m radius around each site and 2010 NOAA C-CAP land cover data. They calculated the contribution of forest and wetlands as 75% with 0% developed land; forest and wetlands at Bulls Creek contributed 37%, while "developed-high" and "low" intensity land categories at Bulls Creek were 7% and 35%, respectively.

In addition to land cover, population density was calculated for the EDNA watersheds as an indicator of level of development in each of the creek systems. As expected, the ACE Basin Creeks had the lowest population density with 0.21 people/hectare (ha) at Wimbee and 0.41 people/ha at Big Bay, and the larger population densities were found at Horlbeck (4.63 people/ha) and Bulls Creeks (12.84 people/ha).

STAGE AND DISCHARGE RELATIONSHIPS

The stage and discharge relationship for the tidal creeks had a cyclic pattern and not the traditional "rating curve" unidirectional pattern (downstream flow), which is usually observed in nontidal systems. Starting at high-water slack (HWS, Figure 2), where discharge would be zero with the stage at or near the maximum, discharge increased as the stage decreased as tide ebbs out of the estuary. Peak discharge occurred midway between HWS and low-water slack (LWS); once peak discharge was attained, the discharge rate decreased as the stage decreased to the point of LWS. As the subsequent flood tide commenced after LWS, the discharge increased until nearly the stage of HWS. Rather than a rating curve describing stage versus discharge, the pattern can better be described as a rating ellipse in tidal systems. This illustrates additional important characteristics of the circular stage-discharge "rating ellipse." First, for the same stage, a different discharge on the flood and ebb tide was observed, and therefore the same discharge value occurred at different stages. Generally, for the same stage value, the discharge in the creek was greater for the ebb tide period than for the flood tide. At our four study sites, the peak ebb discharge was always greater than the peak flood discharge. Also, the peak flood discharge occurred at a higher stage than that for peak ebb discharge for all four of our study sites. Wimbee showed the most ebb-dominant and asymmetric pattern of the rating ellipse of all four sites. This is likely due to the large terrestrial land area that drained from the upper Combahee River basin past our monitoring site (Figure 1).

DISCHARGE AS A FUNCTION OF TIME

Discharge data for each site were plotted in relation to time before or after HWS. It is important to note here that HWS and high tide are not coincident; neither is LWS and low tide, as is illustrated in Figure 4. As found in other studies (Leopold et al., 1993), we have observed a lag between the time at which the water is at its highest stage (part B of Figure 4; high tide) and when the water stops moving upstream (part C of Figure 4; HWS). Similarly, a lag can be seen between when the water reaches its lowest stage (low tide) and when the water stops flowing downstream. In a tidal creek study in California, velocity continued for one-half to one hour after the gage height reached its maximum or minimum; the researchers stated that the inertia of flowing water kept the water velocity flowing in a particular direction until the slope (water-surface elevation of the creek at the mouth compared to headwaters) reversed (Leopold et al., 1993). The durations of the flood and ebb tides were not symmetrical at the field sites, supported by qualitative observation evidence and previous studies (Blanton et al., 2002). In general, the

predicted (and observed) duration of the flood tide was longer than that for the ebb (Table 1) for all four study sites.

We evaluated three different methods for describing the relationship between discharge and time using a nonlinear regression: (1) we modeled the data collectively (flood and ebb) as a sine function; (2) we separated the data and modeled a unique sine function for the flood and ebb; and (3) we modeled the separate flood and ebb data as individual polynomial equations. We found that each of the three regression models had differences in residual standard error (RSE), cycle duration, peak discharge, and discharge volume (or tidal prism), as shown in Table 1. The polynomial regression expressions (example in Figure 2) appear to more accurately model discharge at each of our four study sites, having the smallest RSE values; however, we believe that a sine function more accurately represents the physical

Table 1. Summary of Tidal Hydraulic Characteristics and Statistical Analysis for Each Site

Site	Analytical Model	RSE (Flood/Ebb)	Flood Duration (hr)	Ebb Duration (hr)	Total Duration (hr)	*Flood Peak Discharge (m^3/s)*	*Time of Flood Peak (hr)*	*Flood Volume (m^3)*	Ebb Peak Discharge (m^3/s)	Time of Ebb Peak (hr)	Ebb Volume (m^3)
Wimbee	Polynomial	8.221/14.93	**6.75**	**5.99**	**12.74**	*-75.48*	*-2.67*	*1,177,969*	**133.32**	**3.44**	**1,880,482**
	Sine	10.05/16.10	**6.97**	**6.33**	**13.30**	*-74.19*	*-2.89*	*1,168,448*	**133.89**	**3.20**	**1,867,574**
	Sine All	21.22	**5.99**	**7.02**	**13.01**	*-90.60*	*-3.32*	*1,254,095*	**116.20**	**3.19**	**1,853,833**
Big Bay	Polynomial	27.83/47.46	**7.30**	**5.37**	**12.67**	*-288.06*	*-2.68*	*4,498,690*	**359.66**	**2.05**	**4,385,956**
	Sine	43.19/55.66	**8.08**	**5.66**	**13.74**	*-278.60*	*-2.97*	*4,596,908*	**354.40**	**2.35**	**4,334,732**
	Sine All	81.94	**6.57**	**5.96**	**12.53**	*-310.00*	*-3.40*	*4,644,480*	**266.20**	**2.87**	**3,656,199**
Horlbeck	Polynomial	2.153/3.869	**6.60**	**5.14**	**11.74**	*-8.63*	*-1.97*	*117,086*	**11.71**	**1.63**	**122,598**
	Sine	2.24/3.846	**6.14**	**5.95**	**12.09**	*-8.45*	*-2.16*	*125,004*	**11.73**	**1.85**	**128,486**
	Sine All	4.166	**5.62**	**5.30**	**10.92**	*-13.47*	*-3.13*	*124,791*	**8.89**	**2.33**	**108,434**
Bulls	Polynomial	3.431/5.156	**7.67**	**6.01**	**13.68**	*-13.52*	*-2.25*	*218,449*	**16.55**	**1.92**	**203,245**
	Sine	3.603/5.266	**9.38**	**7.12**	**16.50**	*-13.23*	*-2.54*	*236,455*	**16.29**	**2.20**	**213,816**
	Sine All	5.728	**6.14**	**5.68**	**11.82**	*-15.30*	*-3.20*	*214,437*	**13.56**	**2.71**	**177,249**

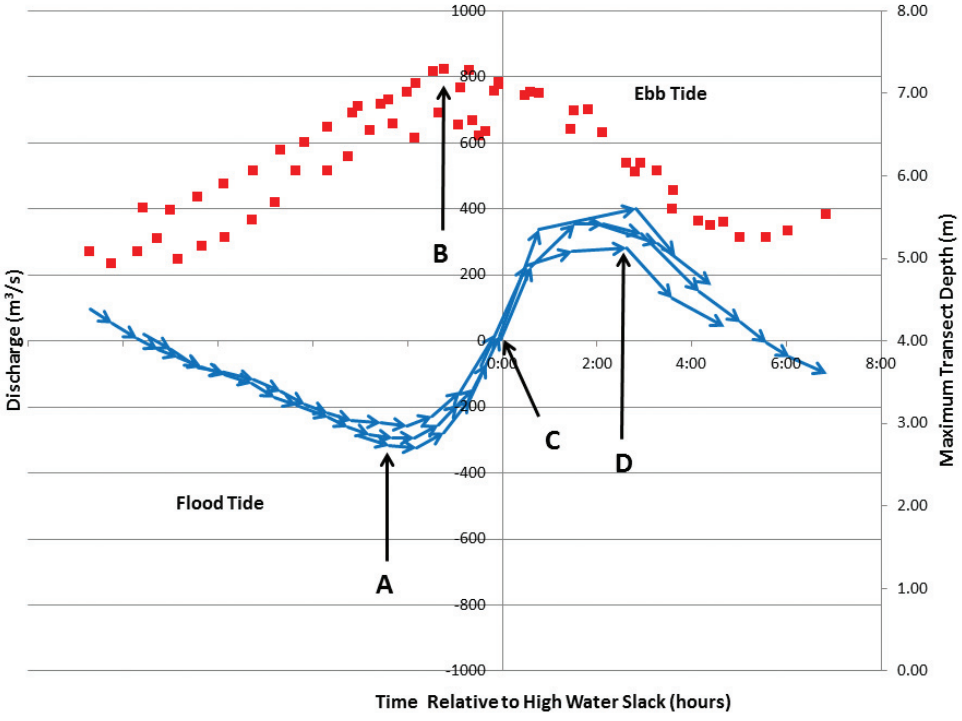

Figure 4. Discharge as a function of time after high water slack tide for the Lag times between peak flood discharge (A), high tide (B), high water slack (C), and peak ebb discharge (D). Blue arrowed lines indicated water discharge rate (left-hand y-axis); red box symbols represent transect maximum water depth (right-hand y-axis).

phenomena of tidal influence than a polynomial equation, as supported by previous tidal creek research (Boon, 1975; Pethick, 1980; Blanton et al., 2002).

Using the sine functions involves tradeoffs as well. The model that incorporates both the flood and ebb data appears to better reflect the transition of the discharge from flood to ebb; when the data are analyzed separately, the duration of the flood or ebb tide can become too long (e.g., the predicted flood tide duration at Big Bay and Bulls Creeks, as listed in Table 1) because the regression model tries to minimize the residuals between the data points rather than match the observed physical phenomena of HWS or LWS (it ends up overshooting the HWS or LWS points). We know that a complete tidal cycle (low tide and high tide) should take about 12 hours and 25 minutes; but the division between flood and ebb tides is unequal in an ebb-dominate system. We expect the flood tide to be longer than the ebb in all models for these systems (Blanton et al., 2002), but the total duration should be close to 12.5 hours. In Table 1, the "sine" (separate for flood and ebb) model consistently predicts the longest total tidal cycle duration and actually predicts an irrationally long tidal cycle (16.5 hours) for Bulls Creek.

Conversely, when modeling the complete flood and ebb data as one sine function, the model tends to undershoot the peak ebb discharge values and overshoot the peak flood discharge (as is especially evident for Big Bay Creek in Figure 5). In Table 1, the peak flood discharge predicted by "sine all" is always greater than the other two models, and peak ebb discharge is always smaller than the other two models. This shows that the model is making tradeoffs in minimizing residuals to try to come up with a single expression to describe two related but very different hydraulic processes.

In summary, the three different regression models predict an "average" discharge with respect to time at each of the study sites. While the polynomial regression most accurately fits the actual observations, it has no relevance to tidal functions. The sine regression model with the flood and ebb data separated may not provide an accurate prediction for flood or ebb duration, but it appears to predict the peak discharge more accurately. Finally, the sine regression model that incorporates both the flood and ebb data gives a more accurate depiction of duration but underestimates the peak discharge, as shown in Figure 5. This figure illustrates the results of interpreting all the flood and ebb data at each site to generate a single sine function regression model and parametric bootstrap, which represents the 95% confidence interval for discharge data.

PEAK DISCHARGE

At all four sites, the peak discharge on the ebb was larger than the peak on the flood (Table 1). The greatest peak discharge was estimated for Big Bay Creek (359.66 m^3/s on

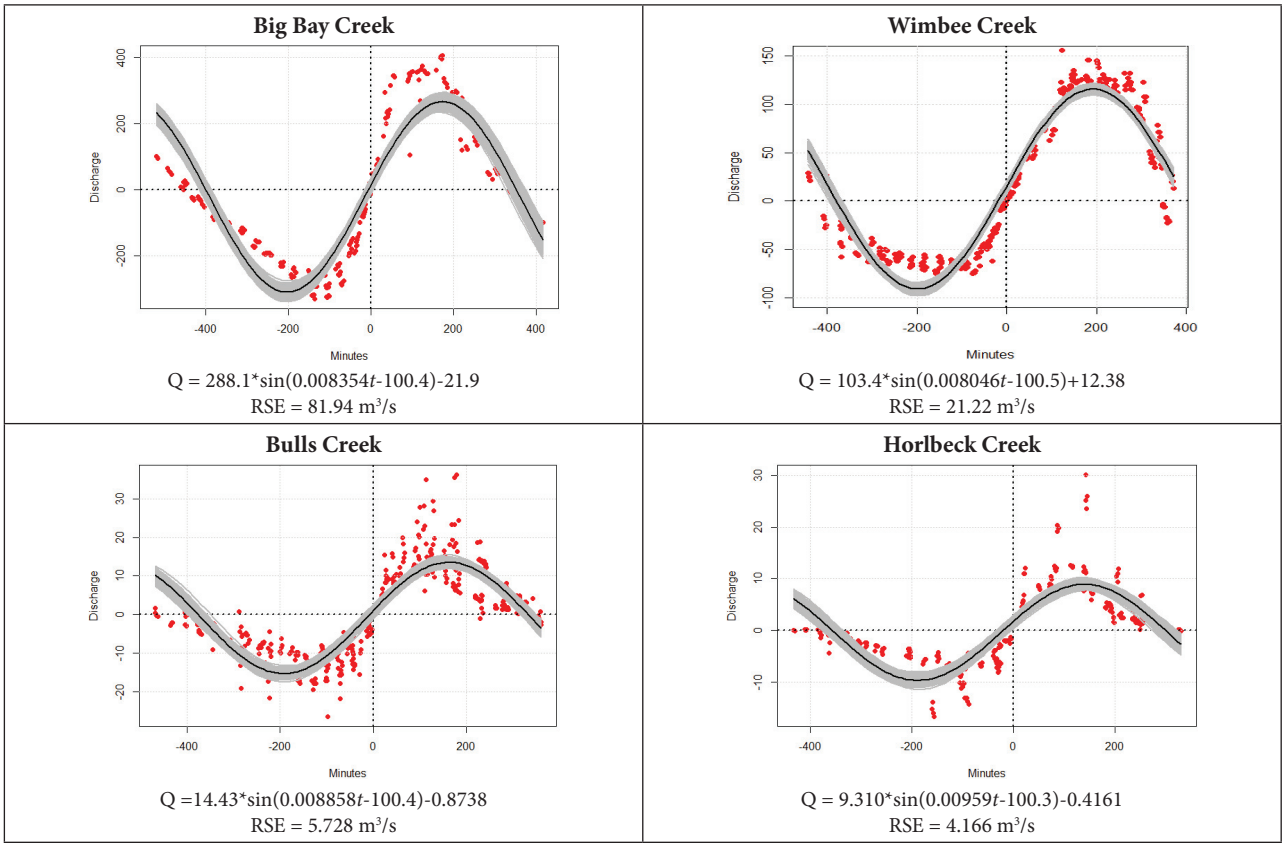

Figure 5a: Tidal creek discharge (Q) as a function of time (t) for all sites with best-fit regression equation defined as a single sine wave function for both flood and ebb tide.

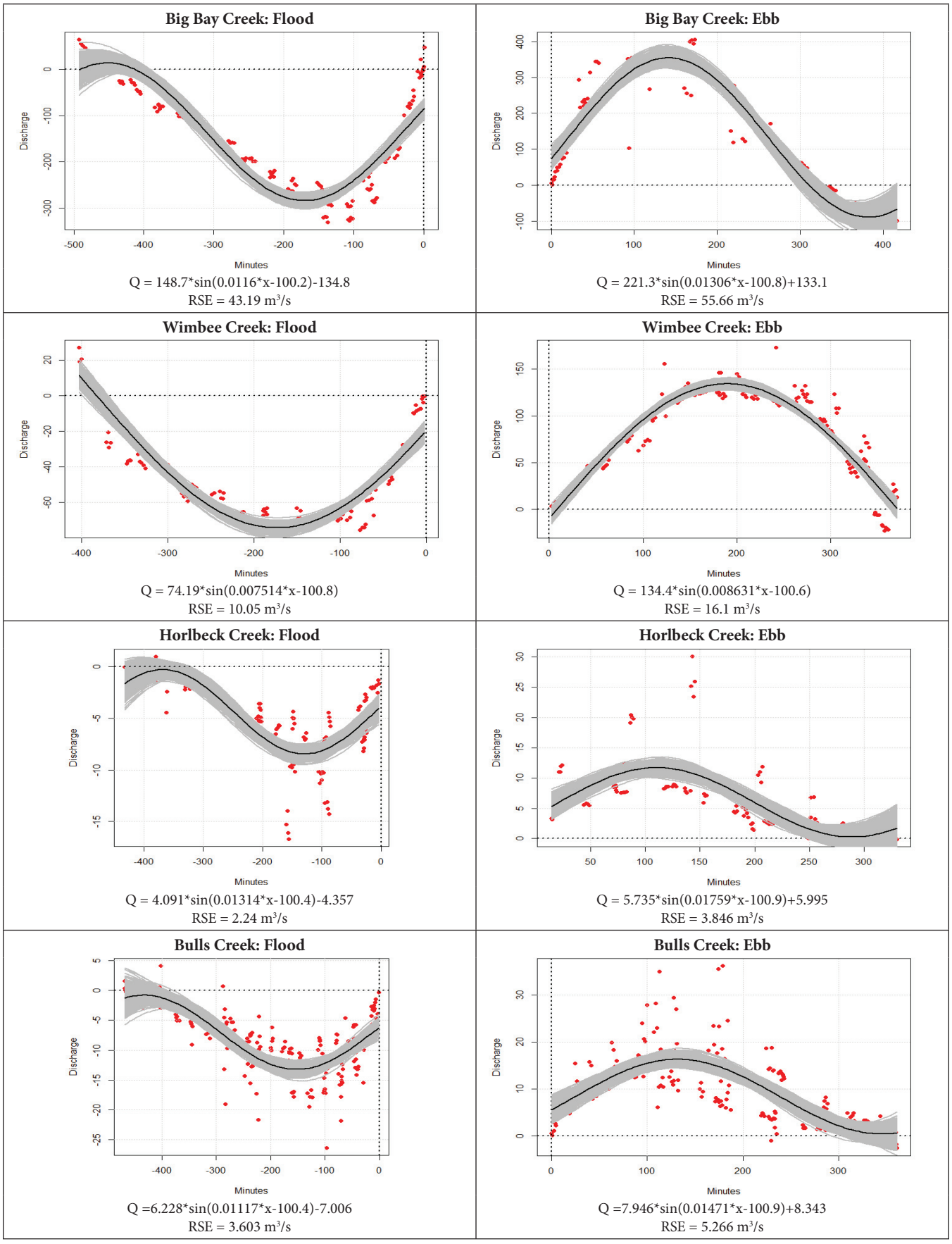

Figure 5b: Tidal creek discharge (Q) as a function of time (t) for all sites with best-fit regression equation defined as a separate sine wave function for both flood and ebb tide.

Big Bay Creek: Flood

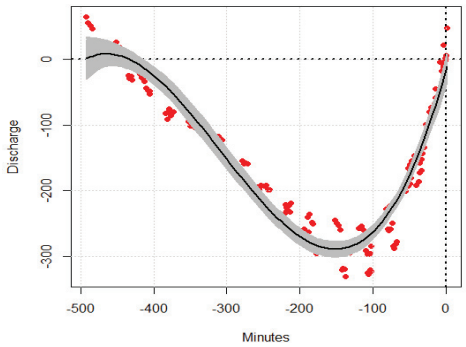

Q = -15.23+(4.057*x)+(0.01777*x^2)+(0.00001922*x^3)
RSE = 27.83 m^3/s

Big Bay Creek: Ebb

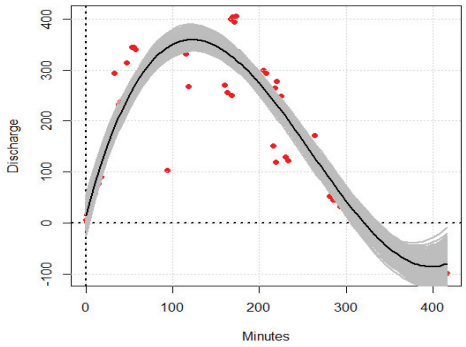

Q = 15.6+(6.247*x)-(0.03333*x^2)+(4.271e-05*x^3)
RSE = 47.46 m^3/s

Wimbee Creek: Flood

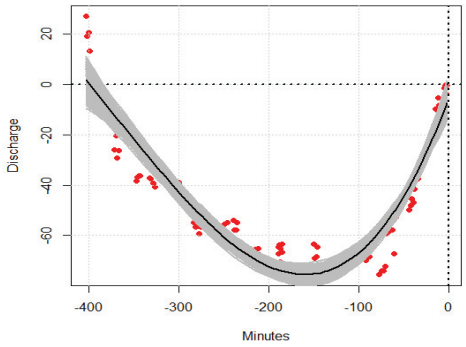

Q = -5.658+(0.9631*x)+(0.003856*x^2)+(0.000003526*x^3)
RSE = 8.221 m^3/s

Wimbee Creek: Ebb

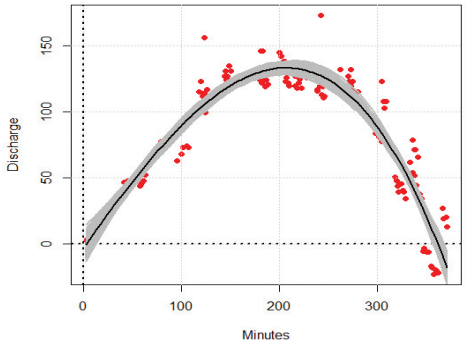

Q = -2.238+(1.036*x)+(-4.982e-04*x^2)+(-6.488e-06*x^3)
RSE = 14.93 m^3/s

Horlbeck Creek: Flood

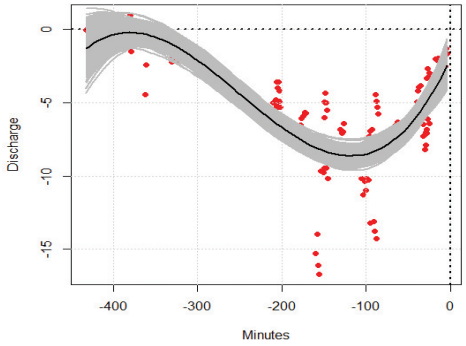

Q = -1.992+(0.1253*x)+(6.943e-04*x^2)+(9.269e-07*x^3)
RSE = 2.153 m^3/s

Horlbeck Creek: Ebb

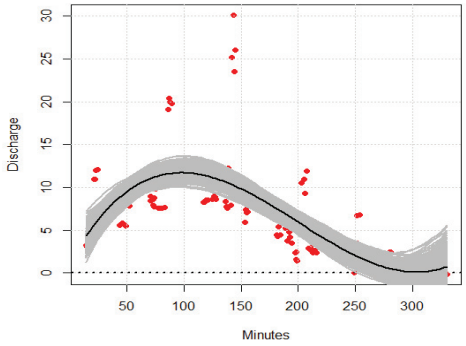

Q = 1.303+(0.2385*x)+(-1.613e-03*x^2)+(2.683e-06*x^3)
RSE = 3.869 m^3/s

Bulls Creek: Flood

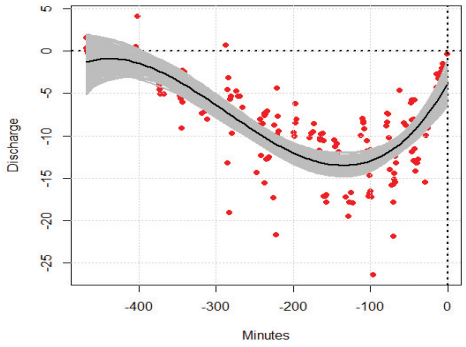

Q =-3.804+(0.1604*x)+(0.0007771*x^2)+(0.0000009034*x^3)
RSE = 3.431 m^3/s

Bulls Creek: Ebb

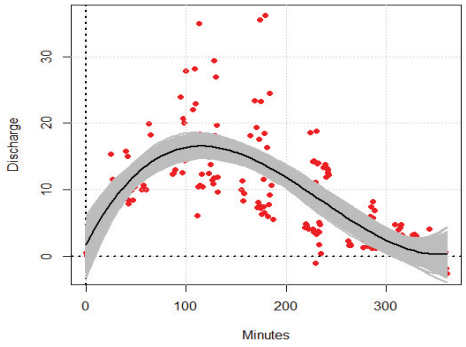

Q =1.705+(0.2894*x)+(-1.666e-03*x^2)+(2.364e-06*x^3)
RSE = 5.156 m^3/s

Figure 5c: Tidal creek discharge (Q) as a function of time (t) for all sites with best-fit regression equation defined as a separate polynomial function for both flood and ebb tide.

the ebb), and the smallest peak discharge was estimated for Horlbeck Creek (-8.63 m^3/s on the flood). The predicted timing of the peak ebb discharge occurred closer to HWS than peak flood discharge, except for on Wimbee Creek. For example, the average peak flood discharge on Big Bay Creek occurred 2.68 hours before HWS, whereas the average prediction for peak ebb discharge occurred about 2.05 hours after HWS, a 37-minute difference. The magnitude of the predicted peak discharge values for both the flood and ebb at Horlbeck and Bulls sites appear more similar than those measured at Big Bay and Wimbee, which show a larger skew toward ebb dominance. Perhaps the larger creek sizes or larger upstream watershed size would also contribute to the more pronounced ebb dominance seen in Big Bay and Wimbee.

VOLUME CALCULATIONS

The resulting regression equations were integrated to determine a total average volume discharged (tidal prism) on the flood and ebb tide for the sampling point along each creek system. From smallest to greatest discharge, the creeks ranked as Horlbeck, Bulls, Wimbee, and Big Bay (Figure 6). All of the creeks, except for Wimbee, had relatively equal discharge on the flood and ebb with the differences being less than 10%. A previous study in tidal creek hydrology found that peak ebb discharge exceeded the flood by more than 50% in some cycles, but the measured volumes entering and leaving the marsh typically differ less than 7% (Boon 1975). Thus, Wimbee was a clear outlier, with the ebb discharge exceeding the flood by more than 50%. We believe that Wimbee's ebb dominance was influenced by its distance from the open ocean (it is the furthest inland sampling site) and the fact that the Combahee, a large river that extends even farther inland, discharges into Wimbee; our assumption is that the flood tide influence is less pronounced at this site due to greater inland nontidal water sources (flowing in the ebb direction) and frictional losses to flood tidal energy as the water moves upstream (Blanton et al., 2002).

YEARLY PRECIPITATION OBSERVATIONS

Precipitation for water years October 2014–September 2015 and October 2015–September 2016 are illustrated in Figure 7. Precipitation for each site was referenced to a NOAA climate monitoring station at Charleston International Airport (CHS) for Bulls and Horlbeck Creeks, Yemassee, SC, for Wimbee Creek, and Middleton Plantation on Edisto Island for Big Bay Creek. In 2014–2015, the total precipitation for Charleston Airport (CHS) was 1,360 mm, 1,258 mm for Edisto, and 1,258mm for Yemassee. The annual precipitation increased at all three sites for 2015–2016: 1,895 mm recorded at CHS, 1,524 mm at Edisto, and 1,700 mm at Yemassee. The wettest month for 2015–2016 was October 2015, which is a reflection of Hurricane Joaquin; the precipitation totals for

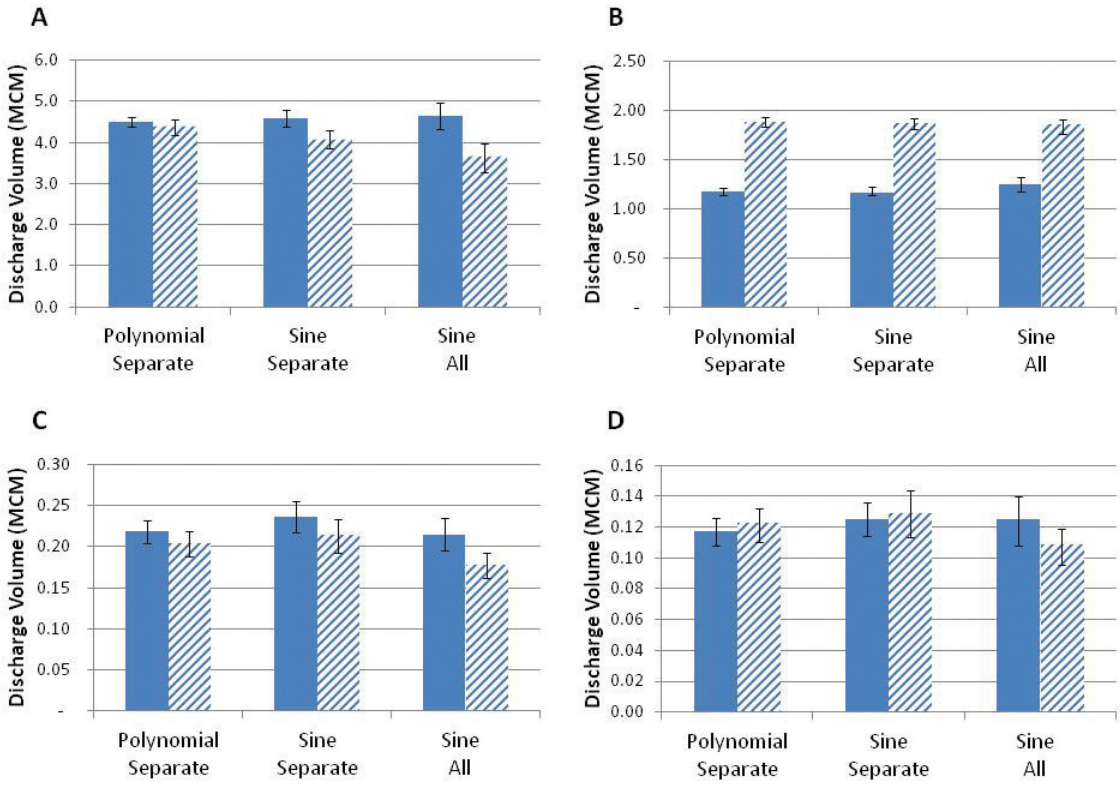

Figure 6: Summary of calculated discharge for one tidal cycle volume in million cubic meters (1 MCM = 264.17x10^6 gallons). From greatest to smallest discharge volume starting at top left: (A) Big Bay, (B) Wimbee, (C) Bulls, and (D) Horlbeck Creek. The volumes for flood (solid bars) and ebb (patterned bars) discharge are most asymmetric for Wimbee Creek.

the duration of the storm accounted for about 25% of total yearly precipitation for CHS and Edisto and 15% of the yearly total for Yemassee. Previous work by Reed et al. (2015) showed that precipitation was significantly and positively correlated with concentrations of DOC, including Wimbee Creek and Bulls Creek, suggesting that rainfall markedly impacts the delivery of DOC and potentially other nutrients from the land to the receiving waters.

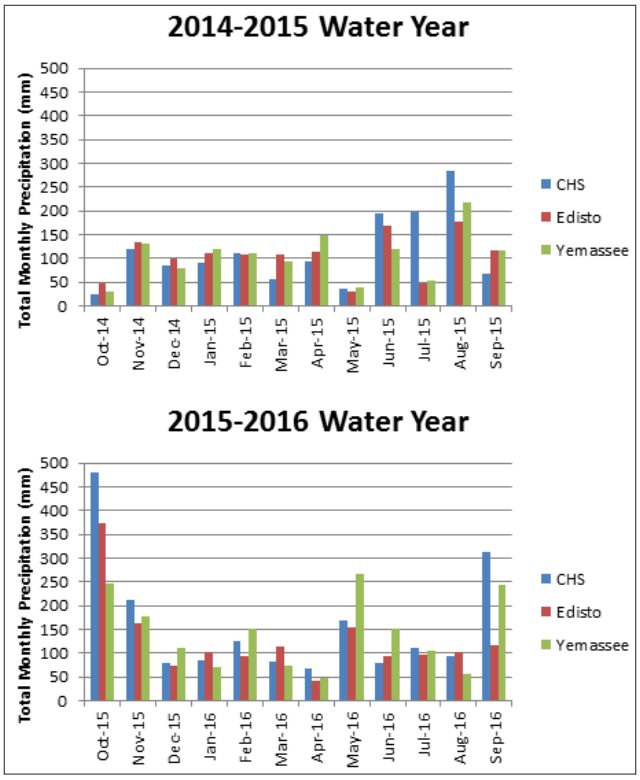

Figure 7. Summary of precipitation data for October 2014–-September 2016 for Charleston Airport (CHS), Edisto Island Middleton Plantation (Edisto), and Yemassee 7.6 NE (Yemassee) obtained from NOAA National Centers for Environmental Information climate data.

STORMWATER RUNOFF MODELING

Stormwater runoff volume was calculated for three study watersheds (Big Bay, Horlbeck, and Bulls) for two scenarios: a 2-inch (50-mm) and 4.5-inch (114-mm) design storm. The 50-mm storm reflects a stormwater volume control requirement in Beaufort County, and the 114-mm storm is an approximation of the 2-year, 24-hour design storm typically used in engineering design to account for flood protection. SWARM calculated a modified curve number (CN) of 83 for Bulls Creek and 77 for both Big Bay and Horlbeck Creeks. We have observed that the differences in the potential impact of stormwater runoff are related to both watershed land cover and size of the individual creeks. Big Bay Creek is a third order creek system, and thus has a larger overall discharge volume than either Bulls (second order) or Horlbeck (first order). Although the overall watershed size, creek volume, and modeled stormwater runoff volume were largest at Big Bay, the potential stormwater volume was a very small proportion of the flood or ebb volume in Big Bay Creek. Bulls Creek was the only site out of the three different locations in which the predicted stormwater runoff surpassed the volume of the tidal prism (Figure 8). Whereas Big Bay and Horlbeck have relatively small runoff volumes compared to design storms, especially for the 95th percentile and 2-year, 24-hour storms, the runoff volume at Bulls Creek for the smallest design storm is equivalent to about one-third of the tidal prism. The runoff generated for the 2-year, 24-hour storm surpasses the tidal prism volume by about one-third. The runoff predicted for the 25-year, 24-hour storm is about 300% of the tidal prism. The runoff volume at Big Bay does not surpass the tidal prism volume for the four different design storm scenarios. The runoff from the 25-year, 24-hour storm (203 mm) is equivalent to about 22% of the tidal prism in Big Bay Creek. The runoff volume at Horlbeck does not surpass the tidal prism volume for the four different design storm scenarios. The runoff from the 25-year, 24-hour storm

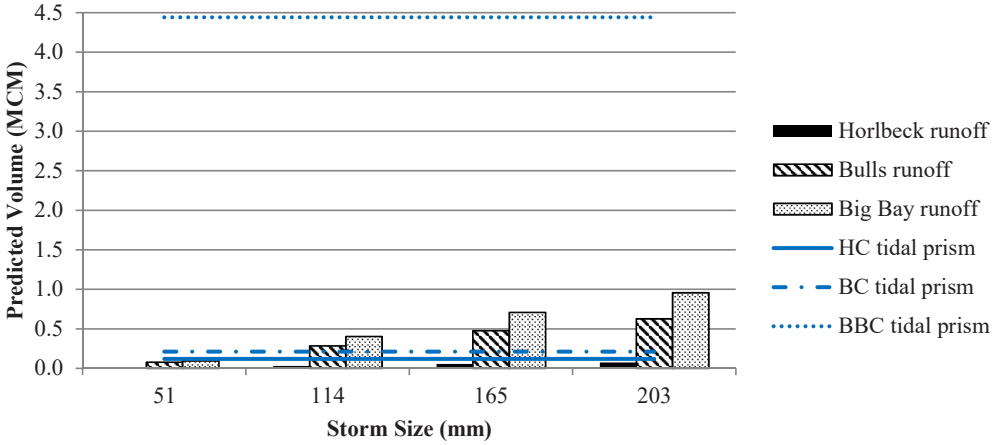

Figure 8. Tidal creek discharge volume (horizontal lines, million cubic meters) for Big Bay, Bulls, and Horlbeck sites compared to stormater runoff volume (vertical bars) as predicted by SWARM. Runoff never exceeds the tidal prism volume for Big Bay.

(203 mm) is equivalent to about two-thirds of the tidal prism in Horlbeck Creek.

Watersheds with more development and higher population, such as Bulls Creek, have the potential to generate more stormwater runoff as a result of increased impervious surfaces from roads, homes, and soil compaction. Previous research has used the amount of impervious cover in tidal creek watersheds as an indicator of coastal development; in fact, documented impacts of coastal development on the ecology of tidal creek systems include increased flooding potential and impairment of headwater and intertidal sections due to increases in nonpoint source pollution (Sanger et al., 2015). Reed et al. (2015; 2016) found that biological (i.e., phytoplankton) growth and biomass responses were augmented in developed systems following inorganic N (ammonium and nitrate) and organic N (urea) additions.

Hypothetically, a rainfall event during high tide could generate more stormwater runoff because more of the marsh platform is inundated or saturated with water. However, the larger volume of water present in the creek at high tide could also help dilute the effect of the influx of nonpoint source pollutants such as nutrients, sediments, and chemicals. Nutrient concentrations in tidal creeks from the two NOAA National Estuarine Research Reserve Systems (NERRs) in South Carolina are highest at low tide and lowest at high tide (NOAA National Estuarine Research Reserve Systems, 2016). Although nutrient concentrations in the creek water are generally highest at low tide, a storm event occurring at or near low tide could deliver additional chemical or sediment load to the wetland and/or creek due to higher concentrations in the stormwater.

IMPLICATIONS

Tidal distortion in these coastal wetland systems is a result of the frictional distortion in creek channels and intertidal storage in marshes and tidal flats (Friedrichs et al., 1988). The distortion of the time it takes for the water to move from HWS to LWS (ebb tide) or LWS to HWS (flood tide) affects the water velocity and thus discharge. In the four creeks in this study, we have observed ebb-dominated creek systems typical of the Southeast. In an ebb-dominated system, the length of time of the flood is longer than that of the ebb, but the peak discharge on the ebb is greater. This has two implications. First, the systems are essentially moving the same volume of water, or tidal prism. If the duration of the ebb tide is shorter than the flood tide, the water velocity on the ebb must be higher to get the same volume of water out. Second, if the ebb current is dominant, the higher velocities on the ebb have the potential to move a greater load of sediment (Dronkers, 1986; Friedrichs et al., 1988; Huang et al., 2008) and other nonpoint source pollution, such as chemicals, bacteria, and viruses, from the headwaters out to the estuaries (Sanger et al., 2015). The ebb dominance was most pronounced at Wimbee Creek, which had almost twice the volume of water moving past our study site on the ebb than for the flood tide (Figure 6). We suspect that this creek behaved differently from our other three sites because it is located relatively further inland and away from the coast. The flood tide loses more energy as it moves father up the tidal creek, reducing the total volume of water delivered to this site. Furthermore, Wimbee Creek is connected to the Combahee River, a large system that has nontidal and tidal inputs and does not have true headwaters. We believe that the force of the nontidal headwater inputs from the Combahee River contribute to the overall larger ebb discharge on Wimbee Creek.

We found that for site-specific discharge data related to time, a polynomial regression model provided the best fit for the data. However, future work could include developing a more robust regression equation incorporating multiple sine functions to more accurately predict discharge as a function of time. We still believe the single sine function has merit for predictive capabilities, and we are working to develop relationships between the discharge and the morphometric characteristics of each creek (such as velocity, width, and depth, as shown in Appendix B) to allow discharge estimates to be made at other tidal creek systems that are not gauged.

Due to limitations of time and funding, we were only able to make seven visits to each site (except Big Bay, which we visited six different days). As we will be able to add more time/discharge observations in the future, we should be able to generate regression models for more specific tidal conditions. For example, we could choose to analyze the data from spring and neap tidal conditions separately. Currently (2017), our regression models include a wide variation of tidal conditions, and even our 95% confidence intervals on the discharge predictions miss many "outlier" conditions (as can be seen in Figure 5, with many data points lying outside of the gray swath of curves).

Future work will build off of these models to estimate nutrient fluxes in tidal wetlands. Moving forward, we will evaluate the nutrient types and concentrations at mid-ebb and mid-flood at each of the four study sites for spring and summer samplings in 2015 and 2016. We hope to determine (1) if there are significant differences in nutrient concentrations and loads on the ebb versus the flood and (2) if there are differences between nutrient loads between sites and (3) if these loading differences are indicative of an underlying hydrodynamic phenomena that may help explain nutrient (nitrogen and phosphorus) fluxes and the respective biologic responses (e.g., phytoplankton growth). The future work will focus on not just how much nitrogen is in the water (loading) but also how the specific type of nitrogen (chemical form) influences phytoplankton composition. Furthermore, we postulate that the changes in nutrient concentrations are

not as significant to the loading calculation as compared to the tidal prism volume for flood or ebb discharge.

ACKNOWLEDGEMENTS

Funding for this study was courtesy of the Environmental Protection Agency, award #CD-0-00D24114 to Drs. Greenfield, Callahan, and Sanger. Funding for this effort in the ACE Basin NERR was provided, in part, by a grant under the Federal Coastal Zone Management Act, administered by the Office for Coastal Management, National Oceanic and Atmospheric Administration, Silver Spring, MD.

We thank Nick Wallover (SCDNR) and Dr. Scott Harris (CofC) who served as boat captains and made it possible for us to collect data at Big Bay and Wimbee Creeks. We also thank the following organizations and individuals for access to creeks and their support for this study: the ACE Basin National Estuarine Research Reserve, Palmetto Islands County Park staff, Beau Bauer from the Nemours Wildlife Foundation, the Ashley Harbor community, Dr. Barbara Beckingham (faculty at CofC), Austin Morrison, Will Vesely, Kimberly Sitta, Mikala Randich, Sarah Nell Blackwell, Michael Shahin, and numerous other College of Charleston undergraduate students in Geology and graduate students in Environmental Studies who assisted with the field work. Also, Dr. Andrew Tweel (SCDNR) helped generate the GIS watershed delineations, and Anne Blair (NOAA) provided guidance and feedback on the SWARM modeling.

We also thank the anonymous reviewers for comments that significantly improved the manuscript. These are contribution Nos. 768 from the South Carolina Department of Natural Resources Marine Resources Research Institute and 1853 from the Belle W. Baruch Institute for Marine and Coastal Sciences, University of South Carolina.

LITERATURE CITED

Alber, M., M. Frischer, D.I. Greenfield, J.D. Hagy, J.E. Sheldon, E. Smith, R.F. Van Dolah, and C.B. Woodson, 2015. An approach to develop nutrient criteria for Georgia and South Carolina estuaries. A task force report to the EPA, GA EPD, and SCDHEC. 59 pp.

Barwis, J. H., 1977. Sedimentology of some South Carolina tidal-creek point bars, and a comparison with their fluvial counterparts. *Fluvial Sedimentology—Memoir 5*: 129–60.

Blair, A., S. Lovelace, D. Sanger, A.F. Holland, L. Vandiver, and S. White, 2014a. Exploring impacts of development and climate change on stormwater runoff. *Hydrological Processes* 28: 2844–54.

Blair, A., D. Sanger, D. White, A.F. Holland, L. Vandiver, C. Bowker, and S. White, 2014b. Quantifying and simulating stormwater runoff in watersheds. *Hydrological Processes*, 28: 559–69.

Blanton, J.O., F. Andrade, and M.A. Ferreira. 2006. The relationship of hydrodynamics to morphology in tidal creek and salt marsh systems of South Carolina and Georgia. In G.S. Kleppel, M. Richard DeVoe and Mac V. Rawson (eds.), *Changing Land Use Patterns in the Coastal Zone: Managing Environmental Quality in Rapidly Developing Regions* (Springer: New York, NY).

Blanton, J.O., G. Lin, and S.A. Elston, 2002. Tidal current asymmetry in shallow estuaries and tidal creeks. *Continental Shelf Research*, 22: 1731–43.

Boon, J.D, 1975. Tidal discharge asymmetry in a salt marsh drainage system1,2. *Limnology and Oceanography* 20: 71–80.

Chow, A., J. Dai, W. Conner, D. Hitchcock, and J.-J. Wang, 2013. Dissolved organic matter and nutrient dynamics of a coastal freshwater forested wetland in Winyah Bay, South Carolina. *Biogeochemistry* 112: 571–87.

Dronkers, J., 1986. Tidal asymmetry and estuarine morphology. *Netherlands Journal of Sea Research* 20: 117–31.

Friedrichs, C.T., and D.G. Aubrey, 1988. Non-linear tidal distortion in shallow well-mixed estuaries: a Synthesis. *Estuarine, Coastal and Shelf Science* 27: 521–45.

Huang, H., C. Chen, J.O. Blanton, and F.A. Andrade, 2008. A numerical study of tidal asymmetry in Okatee Creek, South Carolina. *Estuarine, Coastal and Shelf Science* 78: 190–202.

Leopold, L. B., J. N. Collins, and L. M. Collins, 1993. Hydrology of some tidal channels in estuarine marshland near San Francisco. *CATENA* 20: 469–93.

NOAA National Estuarine Research Reserve System (NERRS). System-wide Monitoring Program, 2016. Data accessed from the NOAA NERRS Centralized Data Management Office website: http://www.nerrsdata.org/; accessed 7 December 2016.

NOS, 2008. Tides and water levels: frequency of tides – the lunar day. National Ocean Service, Accessed 23 October 2015. http://oceanservice.noaa.gov/education/kits/tides/tides05_lunarday.html.

Pethick, J. S., 1980. Velocity surges and asymmetry in tidal channels. *Estuarine and Coastal Marine Science* 11: 331–45.

Reed, M. L., G. R. DiTullio, S. E. Kacenas, and D. I. Greenfield., 2015. Effects of nitrogen and dissolved organic carbon on microplankton abundances in four coastal South Carolina (USA) systems. *Aquatic Microbial Ecology* 76: 1–14.

Reed, M. L., J. L. Pinckney, C. J. Keppler, L. M. Brock, S. B. Hogan, and D. I. Greenfield, 2016. The influence of nitrogen and phosphorus on phytoplankton growth and assemblage composition in four coastal, southeastern USA systems. *Estuarine, Coastal and Shelf Science* 177: 71–82.

RStudio Team, 2016. *RStudio: Integrated Development for R*. Boston, MA: RStudio, Inc.

Sanger, D., A. Blair, G. DiDonato, T. Washburn, S. Jones, G. Riekerk, E. Wirth, J. Stewart, D. White, L. Vandiver, and

A. F. Holland, 2015. Impacts of coastal development on the ecology of tidal creek ecosystems of the US Southeast including consequences to humans. *Estuaries and Coasts* 38: 49–66.

Speer, P. E., D. G. Aubrey, and C. T. Friedrichs, 1991. Nonlinear hydrodynamics of shallow tidal inlet/bay systems. *Tidal Hydrodynamics*: 321–39.

Teledyne RD Instruments, 2007. *WinRiverII Quick Start Guide*. Poway, California: Teledyne RD Instruments. 1–48.

Teledyne RD Instruments, 2011. *Acoustic Doppler Current Profiler Principles of Operation: A Practical Primer*. Poway, California: Teledyne RD Instruments. 1–62.

Teledyne RD Instruments, 2014. *Workhorse Sentinel, Monitor & Mariner Operation Manual*. Poway, California: Teledyne RD Instruments. 1–226.

Van Dolah, R. F., P. C. Jutte, G. H. M. Riekerk, M. V. Levisen, L. E. Zimmerman, J. D. Jones, A. J. Lewitus, D. E. Chestnut, W. McDermott, D. Bearden, G. I. Scott, and M. H. Fulton, 2002. *The Condition of South Carolina's Estuarine and Coastal Habitats During 1999–2000: Technical Report No. 90*. Charleston, SC: South Carolina Marine Resources Division.

Appendix A:
Sample Velocity Measurements and Hydraulic Geometry Curves

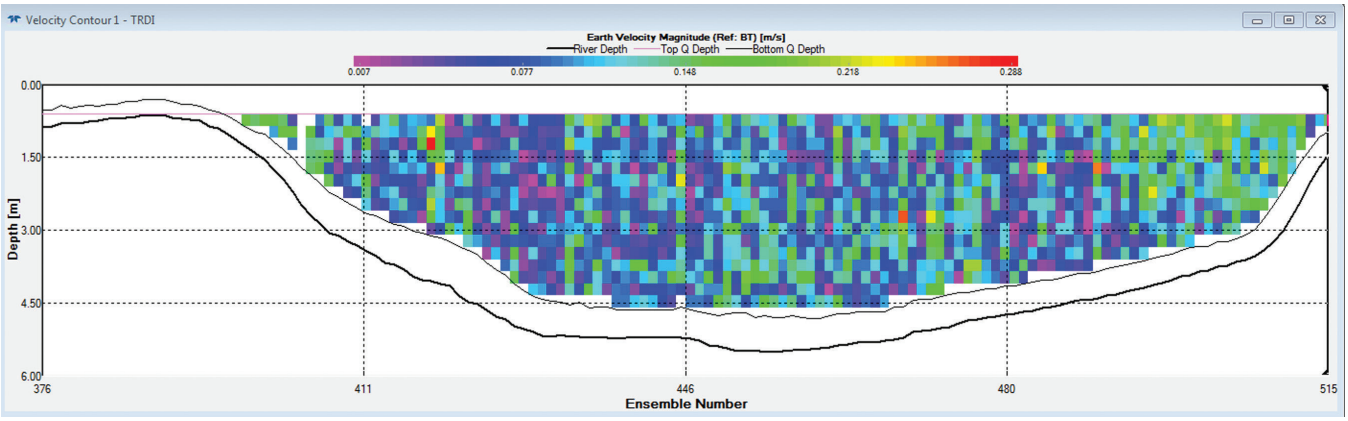

Figure A-1. Velocity magnitude profile for transect 002 at Big Bay Creek on June 14, 2016. Average transect velocity was -0.08 m/s, and total discharge was -29.5 m^3/s.

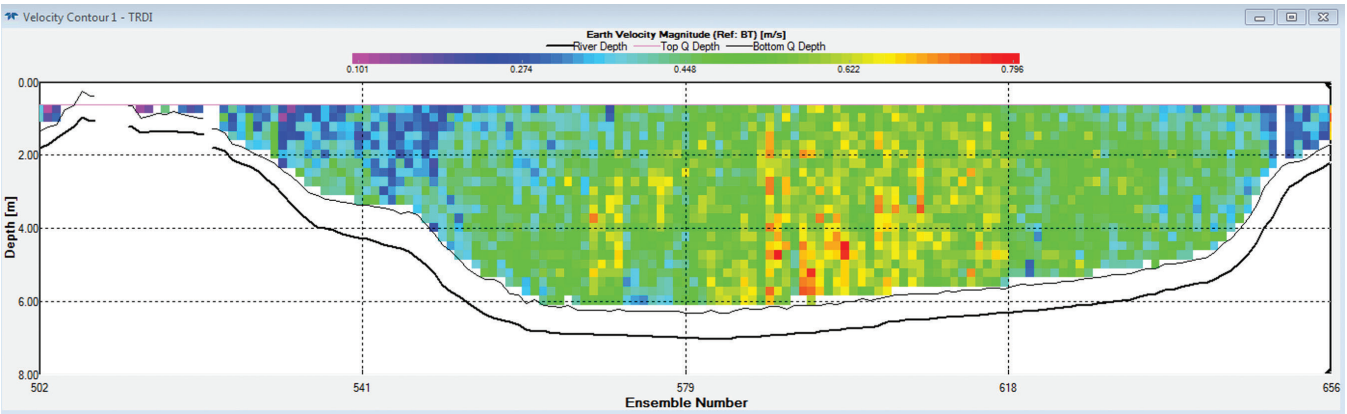

Figure A-2. Velocity magnitude profile for transect 042 at Big Bay Creek on June 14, 2016. Average transect velocity was -0.47 m/s, and total discharge was -228 m^3/s.

Table A-1. Summary of Measurements Collected by ADCP

Date	Transect	Time from HWS (hours)	Max Depth (m)	Discharge (m^3/s)	Transect Width (m)	Cross-Sectional Area (m^2)	Mean Water Velocity (m/s)
6/14/2016	000	-7:34:00	5.60	23.1	88.5	376.3	0.06
6/14/2016	001	-7:31:00	5.60	25.8	85.8	360.2	0.07
6/14/2016	002	-7:29:00	5.60	14.8	89.0	372.5	0.04
6/14/2016	003	-7:27:00	5.60	18.1	88.6	377.6	0.05
6/14/2016	000	-6:59:00	5.58	-22	84.7	361.3	-0.06
6/14/2016	001	-6:57:00	5.58	-28.4	86.5	380.6	-0.07
6/14/2016	002	-6:55:00	5.58	-29.5	88.7	368.6	-0.08
6/14/2016	003	-6:53:00	5.58	-33.4	91.8	387.5	-0.09
6/14/2016	004	-6:24:00	5.73	-82	94.5	383.7	-0.21
6/14/2016	005	-6:21:00	5.73	-90.9	93.2	397.8	-0.23
6/14/2016	006	-6:19:00	5.73	-76.9	88.0	371.4	-0.21
6/14/2016	007	-6:17:00	5.73	-85.4	87.9	390.2	-0.22
6/14/2016	008	-5:52:00	5.89	-95.1	85.6	378.3	-0.25
6/14/2016	009	-5:50:00	5.89	-94.5	91.5	404.0	-0.23
6/14/2016	010	-5:48:00	5.89	-97.2	89.7	382.7	-0.25
6/14/2016	011	-5:45:00	5.89	-100	88.9	407.3	-0.25
6/14/2016	012	-5:14:00	6.05	-117	95.1	426.9	-0.27
6/14/2016	013	-5:12:00	6.05	-117	90.4	397.3	-0.29
6/14/2016	014	-5:10:00	6.05	-119	94.7	425.2	-0.28
6/14/2016	015	-5:07:00	6.05	-123	90.5	399.8	-0.31
6/14/2016	016	-4:39:00	6.31	-154	91.5	425.1	-0.36
6/14/2016	017	-4:36:00	6.31	-159	90.9	432.3	-0.37
6/14/2016	018	-4:34:00	6.31	-158	89.3	420.3	-0.38
6/14/2016	019	-4:31:00	6.31	-159	87.8	431.4	-0.37
6/14/2016	020	-4:09:00	6.40	-193	91.4	427.7	-0.45
6/14/2016	021	-4:06:00	6.40	-192	92.2	441.0	-0.44
6/14/2016	022	-4:04:00	6.40	-199	84.9	443.1	-0.45
6/14/2016	023	-4:01:00	6.40	-199	92.9	451.4	-0.44
6/14/2016	024	-3:40:00	6.58	-221	90.5	442.4	-0.50
6/14/2016	025	-3:38:00	6.58	-226	95.0	479.6	-0.47
6/14/2016	026	-3:35:00	6.58	-222	88.7	437.2	-0.51
6/14/2016	027	-3:33:00	6.58	-219	84.8	466.0	-0.47
6/14/2016	028	-3:09:00	6.75	-240	87.7	459.5	-0.52
6/14/2016	029	-3:07:00	6.75	-236	87.1	466.6	-0.51
6/14/2016	030	-3:04:00	6.75	-248	94.4	467.4	-0.53
6/14/2016	031	-3:02:00	6.75	-250	88.8	466.8	-0.54
6/14/2016	032	-2:32:00	6.86	-245	85.3	471.2	-0.52
6/14/2016	033	-2:30:00	6.86	-249	88.7	483.4	-0.52
6/14/2016	034	-2:27:00	6.86	-253	88.8	476.8	-0.53

Date	Transect	Time from HWS (hours)	Max Depth (m)	Discharge (m^3/s)	Transect Width (m)	Cross-Sectional Area (m^2)	Mean Water Velocity (m/s)
6/14/2016	035	-2:25:00	6.86	-259	88.5	486.3	-0.53
6/14/2016	036	-1:59:00	7.00	-257	84.1	471.8	-0.55
6/14/2016	037	-1:56:00	7.00	-254	86.7	498.6	-0.51
6/14/2016	038	-1:54:00	7.00	-259	86.6	483.2	-0.54
6/14/2016	039	-1:52:00	7.00	-260	86.1	488.7	-0.53
6/14/2016	040	-1:27:00	7.26	-240	83.0	483.6	-0.50
6/14/2016	042	-1:22:00	7.26	-228	87.8	483.1	-0.47
6/14/2016	043	-1:19:00	7.26	-232	88.1	495.1	-0.47
6/14/2016	044	-1:17:00	7.26	-223	90.9	487.3	-0.46
6/14/2016	045	-0:52:00	7.06	-166	86.7	490.7	-0.34
6/14/2016	046	-0:50:00	7.06	-160	86.3	491.4	-0.33
6/14/2016	047	-0:47:00	7.06	-155	89.9	495.5	-0.31
6/14/2016	048	-0:44:00	7.06	-147	86.8	492.5	-0.30
6/14/2016	049	-0:09:00	7.02	-4.87	95.8	494.2	-0.01
6/14/2016	050	-0:04:00	7.02	21.1	100.2	570.9	0.04
6/14/2016	051	0:01:00	7.02	47.8	107.1	515.4	0.09

Appendix B:
Sample Hydraulic Geometry Curves

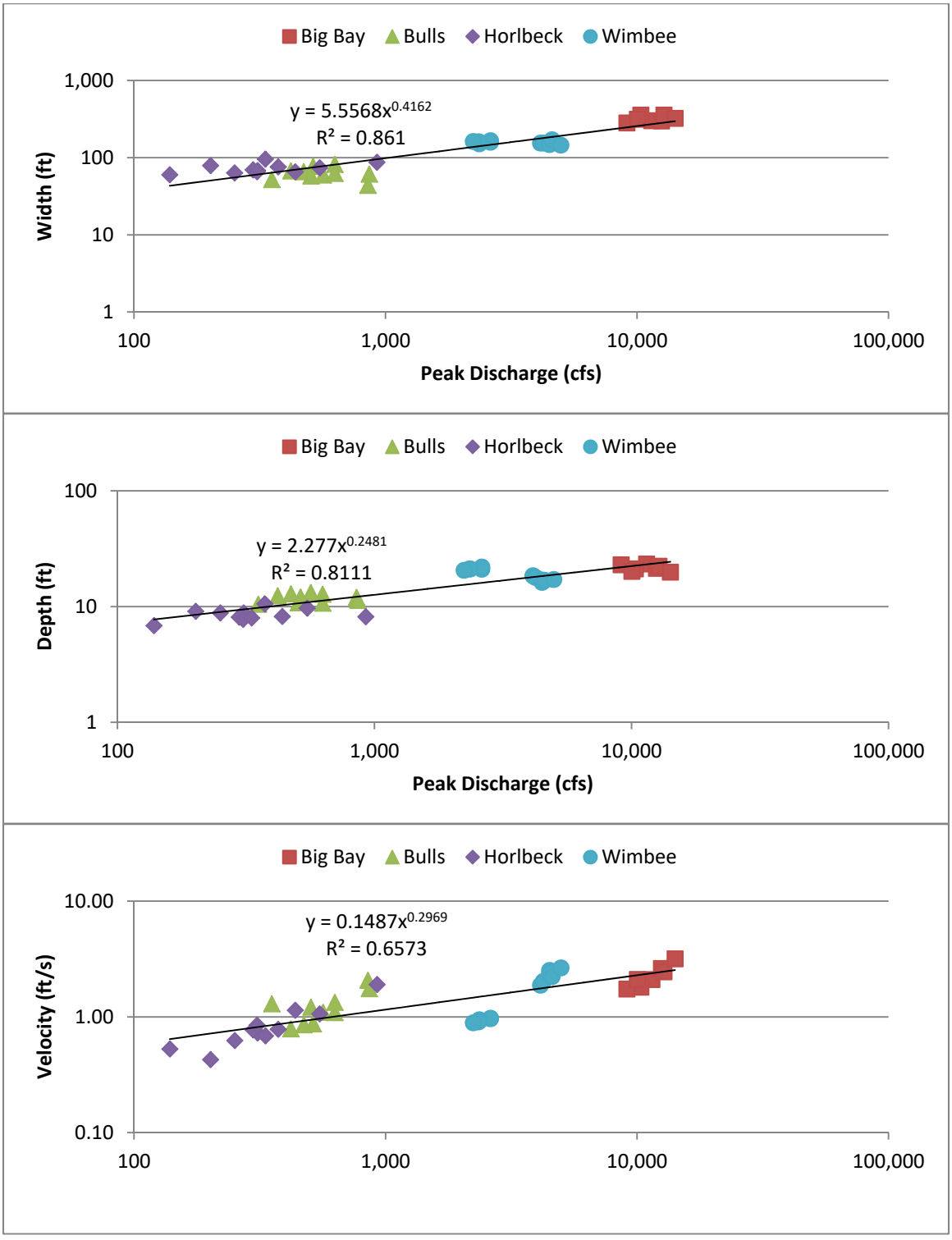

Figure B-1. Hydraulic geometry relationships of velocity, depth, and width to peak discharge (flood and ebb). Original measurements were converted from metric to English units for comparison.

Field Spectroscopy as a Tool for Enhancing Water Quality Monitoring in the ACE Basin, SC

Caitlyn C. Mayer[1] and Khalid A. Ali[2]

AUTHORS: [1,2], Adjunct Professor, Department of Geology and Environmental Geosciences, College of Charleston, Charleston, SC 29424. [2]Assistant Professor, Department of Geology and Environmental Geosciences, College of Charleston, Charleston, SC 29424.

Abstract. The Ashepoo, Combahee, Edisto (ACE) Basin in South Carolina is one of the largest undeveloped estuaries in the Southeastern United States. This system is monitored and protected by several government agencies to ensure its health and preservation. However, as populations in surrounding cities rapidly expand and land is urbanized, the surrounding water systems may decline from an influx of contaminants, leading to hypoxia, fish kills, and eutrophication. Conventional in situ water quality monitoring methods are timely and costly. Satellite remote sensing methods are used globally to monitor water systems and can produce an instantaneous synopsis of color-producing agents (CPAs), including chlorophyll-*a*, suspended matter (TSM), and colored-dissolved organic matter by applying bio-optical models. In this study, field, laboratory, and historical land use land cover (LULC) data were collected during the summers of 2002, 2011, 2015, and 2016. The results indicated higher levels of chlorophyll, ranging from 2.94 to 12.19 µg/L, and TSM values were from 60.4 to 155.2 mg/L between field seasons, with values increasing with time. A model was developed using multivariate, partial least squares regression (PLSR) to identify wavelengths that are more sensitive to chlorophyll-*a* (R^2 = 0.49; RMSE = 1.8 µg/L) and TSM (R^2 = 0.40; RMSE = 12.9 mg/L). The imbrication of absorption and reflectance features characterizing sediments and algal species in ACE Basin waters make it difficult for remote sensors to distinguish variations among in situ concentrations. The results from this study provide a strong foundation for the future of water quality monitoring and for the protection of biodiversity in the ACE basin.

INTRODUCTION

Coastal watersheds are essential components of the hydrologic cycle, as these are the regions where all the water from the surface and the ground converge into a single area and drain into the ocean (USEPA 2012). Since these geographic regions consist of a variety of water sources, they are an essential focus of study for managing and monitoring coastal resources in South Carolina. Coastal watersheds begin with the headwaters of rivers and streams, including adjacent wetlands, and as the water drains toward the coast, it is influenced by a variety of land and water uses (i.e., agricultural and industrial operations and urban development). As these waters reach coastal areas, the rivers empty into estuaries, along with any nutrient-enriched runoff from the different lands it passes through, before discharging into the ocean.

The Southeastern United States is one of the fastest growing populations nationwide, with the state of South Carolina experiencing some of the fastest rates of urbanization (7.24 % per year), which exceed the average U.S population growth rate (Allen and Lu 2003). To accommodate this growth, land is urbanized, which is one of the major causes of coastal wetland and estuarine loss. Urbanization also influences the hydrological and geological dynamics of coastal systems by causing concentrated flows of nutrients and chemical pollutants to flow into estuaries during flood events (storm water runoff), while non-flood events receive diffused discharge into groundwater (Lee et al., 2006). Urbanization changes land from permeable forest or wetlands to impermeable surfaces, such as parking lots, roads, buildings, and rooftops (Leopold, 1968). The increase in impervious areas in a catchment changes the natural hydrogeological regime of a system and results in concentrated areas of rain runoff (Lee et al., 2006). This can lead to the deterioration of water quality, as coastal systems near urban areas interact with nutrient pollution that would normally have been buffered through pervious surfaces (Bannerman et al., 1993).

It is generally recognized that increased levels of nutrient pollution increase eutrophication (nutrient enrichment to waters), which can lead to an abundance of chlorophyll-*a* (Chl-*a*) in the water (from algal blooms) (Anderson et al., 2002). Natural estuarine eutrophication is usually a slow process that stimulates algal growth, resulting in productive ecosystems (Bricker et al., 1999). However, in recent decades, anthropogenic activities have accelerated nutrient input into estuarine systems, and research has shown that more coastal algal blooms have occurred than in past decades (Gilbert et al., 2005). Agriculture is one of these activities, contributing large concentrations of carbon, nitrogen, and phosphorous into estuaries via colored dissolved organic matter (CDOM), especially after it rains. CDOM is the largest source of organic carbon in the aquatic environment, contributing to light absorption and bacterial respiration in estuarine systems. It can transport large concentrations of nutrients to estuaries, which can indirectly promote algal growth (Corbert, 2007). Agriculture, along with urban development, can also cause soil erosion. When eroded soil enters the water system, the concentration of total suspended matter (TSM) increases. TSM are particles in water that cannot pass through a 0.7 µm glass fiber filter, including inorganic sediments and organic particles (phytoplankton). Suspended matter can affect aquatic habitats as they absorb heat from the sun, increase the water temperature, and consequently lower the available concentrations of dissolved oxygen necessary for aquatic life (Etheridge et al., 2015).

To assess the health of coastal watersheds, water quality can be used as a key index to evaluate the stressors posed on the environment. Obtaining water quality measurements using conventional methods is labor intensive, costly, and time consuming, and they lack spatial and temporal resolution, making it difficult to monitor water quality dynamics in real time. In response to increasing terrestrially derived constituents from agriculture and urbanization, coastal watersheds, especially in South Carolina, may potentially be exposed to higher fluxes of sediments and nutrients. Therefore, it is imperative to seek more robust methods of monitoring coastal systems.

Remote sensing methods are used globally to monitor water systems and can produce an instantaneous synopsis of the water quality (McClain, 2009). Remote sensing operates by measuring the quantity and type of electromagnetic radiation (EMR) exiting the water; which is a function of the various color-producing agents (CPAs) present in the water column. The universality of satellite-based remote sensing data has assisted in the efforts to identify CPAs, which are materials in the water that can change water color (reflectance) and affect water quality. The three primary CPAs in coastal watersheds are (1) Chl-*a*, a primary pigment found in all phytoplankton species; (2) TSM, consisting of minerals, sediments, and organic particle such as decomposing phytoplankton and zooplankton; and (3) CDOM from decaying organic matter that can cause yellow color alterations in the water body.

The convoluted interactions of these CPAs have been extensively studied in ocean systems (e.g., Ryan et al., 2016; Yacobi et al., 2011; Gitelson et al., 2008; Schalles, 2006), and as Chl-*a* is prevalent in photosynthetic organisms, estimating these concentrations and understanding the interactions with other CPAs is essential for the remote sensing of water quality (Schalles, 2006). Remote sensing methods measure water quality by correlating co-located satellite-derived or field-derived reflectance with in situ samples of CPAs. Conventional satellite technology uses multispectral sensors to monitor the water quality at moderate to high spatial and temporal resolutions. These sensors can predict the concentrations of Chl-*a* in ocean waters (Klemas, 2011) through the use of global algorithms that relate spectral reflectance features in the blue and green portion of the spectrum to Chl-*a* concentration. However, these algorithms are broadly calibrated (IOCCG, 2000; McClain, 2009) and are limited to waters that are dominated by Chl-*a*, thus resulting in low accuracy model predictions in ACE type waters that possess multiple CPAs.

To model the varying CPAs found in turbid coastal waters, empirical remote sensing algorithms that employ reflectance values in the near-infrared (NIR) regions of the EMR have been found to be successful for modeling Chl-*a*, as a limited amount of absorption by suspended solids and CDOM is observed in these regions of EMR (Doxaran et al., 2002; Robertson et al., 2009; Moses et al., 2012). Empirical models using ratios of bandwidths are found by rationing spectral bands that display reflectance and absorption features due to phytoplankton:

$$\mathbf{(1)}\quad \mathbf{R} = \left(\frac{R_{RS}(\lambda_1)}{R_{RS}(\lambda_2)}\right),$$

where $R_{RS}(\lambda)$ represents a specific band (wavelength) within a sensor dataset. The reflectance (R) value derived from the ratio can then be correlated to known concentrations of in situ CPAs that were collected within the same spatial and temporal constraints as the satellite image (Witter et al., 2009). From this band ratio, the specific wavelengths where Chl-*a* absorption features are observed can be used to calibrate the equation and is represented by

$$\mathbf{(2)}\quad [\textbf{Chl-}a\ ] \propto = \frac{R_{RS}(\lambda_{NIR})}{R_{RS}(\lambda_{Red})},$$

where λ_{NIR} is the Chl-*a* maximum reflectance peak near 700 nm due to decreasing Chl-*a* absorption and increasing absorption by water, and λ_{Red} is the absorption maximum around 670 nm due to increasing Chl-*a* absorption (Vasilikov and Kopelevich, 1982; Gitelson, 1992; Han, 1997; Moses et al., 2012). Spectral features may vary depending upon the

concentration and type of Chl-*a*, as well as the resolution of the satellite sensor. These ratio models have produced accurate estimates of Chl-*a* concentration in coastal watersheds and turbid estuarine environments around the world (Gurlin et al., 2011; Moses et al., 2012). A summary of six published band-ratio algorithms that utilize blue/green and red/near-infrared spectral regions is detailed in Table 1. The development of these models was examined briefly as an implication to the applicability of the PLSR method when adapted to the in situ reflectance dataset.

Hyperspectral sensors collect reflectance signals across the EMR using many narrow bands (with high spectral resolution), which enhances the retrieval of Chl-*a* signals in optically complex waters. With consecutive narrow bands, hyperspectral sensors are capable of quantifying reflectance values regardless of any shift in crucial spectral features due to the presence of multiple CPAs (Ryan et al., 2016). These sensors can be field based or secured on spaceborne and airborne platforms, resulting in high spectral and spatial resolution. In situ hyperspectral measurements have previously been used to calibrate algorithms for smaller water bodies, such as estuarine sites, specifically studies in the Altamaha and St. Mary's River, Georgia and Long Bay, South Carolina, which resulted in the development of successful regression models ($R^2 = 0.88$, $R^2 = 0.72$, $R^2 = 0.80$) that showed correlations with Chl-*a* and successful applications for estimating CPAs in estuarine surface waters (Bhatti et al., 2010; Ryan et al., 2016).

MULTIVARIATE APPROACHES:

As advances in technology lead to the availability and accessibility of hyperspectral (continuous bandwidths) remote sensors, approaches that can address the multidimensionality and collinearity of large, higher resolution satellite datasets must be applied. Factor analysis approaches, which consider what factors influence the data the most, involve a varimax-rotated method of principal component analysis (VPCA) and regression model methods, such as PLSR. These methods can reduce the dimensionality of large datasets and allow the end user to identify potentially correlated variables.

VPCA identifies the least number of linear combinations of the available variables that summarize the data without compromising its variability (Maitra and Yan, 2008). This variance is exemplified by several primary orthogonal components with scores that help define the specific

Table 1. Band ratio algorithms used to estimate chlorophyll-*a* concentrations (C) from remote sensing reflectance (R_{RS}) in the ACE Basin. Validation parameters were determined using the r-squared value (R^2) and root-mean-square error (RMSE) in micrograms per liter (µg/L) of the predicted versus actual Chl-*a* concentrations.

Algorithm	Algorithm Equation	Reference	Validation Parameters (µg/L)
Blue Green Models			
Morel-1	R = log(R443/R555) C = 10^(0.2492-1.768R)	O'Reilly *et al.* (1998)	R^2 = 0.0026 RMSE = 9.92
Morel-3	R = log(R490/R555) C = 10^(0.20766-1.82878R+0.75885R^2 0.73979R^3)	O'Reilly *et al.* (1998)	R^2 = 0.0096 RMSE = 10.04
OC4v4	R = log(max[R443,R450,R510]/R555) C = 10^(0.366-3.067R+1.930R^2+0.649R^3-1.532R^4)	O'Reilly *et al.* (1998)	R^2 = 0.0021 RMSE = 2.83
*Adapted Morel-1 Model	R = log(R443/R570) C = 10^(0.2492-1.768R)		R^2 = 0.0082 RMSE = 3.71
*Adapted Morel-3 Model	R = log(R443/R560) C = 10^(0.20766-1.82878R+0.75885R^2-0.73979R^3)		R^2 = 0.012 RMSE = 3.74
*Adapted OC4v4 Model	R = log(max[R440,R450,R510]/R580) C = 10^(0.0162-9.372R-25.55R^2+0.649R^3-1.532R^4)		R^2 = 0.148 RMSE = 2.22
Red-Near Infrared Models			
2-Band MODIS	R = R^{-1}(667)*R(748) C = 0.7843-0.1573R+0.0319R^2)	Yacobi et al. (2011)	R^2 = 0.0028 RMSE = 6.36
3-Band MERIS	R = R^{-1}(665)-R-1(708)*R(753) C = -0.1305-0.011R+0.0088R^2	Yacobi et al. (2011)	R^2 = 0.0028 RMSE = 6.36
Red-NIR and Blue Green Models			
Hladik	R = (aveR650 + R700) - R675/(aveR440 + R550) C = 3.72 + 34.92R + 67.63R^2	Hladik (2004)	R^2 = 0.096 RMSE = 6.70
* Adapted Hladik Model	R = (aveR650 + R700) - R675/(aveR440 + R550) C = 5.811 + 20.39R - 49.81R^2		R^2 = 0.0991 RMSE = 2.33

wavelengths responsible for characterizing water quality parameters (Fu et al., 2013). VPCA was selected as an applicable multivariate statistical approach for its ability to decrease the dimensionality of the data, eliminate collinearity among the data, and transform large datasets into smaller datasets of unrelated indices. This approach has been applied successfully in previous ocean color modeling research studies, where strong correlation models for Chl-*a* prediction were produced (Sathyendranath et al., 1994; Gao et al., 2000; Gross-Colzy et al., 2007; Ortiz et al., 2013; Ali et al., 2013; Ryan et al., 2016).

PLSR was developed in the 1980s by Herman Wold and has since gained acceptance in its use for spectral analysis. Like VPCA, this approach extracts the least number of eigenvectors from the explanatory variables (Ortiz et al., 2013) but expands the statistics further by incorporating a response variable during the extraction and performing a least-squares regression on the components instead of the original data, which provides correlations specific to the observed data.

This technique is more biased than the VPCA approach because it is suited to the observational data, and because of that, it has been employed in several successful remote sensing studies (Ryan et al., 2016; Ali et al., 2013; Robertson et al., 2009). Modeling using PLSR assumes that observations of reflectance are directed by factors that are linear combinations of explanatory variables (Roberston et al., 2009). The vector loadings (P) of the spectra are approximated by a matrix consisting of explanatory variables (X) and the response variables (Y) (i.e., CPAs). The result is then normalized over a length of 1, and the reflectance data, X, and first loading vector, P, are used to estimate the first column of the regression factor matrix, T (Eq. 3). The process of multiple linear regressions determines the vector loadings of the CPAs, Q, and computes their residuals, F (Eq. 4). Using these residuals, these calculations are replicated for the second regression factor and so on, with F and E representing the error matrices that are accepted as independent. The goal of PLSR modeling is to decrease the normalization of F while maximizing the covariance between X and Y. The general model of multivariate PLSR is described as follows:

$$X = TP^T + E \quad (3)$$

$$Y = UQ^T + F \quad (4)$$

PLSR was chosen for this study because of its ability to recognize significant relationships between X and Y variables. The Ashepoo Combahee Edisto (ACE) Basin is one of the largest undeveloped estuaries in the nation, with a variety of optical properties, draining approximately 8,000 km^2 into the Atlantic Ocean (Nobel et al., 2003) and is part of the National Estuarine Research Reserve System (NERRS; a partnership between NOAA and coastal states, to protect and monitor 28 different estuaries). The models developed from this study were used to retrieve water quality data at higher spatial and temporal resolution. This will enhance monitoring methods in South Carolina and may be used by water managers and coastal resource managers to respond to environmental concerns more efficiently.

Prior to this study, no remote sensing-based models of the biogeochemical processes for the ACE Basin NERRs had been developed. To accurately characterize the local biogeochemical, spectral, and temporal dynamics of this coastal environment, regionally tiered algorithms were developed using empirical and multivariate approaches with in situ water samples and multispectral and hyperspectral reflectance data. The goal of this study was to develop models that could accurately assess the water quality of a coastal watershed by determining the visible infrared (VIR) signatures of select CPAs and to establish a historical comparison of the relationships between urbanization and water quality over time.

STUDY AREA

St. Helena Sound estuary, along the coast of South Carolina between Edisto Island and Hunting Island (Figure 1), is a

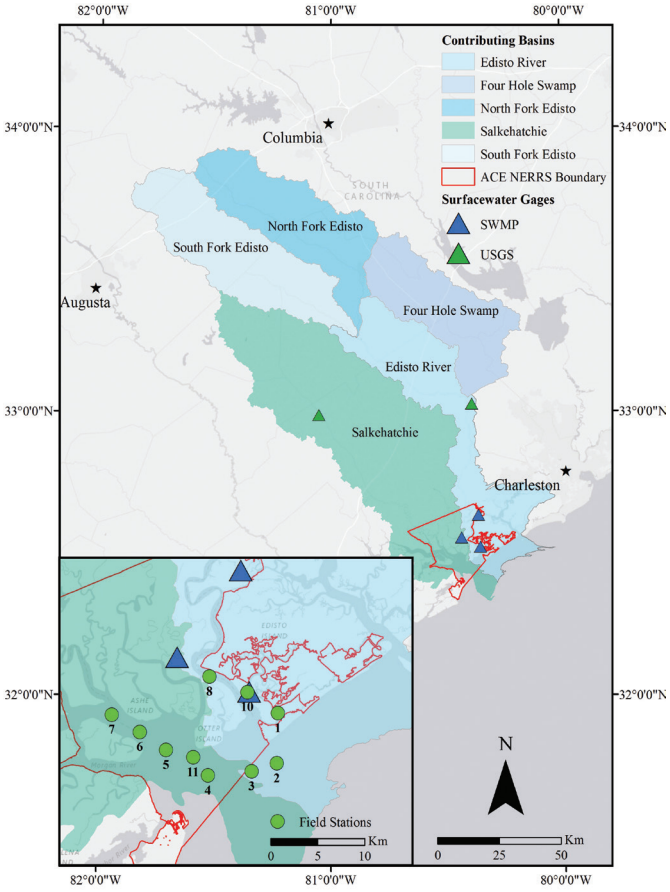

Figure 1. Map of ACE Basin. Salkehatchie (left) and Edisto (right) 6-digit HUCs overlaid with USGS gauges (dark green triangles) and SWMP gauges (dark blue triangles). Inset shows field stations in St. Helena Sound (neon green circles), Coastal South Carolina U.S.A.

drowned river valley that likely formed during the Pleistocene and was flooded during a high sea level stage (Cooke, 1936; Bearden et al., 1985). Historical weather data indicate that the ACE Basin has a subtropical climate, with average water temperatures of 20 ˚C and average annual precipitation of 2.8 cm from June 2015 to September 2016 (NOAA, 2015b). This coastal portion of the ACE Basin is characterized by marsh islands, barrier islands, and tidal creeks (Mathews et al., 1980; Bearden et al., 1985) with elevations ranging from 0.5 to 12 m and inland sub-basins ranging from 12 to 214 m. All the surface water from the ACE Basin discharges into the Atlantic Ocean via St. Helena Sound (SCWRC 1972), and this area has an extensive set of LULC data as well as gauging stations for both water quality and quantity, making this estuary an ideal study area for monitoring the water quality in the ACE Basin, as CPA concentrations may have more variability.

The barrier islands that surround St. Helena Sound are composed of beach ridges that formed during the Holocene (Stapor, 1984), and terrestrial and back-barrier sediments including kaolin clays are the primary source of riverine deposits (McIntyre et al., 1991; Soller and Mills, 1991).

An increase in population will inevitably lead to urbanization around the ACE Basin and may result in human-induced stress on the ecosystem. Results from state monitoring programs, specifically the South Carolina Estuarine and Coastal Assessment Program (SCECAP), have already indicated high levels of total nitrogen (34.6–98.5 µM), total phosphorous (2.3–12.49 µM) and Chl-*a* (4.1–49.85 µg/L) when compared to other SC estuaries (Bricker et al., 1999; SCDHEC, 1998). SCECAP randomly samples 30 different sites per year along the SC coast, and resulting water quality data are defined as "good" (<75th % of historical SC records), "fair" (>=75th – <90th %), and "poor" (>= 90th %). The samples from the ACE Basin revealed that 83% of open water habitats and 42% of tidal creek habitats were classified as good, compared to 89 % and 70% statewide (Van Dolah et al., 2004). Due to the ACE Basin's relatively higher levels of nitrogen, phosphorous, and Chl-*a*, in comparison with levels at another SC NERR in the North Inlet (SC) during 1999-2000, the estuary was classified as moderately eutrophic (Bricker et al., 1999).

In a recent study in the ACE Basin, measured Chl-*a* served as a proxy for phytoplankton and indicated the presence of over a hundred phytoplankton species. The majority of these phytoplankton were diatoms, ciliates, and dinoflagellates (including three species associated with harmful algal blooms, *Akashiwo sanguinea*, *Gymnodinium sp*., and *Heterocapsa rotunda*), although no blooms were associated with the samples collected (Keppler et al., 2014).

Harmful algal blooms (HABs) are broadly defined as potentially toxic algal species and high-biomass producers that can cause low oxygen (hypoxia) conditions in the environment and indiscriminant mortalities of aquatic life as they reach dense concentrations, whether or not toxins are present (Heisler et al., 2008). No toxic blooms have been recorded, but low dissolved oxygen (DO; 4.4 mg/L) levels in the ACE Basin have been measured, as well as in similarly sized southeastern estuaries (Keppler et al., 2014).

METHODS

FIELD TECHNIQUES:

Field campaigns were conducted in summer 2015 and 2016 during the months of June, July, and August, as Chl-*a* concentrations tend to be higher in summer months. Field days were scheduled to correlate with the day closest to the Landsat 8 TM flyover, and no field day occurred more than 3 days from the time of satellite flyover so that water conditions at time of collection were similar to water conditions at the time of satellite flyover. Field stations were evenly distributed

Table 2. Field station descriptions. Site coordinates, mean depth, distance to nearest land, and land cover type listed by associated water body type.

Station	Description	Water Body Type	Latitude (dd)	Longitude (dd)	Mean Depth (m)	Distance to Nearest Land (km)	Land Cover Type
2	Atlantic Ocean	O	32.45697	-80.32369	5.75	2.5	D
3	Atlantic Ocean	O	32.44956	-80.35464	4.97	3.6	D
4	St. Helena Sound	E	32.44611	-80.40414	9.81	3.3	H
5	St. Helena Sound	E	32.46989	-80.45122	7.77	3.4	H
6	St. Helena Sound	E	32.48672	-80.48078	8.88	1.2	H
11	St. Helena Sound	E	32.46289	-80.42064	5.64	1.5	H
7	Ashepoo/Combahee River	R	32.50286	-80.5125	8.84	3.6	EF
8	Edisto River	R	32.53761	-80.40169	6.94	0.7	EF
10	Edisto River	R	32.523	-80.35894	1.95	1.0	EF
1	Big Bay Creek	R	32.50339	-80.32475	4.77	0.2	DF

through varying environments in the basin (riverine, estuarine, and offshore) and land classes to capture a range of water quality variability. With a total of 10 stations (Table 2), 4 were riverine (R), 4 were estuarine (E), and 2 were offshore (O); all were near developed (D), herbaceous (H), evergreen forest (EF), and deciduous forest land types (DF) (Table 2). GPS waypoints were also taken at each field station using a Garmin GPSMAP 78c with an accuracy of 3 m to confirm accurate revisits on each cruise and to further aid in navigating around sandbars, based on previous track lines. Each environment was representative of different interactions between hydrologic, geologic, and biologic cycles.

At each site, subsurface water samples were collected at a depth of 0.5 m and preserved on ice during transport for laboratory processing. The water samples for CDOM were collected in 50 mL glass amber bottles to reduce exposure to sunlight and stored on ice. The samples were transported on ice at the completion of the field day and immediately stored in a 4˚C refrigerator at the aquatic remote sensing laboratory at the College of Charleston until further analysis. Using the following methods outlined in Arar and Collins (1997), water samples for Chl-*a* analysis were filtered under minimal light exposure using handheld pumps, filtering 500 mL of water through 0.7 µm ashed GF/F™. The filters were then folded inward two times and inserted into a 15 mL plastic screw cap centrifuge tube, wrapped in aluminum foil to prevent further light penetration, and transferred to a -20˚C freezer until further analysis.

The same method of filtering was used for TSM, using preweighed ashed filters for the preparation of gravimetric analysis. Once filtration was complete, the TSM filters were placed in a sealed plastic container wrapped in aluminum foil and stored in a dark environment. The field water quality parameters of pH, salinity, temperature, turbidity, total dissolved solids, and fluorescence were measured in situ using a submersible multiparameter sonde (YSI 6600V2). At each station, the YSI was deployed from the research vessel and lowered to approximately 1 meter below the surface before measurements were recorded.

The spectral radiance of the water was measured from above the water surface, and downwelling irradiance was measured from a ground platform aboard the research vessel at each station using a GER1500 spectroradiometer. This sensor can measure wavelengths in the 350–1050 nm portion of the spectrum and has a resolution of 1 nm. At each station, four measurements were captured: (1) 45˚ down from the horizon of the water (TAR 45), (2) 90˚ from the horizon into the water (TAR 90), (3) 45˚ from the zenith into the sky (TAR Sky), and (4) zenith into the sky using a cosine diffuser for solar irradiance (Mobley, 1999). The sensor was programmed to take the average of three spectral readings to reduce noise, and multiple spectral readings were taken at each site to account for differences in the target and to decrease potential error in the data. A white reference spectralon was used to calibrate the sensor at each site prior to taking target measurements. This method is described by Duffie and Beckman (2013) and has been successfully applied in similar remote sensing studies (Rodriguez-Guzman and Gilbes-Santaella, 2009; Ali et al., 2013). Remote sensing reflectance (R_{RS}) was calculated using Eq. 5:

$$(5)\quad R_{RS} = \frac{L_t - fL_s}{E_d},$$

where $L_t(\lambda)$ is the radiance measured 45˚ from the horizon to the water; f is the Fresnal number, which is the percent of radiation reflected back into the atmosphere; $L_s(\lambda)$ is the radiance from the sky; and E_d is the solar irradiance measured at the surface (f = 0.028 at a 45˚ angle into the water). Remote sensing reflectance, measured in units of steradians (sr^{-1}) from radiometric measurements, was used during model development. The R_{RS} spectra from each station were averaged to a 10 nm spectral resolution to enhance the signal-to-noise ratio and trimmed to reflectance data between 400 nm and 800 nm, as spectral features of observed CPAs are most prominent in this range, and absorption by water is observed in lower wavelengths.

LABORATORY ANALYSIS

The Chl-*a* concentrations were measured following the US EPA 445 acetone extraction protocol outlined in Arar and Collins (1997). Once ready to process, the samples were removed from the freezer and thawed until they reached room temperature, and 10 mL of 90% buffered acetone solution was added to the centrifuge tube to degrade the filter. The filter in each sample was macerated to disintegrate the Chl-*a* samples from the GFF. Samples were then placed in a 4C refrigerator for 24 hours to complete the extraction process. Subsequently, the samples were removed from the refrigerator and spun in a centrifuge at 4,000 RPM for 10 minutes at 10C. This controlled temperature during centrifugation allows the samples to undergo a slower warming process while the filters are separated from the supernatant. The Chl-*a* concentration was measured by the fluorescence value of each sample, using the Turner Designs Trilogy Fluorometer fitted with a chlorophyll optical module (485 nm excitation and emission filter 665 nm).

Gravimetric analysis was used to measure the concentrations of inorganic and organic material in the water at each sampling location. Following the EPA protocol outline in Arar and Collins (1997), ashed filters were weighed before the samples underwent gravimetric analysis. After 500 mL of water from each site was filtered, the filters were dried at 60C for 12 hours in an Isotemp oven. The dried filters were then removed from the oven and weighed once they reached room temperature to determine the mass of TSM

(TSM = dry filter weight – pre-filter weight). After the TSM concentrations were determined, the relative reflectance of the remaining particles on the filter samples was measured at 1 nm resolution using a portable ASD spectroradiometer and R-software. Once relative reflectance was measured, the filters were combusted in an Isotemp Muffle Furnace at 550˚ C for 4 hours to remove organics and weighed again to measure the organic carbon content lost on ignition (LOI). The relative reflectance of the combusted filters was measured a second time to characterize the inorganic particles. These signatures were then utilized during data processing, analyzing, and developing models.

Organic materials that have dissolved into the water system strongly contribute to the water's ability to absorb or reflect and are therefore a main focus in many ocean color optics studies (Babin et al., 2003; Miller et al., 2002). The water samples stored in the 50 mL amber bottles were prepared using the methods proposed by Mitchell et al. (1998). Each sample was filtered through a nylon filter with a 0.2 µm pore size to remove any suspended particles. The absorption spectra of the CDOM samples were then measured using an Evolution 220 spectrophotometer fitted with a 100 mm long quartz cell to provide an appropriate path length for light absorption. The concentration of CDOM is a function of the slope of absorption. Higher slopes in the UV-blue portion of the spectrum indicate higher concentrations and vice versa. The spectral slope was calculated from 400-450 nm and graphed by station to identify stations with greater concentrations of CDOM.

PARTIAL LEAST SQUARES REGRESSION MODEL DEVELOPMENT:

Multivariate data analysis and feature extraction methods were applied to in situ hyperspectral data as a means to identify the CPAs in the water. Statistical analyses of the hyperspectral data included partial least square regression (PLSR), multivariable regressions, and principal component analysis (PCA) using Minitab and ExcelStat. These methods have numerous advantages over traditional band ratios, as they can be calibrated using the full available spectrum, rather than specific spectral ranges.

Hyperspectral datasets can identify important absorption features that may be characteristic of various CPAs, including Chl-*a*, which can be undetectable by sensors with moderate resolution (Cole et al., 2014). Due to the amplified spectral resolution, these datasets contain a vast quantity of repetitive information that increase the multidimensionality of the data, which consequently needs a method of its own to decrease the dimensionality between variables in the data (Gomez-Chova et al., 2003). Prior to statistical analysis, in situ GER data was standardized to relative reflectance values and normalized to establish proper modeling across varying spectral characteristics, and the radiometric resolution was decreased from 1 nm to 10 nm to reduce noise.

Recall that VPCA is a statistical method that forms new variables that are linear transformations of the original variables (Nwaodua et al., 2014). The new variables produced after reducing the dimensionality of the initial dataset are uncorrelated and exemplify a large percentage of the information from the original variables. VPCA was applied to first-derivative in situ GER data using XLSTAT Statistical Software to decrease the dimensionality of the data and to identify the relevant band characteristic of each component. The relative reflectance values between 400 and 800 nm were evaluated at a 10nm resolution to produce principal component scores in each band. These scores were compared with spectrums of known constituents in southeastern and ACE Basin waters.

PLSR is comparable to PCA in that reflectance spectra are influenced by components of linear combinations for observed explanatory variables (spectral bands), but PLSR surpasses PCA as it can correlate components to response variables (CPAs). PLSR was applied to relative reflectance of in situ GER data and in situ Chl-*a*, TSM, TSS, and CDOM concentrations to develop a regression model with an optimal number of factors to be useful for predicting CPAs. The "leave one out" cross-validation method described in Haaland and Thomas (1988) was used to select the optimal number of factors without over-fitting the concentration data using XLSTAT Statistical Software and Minitab 17. This method was chosen for this study as it considers the complexity of the datasets and contributes a more robust predictive model calibrated to the estuarine waters of the ACE Basin.

RESULTS AND DISCUSSION

COLOR-PRODUCING AGENTS

ACE Basin waters are characterized by multiple nonlinearly related optically active constituents (Figure 2). Minor to no correlations between Chl-*a* and TSM ($R^2 = 0.19$) in Figure 2a and Chl-*a* and CDOM ($R^2 = 0.06$) in Figure 2b indicate that the CPAs are independent of one another. The measurements of CPAs were relatively high when compared to turbid waters in similar coastal watersheds (Schalles, 2006; Keppler et al., 2015). The TSM values ranged between 60.4 and 155.2 mg/L, with an average concentration of 87.7 mg/L and a SD of 15.6 mg/L. The greatest average TSM concentrations were measured at stations 1 and 8, which had the highest TSS concentrations and were closest to land. The lowest concentrations were measured at stations 5 (60.8 mg/L) and 7 (60.4 mg/L) (Figure 3). However, these stations were near major sandbars within the Sound, so the rates of flow may have been constrained, causing lower concentrations of suspended matter (Milligan et al., 2001). In

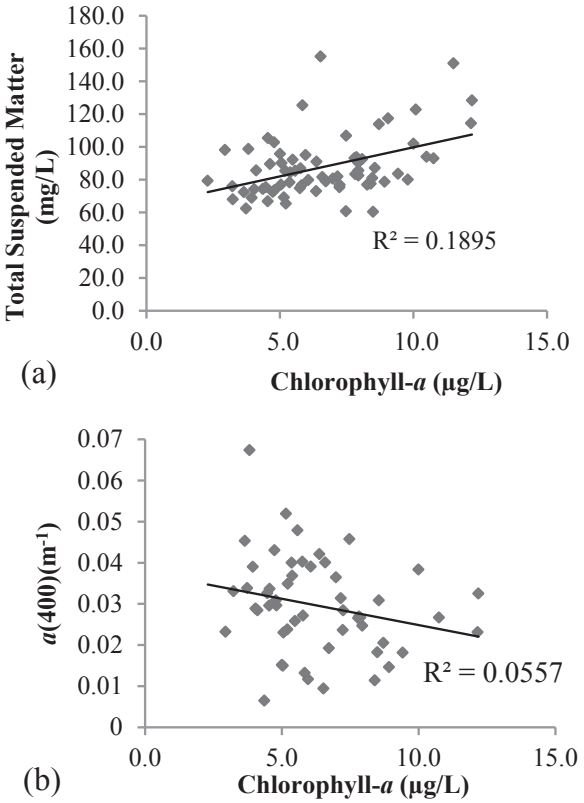

Figure 2. Regression plots of (a) Chl-*a* vs. TSM and (b) Chl-*a* vs. CDOM absorption (*aCDOM*) at 400 m^{-1}.

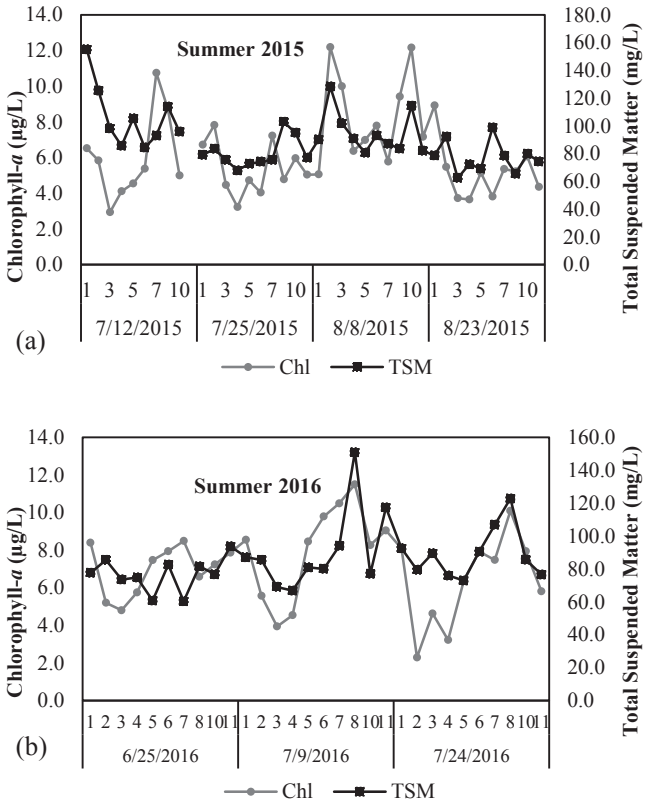

Figure 3. Chl-*a* and TSM concentrations by site and by field sampling day for (a) summer 2015 and (b) summer 2016.

general, the most variations in TSM were observed at stations with the highest average TSM and Chl-*a* concentrations, which were in smaller water bodies with shallower depths. This suggests that the constituents vary independently from each other; however, similar biogeochemical conditions may influence the variations between them. The spatial patterns of these components are essential to understanding the processes influencing their distribution and accumulation throughout the ACE Basin. Only twice were TSM and Chl-*a* concentrations equally high, both times at station 8, which is in Fenwick Cut, where the Edisto River mixes with the Intracoastal Waterway (ICW). This is a highly traversed area known to have high flocculating, low-settling sediments after periods of increased discharge. Bottom stress from current mixing and increased discharge resuspends the flocs (Milligan et al., 2001), causing elevated concentrations of TSM and Chl-*a* in this location.

The results indicate that average CPA concentrations follow a nearshore-offshore gradient, with the stations nearest land having the highest concentrations of Chl-*a* and TSM, and the sites furthest from land having the lowest (Figure 3). These trends are comparable to other nearshore-offshore gradient studies in coastal watersheds (Smith, 2002; Schalles, 2006; Keppler et al., 2015) and support the concept that terrigenous runoff gradually attenuates as it travels farther from land.

In this study, absorption by CDOM decreased exponentially with increasing wavelength. Absorption coefficients at 400 nm (α400) from both field seasons ranged from -0.38 to 10.2 m^{-1}, with an average of 3.16 m^{-1} and a standard deviation (SD) of 1.99 m^{-1} (Figure 4). This wide range and high SD can be attributed to high variability among field stations and possibly temporal variations. To investigate the role of temporal variations, the CDOM values were analyzed by field season. Absorption coefficients at 400 nm for summer 2015 ranged from -0.38 to 5.86 m^{-1}, with an average of 2.32 m^{-1} and an SD of 1.16 m^{-1}(Figure 5a). During the summer of 2016, an increase in values were observed, as the range of absorption coefficients at 400 nm was 0.62 to 9.62 m^{-1}, with an average of 4.17 m^{-1} and an SD of 2.33 m^{-1}

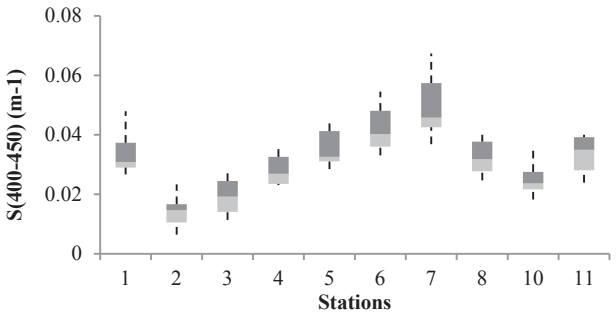

Figure 4. Box plots of spectral slope of CDOM from 400nm to 450 nm. Box plots include minimum, Q1, median, Q3, and maximum.

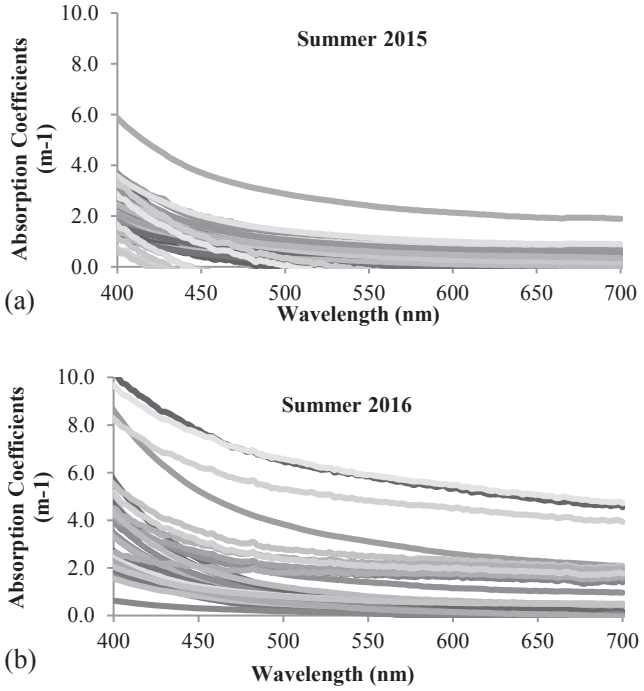

Figure 5. CDOM absorption spectra from 400 to 700 nm using laboratory spectrophotometer: (a) summer 2015 spectra and (b) summer 2016 spectra.

(Figure 5b). The stations that had the highest absorption coefficients for both field seasons were 1, 7, 8, and 11, while the lowest values were observed at stations 2, 3, and 10. The CDOM absorption coefficients were highest at station 1 and 7, which were upstream from the Sound. Station 1 is in Big Bay Creek, adjacent to Live Oak Boat Landing, which is part of Edisto Beach State Park and is influenced by runoff from the boat landing and surrounding areas of anthropogenic activity. Sources of CDOM at this location may include marsh grass and decaying leaves from deciduous trees within the State Park. Station 7 is in the Ashepoo river surrounded by *Spartina alternaflora* (marsh grass), which is an important source of CDOM in estuaries, as it is salt tolerant, making it the dominate plant life. CDOM decreases at mixing gradients (stations 8 and 10) and is lowest in the Sound and offshore due to high loads of seston dominating the water (Schalles, 2006).

REMOTE SENSING

Laboratory-analyzed Chl-*a* and TSM concentrations were correlated with variations in radiometric measurements of TSM filters. Stronger absorption troughs and reflectance peaks coincided with stations with high observed TSM and Chl-*a* concentrations. The troughs (see Figures 2 and 3) indicate spectral absorption features of TSM, while the peaks indicate spectral reflectance features of TSM. The point of inflection at 660 nm is representative of high TSM absorption along with the interplay of seston scattering and higher water absorption in this spectral region (Schalles, 2006) (Figure 6).

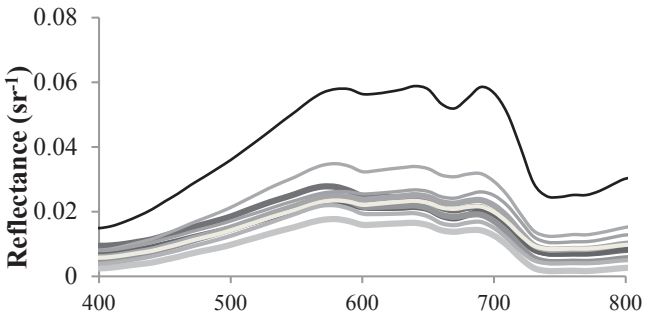

Figure 6. Remote sensing of reflectance spectra from summer 2015 field campaign.

The characteristic troughs and peaks observed throughout each spectra indicate the existence of organic matter (D'Sa and Miller, 2005) along with the low reflectance in the blue portion of the spectrum. Low reflectance in the red portion of the spectrum can be attributed to absorption by Chl-*a*, specifically near 650–690 nm. Absorption troughs from algal particles were no longer present as organics were removed, and the magnitude of the reflectance peaks shifted toward longer wavelengths with an observed peak around 580 nm, consistent with reflectance patterns from high concentrations of kaolin clays (Beck et al., 1976).

APPLICATION OF BAND RATIO ALGORITHMS

Six published algorithms were assessed to model Chl-*a* variability in the study areas, and no correlations were observed between the in situ Chl-*a* data and the modeled data (Table 1). However, the models that preformed relatively better were adapted using estimated correlation coefficients determined from the in situ data. The correlations ranged between 0.0026 and 0.15 for the blue-green band ratios regressed with laboratory-analyzed Chl-*a* concentrations, with the strongest correlation resulting from tuning the OC4v4 algorithm, which was a red-NIR/blue-green model developed for global ocean systems, with a strong reflectance peak at 580 nm. In general, all the band ratio models were equally weak in terms of performance in predicting Chl-*a* concentration. With all the R^2 values consistently < 0.2, no correlations or assumptions could be made using the band ratio models, as they were not statistically significant (Table 1). Even though the waters within the ACE Basin contained moderate amounts of Chl-*a*, the high concentration of suspended sediment and CDOM most likely caused spectral mixing within the blue-green, and red-NIR spectral range, which impeded the reflectance and absorbance by the Chl-*a* to the sensor. The Morel models applied to the hyperspectral GER dataset significantly overestimated Chl-*a*, specifically when the measured concentrations were low at stations 4 and 5 throughout each season. In these cases, strong absorption occurred in the blue and green wavelengths, most likely due to a greater presence of seston (Schalles, 2006), which caused

the logarithm of the blue-green ratio to be negative (D'Sa and Miller, 2005).

For the OC4v4 and Hladik models, predicted Chl-*a* concentrations were lower than the measured concentrations; however, they were closer to actual values, suggesting that models accounting for more spectral features are more successful. Spectral similarities, low-to-moderate spatial variability, and low-to-moderate Chl-*a* concentrations made it difficult for the models to accurately predict Chl-*a*. Additionally, these blue-green models were developed from a global dataset of Case I waters where Chl-*a* is the dominant constituent and with a much broader range in concentrations. Therefore, when applied to the complex waters of the ACE Basin, the models performed poorly.

Tuning and calibration of the OC4v4 model resulted in slightly higher predictive accuracy (0.8%) when applied to the ACE Basin than current global ocean color models. This model used spectral features from both blue-green and red-NIR wavelengths to account for the optical complexity in southeastern estuarine waters (Schalles, 2006). Distinguishing spectral signatures of the water column is vital when choosing bands that exemplify CPAs. However, this model did not result in any accurate predictions of Chl-*a*, as the correlations remained extremely weak (R^2 = 0.15, RMSE = 2.22). The low-to-moderate concentrations of measured Chl-*a* combined with spectral mixing throughout the measured bands contributed to a low signal-to-noise ratio, which likely caused all models to underperform.

APPLICATION OF PRINCIPAL COMPONENT ANALYSIS

The ACE basin has an optically complex environment resulting from the varying biological and sedimentological particles in the water. An awareness of the water constituents that represent this aquatic system is critical for ocean color modeling. The VPCA model, based on the entire dataset, indicated the presence of three significant varimax-rotated factors, which account for 54.9%, 27.7%, and 8.8% of the variance, for a combined total variance explained of 91.3% (Figure 7). A comparison of the factor loadings as a function of wavelength indicated that the components consisted of organic and inorganic materials. PC1 and PC3 did not display any identifiable spectral features indicative of water constituents and were most likely backscatter from high sediment loading and re-suspension within the water column from boats, waves, or high-discharge events. The spectral peaks from PC2 were comparable to the patterns observed in the GER data and were characterized by reflectance trends indicative of Chl-*a* (Figure 8). In situ GER reflectance of surface water indicated moderate concentrations of Chl-*a*, with spectral features at 550 nm comparable to those of the cyanobacteria *Anabaena*, which is known to travel among areas of moist sediment (Romero-Vivas, 2015). This may explain why some stations exhibited high TSM and Chl-*a*, as the sediments may have served as vehicles for the organic particles (Stumpf et al., 1988). The effectiveness of the PCA modeling technique emanates from its capacity to distinguish linear combinations of the original variables that are independent and to acknowledge the issue of correlated variance. The organic and inorganic CPAs present in the ACE Basin characterize these waters as optically complex, particularly after meteorological disturbance events from high wind or precipitation.

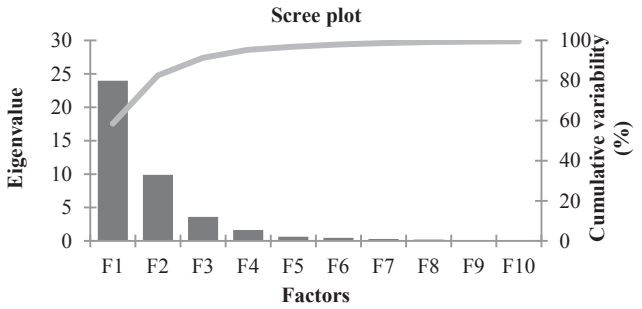

Figure 7. Scree plot of variability (%) and cumulative variability (%) of each component.

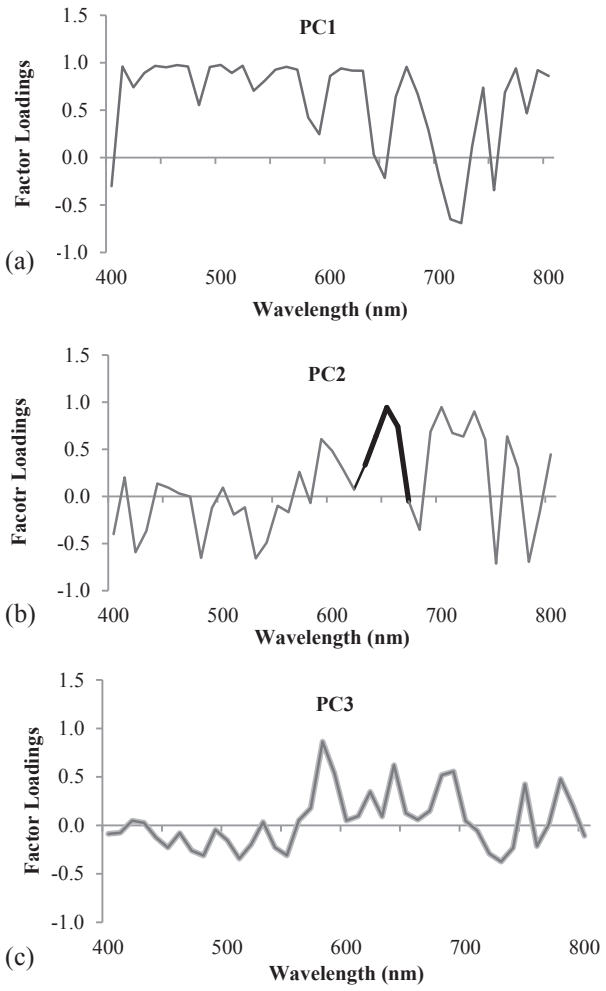

Figure 8. Weighted scores of the first three PCs. Highlighted reflectance peak (black) in PC2 (b) is characteristic of a spectral feature of Chl-*a*.

APPLICATION OF PARTIAL LEAST SQUARES REGRESSION

The PLSR model for the estimation of Chl-*a* using the full spectrum of hyperspectral GER data was stronger with a lower error rate (R^2 = 0.49 and RMSE = 1.77 µg/L) can be observed in Figure 9. Chl-*a* values from station 1 were removed in this model to decrease outliers. A near-linear correlation with few outliers between the predicted and observed Chl-*a* values demonstrates the potential for predictive ocean color monitoring in the ACE Basin (Figure 8a). Standardized coefficients of bands 420, 550, and 680 nm showed the greatest sensitivity for predicting Chl-*a* (Figure 9b). These bands are characteristic of the absorption and reflection features of the planktonic cyanobacteria that are typically found in temperate waters in the southeast.

A PLSR model for the estimation of TSM was not as accurate, with an R^2 = 0.40, and the error rate was much higher in this model (RMSE = 12.9 mg/L), especially at stations 1 and 8, which caused deviation from the model (Figure 9a). This was likely due to the lower spectral variability observed at these stations from high loads of inorganic material that were characterized by absorption features. More absorption was apparent with TSM than with Chl-*a*, with dominating troughs at 460, 490, 660 (Figure 10b), and the NIR portion of the spectrum. TSS preformed less moderately than Chl-*a* and TSM, with an R^2 value of 0.26 (Figure 11a), a strong reflectance peak at 580 and 590 nm, and strong absorption along NIR wavelengths (Figure 11b). Although satellite estimation proved to be difficult in such shallow, spatially confined waters, Stations 1 and 8 provided an understanding of the spectral characteristics of ACE Basin waters with high CPA concentrations. These stations, along with offshore stations, also contributed to the variability in concentrations, which is important when developing a regional model for remote estimation. Using more of these types of signatures to train the model would likely improve the model strength and estimation.

Overall, two primary factors can contribute to the low correlations from PLSR: (1) The optically complex nature of these waters prevented electromagnetic radiation from penetrating the sub-bottom, particularly at shallow sites with high suspended sediments and varying angles of incoming radiation. Significant backscatter from the bottom decreased

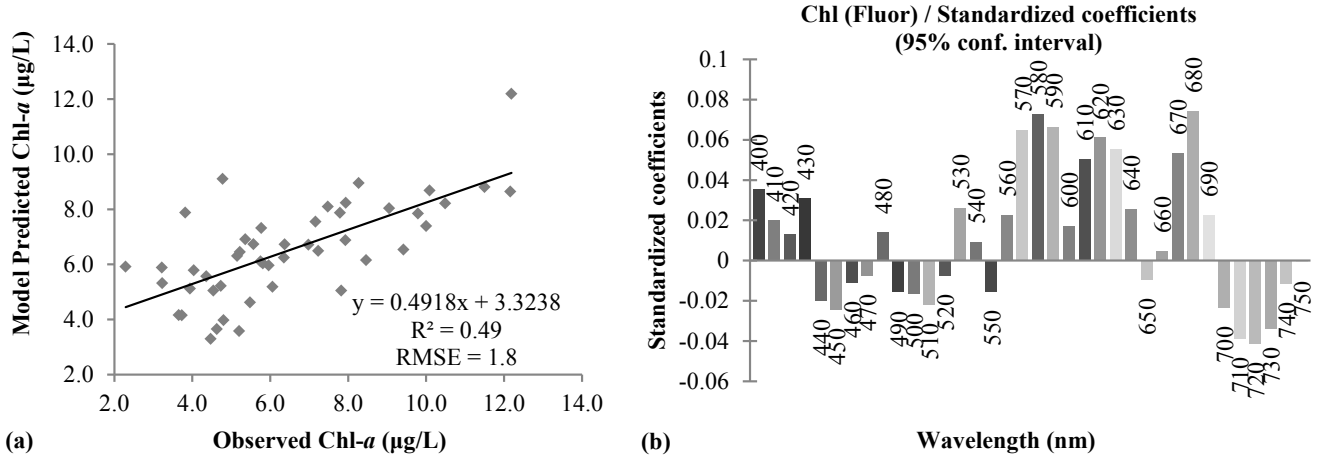

Figure 9. (a) PLSR model accuracies for Chl-*a* prediction and (b) PLSR standardized coefficient plot for Chl-*a* prediction.

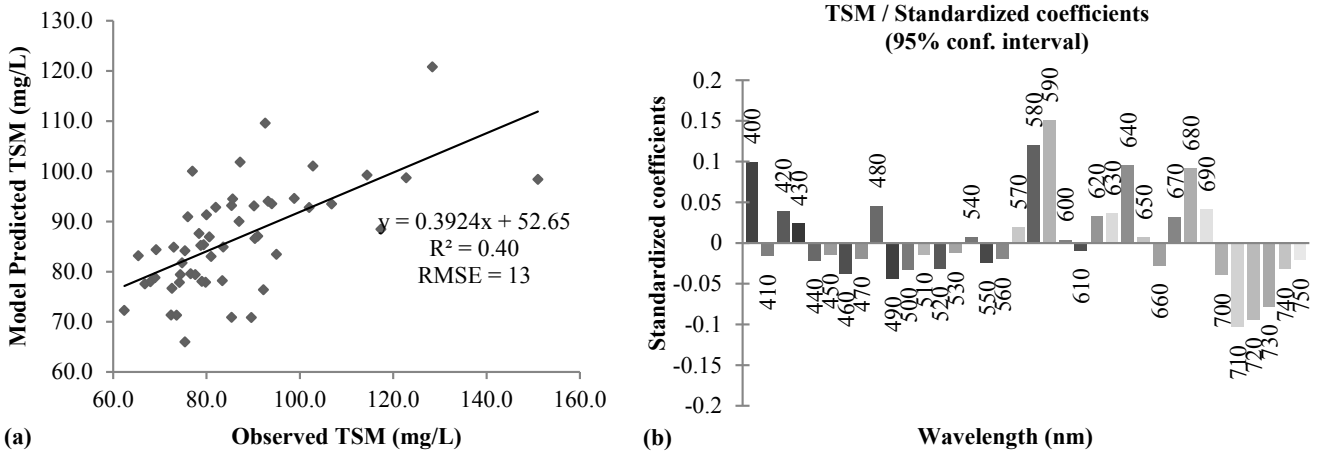

Figure 10. (a) PLSR model accuracies for TSM and (b) PLSR standardized coefficient plot for TSM.

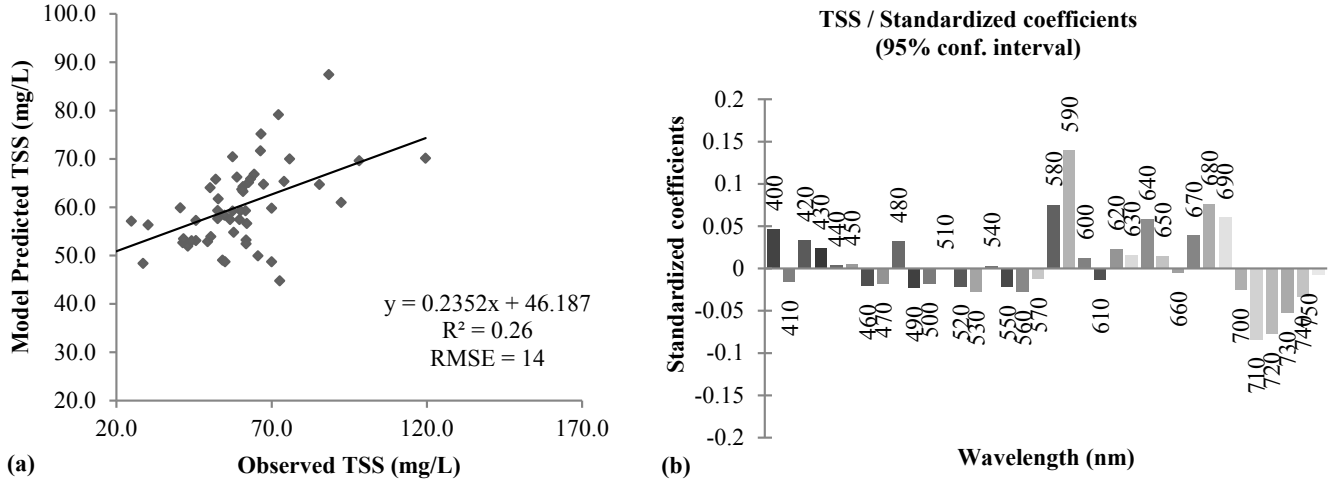

Figure 11. (a) PLSR model accuracies for TSS and (b) PLSR standardized coefficient plot for TSS.

the signal-to-noise ratio from the water surface to the sensor. (2) Significantly high inorganic concentrations observed in all the data, along with high CDOM absorption coefficients, reduced the signal strength and signal variability. The primary factors made it challenging for the model to distinguish background noise (e.g., backscattering from the bottom and other in-water optical constituents) from the spectral features of Chl-*a*. To enhance the signal-to-noise ratio, more refined models or methods are necessary to appropriately distinguish the individual signals. These models should take into consideration the diffuse attenuation coefficients of the water column, bottom reflectance, interference from the sea-air interface, and depth (Lee et al., 2005).

CONCLUSION

In this study, in situ sampling of water quality parameters was used to characterize the temporal and spatial variability in the ACE Basin waters. The results indicate optically complex, moderately eutrophic waters with low-to-moderate concentrations of Chl-*a* and high TSM and CDOM. Distance from land and the degree of watershed development were also parameters that influenced the presence of Chl-*a* and suspended sediments. The results of this study indicate close linkages between physical and bio-optical properties of the water column, which makes satellite remote sensing a useful tool for monitoring changes.

The traditional band ratio models for ocean color or estuarine modeling that have been proposed in previous studies were not found to be a beneficial or an accurate method for estimating Chl-*a* from the in situ radiometric data ($R^2 < 0.099$) due to significant overestimation and underestimation. Tuning the OC4v4 model using model coefficients derived from the in situ data slightly improved the overall accuracy ($R^2 = 0.15$) and lowered the error rate (RMSE = 2.2); however, numerous factors contributed to a low signal-to-noise ratio, which limited its success. More spatially distributed stations with higher spectral variability and more representative data, combined with enhancements in atmospheric correction methods and the availability of higher-resolution sensors, will lead to more conclusive predictions of CPA variability.

The multivariate PLSR approach provided a more accurate model for predicting Chl-*a* ($R^2 = 0.49$) and TSM ($R^2 = 0.40$) than the traditional band ratio approach. Employing the full visible-near infrared spectrum improved the modeling capability, even with a low signal-to-noise ratio. PLSR was useful for reducing the dimensionality and multicollinearity of the extensive hyperspectral dataset while maintaining maximum variability among observations. This approach demonstrated the favorable potential for modeling CPA variability in the ACE Basin despite the dominating properties of inorganic materials in the water.

As operational ocean color satellites become more abundant and higher-resolution technologies are employed, multivariate methods, including PLSR, display considerable potential for estimating CPAs in the ACE Basin. These methods can also be applied to predict CPAs in other coastal systems, but sample collection and field calibration would be required, as the ACE Basin models lack correlations strong enough to predict CPA variability elsewhere. These technologies would also allow for more modeling and prediction of water quality that could be utilized by resource managers to accurately monitor and protect aquatic ecosystems. The absorption and reflectance features characterizing sediments and algal species make it difficult for moderate resolution sensors to distinguish in situ concentrations. The results from this study provide a strong foundation for the future of water quality monitoring and the protection of biodiversity in the ACE basin, and successful application of the PLSR approach demonstrates substantial potential for future remote sensing research. This is a considerable benefit for coastal resource

managers because the technique applies a versatile approach that can be used in an array of waters. The results provide a synoptic view of the water quality variations in a significantly short amount of time, which could facilitate coastal managers in making informed decisions about potential sources of pollution, land development, and health for humans and the surrounding environment.

Finally, communication with coastal managers and local community members would strongly contribute to this research. Interaction with coastal managers would provide localized knowledge regarding primary concerns with water quality, as well as give insight to the different complicated parameters that may affect specific coastal areas. Additionally, correspondence with local community members would aid in determining the level of awareness, understanding, and concern about anthropogenic factors that may be influencing water quality in these coastal systems.

ACKNOWLEDGEMENTS

This research was supported by the Kathryn D. Sullivan Earth and Marine Science Fellowship and the Graduate Research Assistantship through the NASA South Carolina (SC) Space Grant Consortium and NOAA SC Sea Grant Consortium. The authors thank Peter Bierce, captain of the research vessel, and the department of Geology and Environmental Sciences at the College of Charleston, South Carolina, for loaning the research vessel and providing equipment, technology, and laboratory space that were paramount to the completion and success of this project.

LITERATURE CITED

Ali, K. A., Witter, D. L, and Ortiz, J. D., 2013. Multivariate approach to estimate colour producing agents in Case 2 waters using first-derivative spectrophotometer data. *Geocarto International* 29(2): 102–127.

Allen, J. and Lu, K., 2003. Modeling and prediction of future urban growth in the Charleston region of South Carolina: a GIS-based integrated approach. *Conservation Ecology* 8(2): 2.

Anderson, D., Glibert, M., Burkholder, P. M., and Joann, M., 2002. Harmful algal blooms and eutrophication: Nutrient sources, composition, and consequences. *Estuaries* 25(4).

Arar, E.J and Collins, G.B., 1997. Method 445.0: In Vitro determination of chlorophyll a and pheophytin a in marine and freshwater algae by fluorescence. *National Exposure Research Laboratory*. Office of Research Development, U.S. Environmental Protection Agency: Cincinnati, OH.

Babin, M., Stramski, D., Ferrari, G.M., Claustre, H., Bricaud, A., Obolensky, G., and Heopffner, N., 2003. Variations in the light absorption coefficients of phytoplankton, nonalgal particles, and dissolved organic matter in coastal water around Europe. *Journal of Geophysical Research* 108(7):3211.

Bannerman, R.T., Owens, D. W., Dobbs, R. B., and Hornewer, N. J., 1993. Sources of pollutants in Wisconsin stormwater. *Water Science and Technology* 28:241–259.

Bhatti, A. M., Rundquist, D., Schalles, J., Steele, M., and Takagi, M., 2010. Qualitative assessment of inland and coastal waters by using remotely sensed data. *International Archives of the Photogrammetry, Remote Sensing and Spatial Information Science* 38(8).

Bearden, C., Low, R., Rhodes, R., Van Dolah, R., Wenner, C,. Wenner E, and Whitaker, D., 1985. A review and analysis of commercial shrimp trawling in the sounds and bays of South Carolina. *South Carolina Marine Resources Center*. Technical Report 62.

Beck, R. H., B. F. Robinson, W. W. McFee, and J. B. Peterson, 1976. Spectral characteristics of soils related to the interaction of soil moisture, organic carbon and clay content. LARS Information Note 081176. *Laboratory for Applications of Remote Sensing*, Purdue University, West Lafayette, IN.

Bricker, S. B., Clement, C. G., Pirhalla, D. E., Orlando, S. P., and Farrow, D. R. G., 1999. National estuarine eutrophication assessment: effects of nutrient enrichment in the Nation's estuaries. *NOAA. National Ocean Service, Special Projects Office and the National Centers for Coastal Ocean Science*, Silver Springs, MD: 71.

Cole, B., McMorrow, J., and Evans, M., 2014. Empirical modeling of vegetation abundance from airborne hyperspectral data for upland peatland restoration monitoring. *Remote Sensing* 6: 716–739.

Cooke, C. W., 1936. Geology of the Coastal Plain of South Carolina. *United States Department of the Interior*. Bulletin 867.

Corbert, C. A., 2007. Color dissolved organic matter (CDOM) workshop summary. Reports. Paper 2.

D'sa, E. J. and Miller, R. L., 2005. Bio-optical properties of coastal waters. Ch. 6 in, *Remote Sensing of Coastal Aquatic Environments*: 129–155.

Doxaran, D., Froidefond, J. M., and Castaing, P., 2002. A reflectance band ratio used to estimate suspended matter concentrations in sediment-dominant coastal waters. *International Journal of Remote Sensing* 23: 5079–5085.

Duffie, J. A., and Beckman, W. A., 2013. *Solar Engineering of Thermal Processes* (4 ed.). Hoboken, NJ: John Wiley & Sons.

Etheridge, J. R., Brigand, F., and Burchell II, M. R., 2015. Quantifying nutrient and suspended solids fluxes in a constructed tidal marsh following rainfall: The value of capturing rapid changes in flow and concentrations. *Ecological Engineering* 78: 41–52.

Fu, Y., Yang, G., Feng, H., Song, X., Xu, X., and Wang, J., 2013. Comparative analysis of three regression methods for the winter wheat biomass estimation using hyperspectral measurements. *Proceedings of the 2nd International Conference on Computer Science and Electronics Engineering*: 1733–1736. Hangzhou, China.

Gao, B. C., Montes, M. J., Ahmad, Z., and Davis, C. O., 2000. Atmospheric correction algorithm for hyperspectral remote sensing of ocean color from space. *Applied Optics* 39(6): 887–896.

Gilbert, P. M., Anderson, D. A., Gentien, P., Graneli, E., and Sellner, K. G., 2005a. The global, complex phenomena of harmful algal blooms. *Oceanography* 18(2): 136–147.

Gitelson, A. 1992. The peak near 700 nm in the reflectance spectra of algae and water: relationships of its magnitude and position with chlorophyll concentration. *International Journal of Remote Sensing* 13(17):1367–1373.

Gomez-Chova, J. C., Camps-Valls, G., Martín, J. D., Soria, E., Vila, J., Alonso-Chorda, L., and Moreno, J., 2003. Feature selection of hyperspectral data through local correlation and SFFS for crop classification. *IEEE International Geoscience and Remote Sensing Symposium*: 555–557.

Gross-Colzy, L., S. C., Frouin, R., and Henry, P., 2007. A general ocean colour atmospheric correction scheme based on principal component analysis-Part I: Performance on case I and case 2 waters. *Proc. SPIE, 6680, Coastal Ocean Remote Sensing, 668002.*

Gurlin, D., A. A. Gitelson, and Moses, W. J. 2011. Remote estimation of Chl-*a* concentration in turbid productive waters—Return to a simple two-band NIR-red model? *Remote Sensing of Environment* 115: 3479-3490.

Haaland, D. M. and Thomas, E.V., 1988. Partial least-squares methods for spectral analyses. 1. Relation to other quantitative calibration methods and the extraction of qualitative information. *Analytical Chemistry* 60(11): 1193–1202.

Han, L., 1997. Spectral reflectance with varying suspended sediment concentrations in clear and algae-laden waters. *Photogrammetric Engineering and Remote Sensing* 63: 701–705.

Heisler, J., Glibert, P. M., Burkholder, J. M., Anderson, D. M., Cochlan, W., Dennison. W. C,. Dortch, Q., Gobler, C. J., Heil, C. A., Humphries, E,. Lewitus, A., Magnien, R., Marshall, H. G., Sellner, K., Stockwell, D. A., Stoecker, D. K., and Suddleson, M., 2008. Eutrophication and harmful algal blooms: A scientific consensus. *Harmful Algae* 8: 3–13.

IOCCG, 2000. Remote sensing of ocean color in coastal, and other optically complex waters. Dartmouth, Canada: Sathyendranath, S. (ed), *Reports of the International Ocean-Colour Coordinating Group*, No. 3, IOCCG.(India) Private, Ltd.

Keppler, C. J., Bergquist, D. C., Brock, L. M., Felber, J., and Greenfield, D. I., 2014. A spatial assessment of baseline nutrient and water quality values in the Ashepoo-Combahee-Edisto (ACE) Basin, South Carolina, USA. *Marine Pollution Bulletin* 99:332–337.

Klemas, V., 2011. Remote sensing techniques for studying coastal ecosystems: an overview. *Journal of Coastal Research* 27(1).

Lee, Z., Carder, K. L., Hawes, S. K., Steward, R. G., Peacock, T. G., and Davis, C. O. 1994. Model for the interpretation of hyperspectral remote-sensing reflectance. *Applied Optics* 33(24): 5721–5732.

Lee, S.Y., Dunn, R. J. K.,Young, R. A, Connolly, R., Dale, P. E., Dehayr, R., C. J, Lemckert. Mckinnon, J., Powell, S., Teasdale, P. R., and Welsh, D. T., 2006. Impact of urbanization on coastal wetland structure and function. *Austral Ecology* 31(2).

Leopold, L. B., 1968. Hydrology for urban planning, a guidebook on the hydrologic effects of urban land use. *U.S Geological Survey Circular 554*, Washington, D.C: U.S Department of the Interior.

Maitra, S. and Yan, J., 2008. Principal component analysis and partial least squares: two dimension reduction techniques for regression. *Casualty Actuarial Society, Discussion Paper Program.*

Mathews, T. D., Stapor, F. W., Richter, C. R., Miglarese, J. V., McKenzie, M. D., and Barclay, L. A., 1980. *Ecological Characterization of the Sea Island Coastal Region of South Carolina and Georgia, Volume I: Physical Characterization Area.*

McClain, C. R., 2009. A decade of satellite ocean color observations. *Annual Review of Marine Science* 1:19–42.

McIntyre, M. P., Eilers, H. P., and Mairs, J. W., 1991. *Physical Geography*. Wiley and Sons, New York, NY.

Miller, R. L., Belz, M., Del Castillo, C., and Trzaska, R., 2002. Determining CDOM absorption spectra in diverse coastal environments using multiple path length, liquid core waveguide system. *Continental Shelf Research* 22:1301–1310.

Milligan, T. G., Kineke, G. C., Blake, A. C, Alexander, C. R, and Hill, P. S., 2001. Flocculation and sedimentation in the ACE Basin, South Carolina. *Estuaries* 24(5):734–744.

Mobley, C., 1999. Estimation of the remote-sensing reflectance from above-surface measurements. *Applied Optics* 38(36):7442–7455.

Moses, W. J., Gitelson, A. A., Berdnikov, S., Saprygin, V., and Povazhnyi, V., 2012. Operational MERIS-based NIR-red algorithms for estimating chlorophyll-*a* concentrations in coastal waters—The Azov Sea case study. *Remote Sensing of the Environment* 121:118–124.

Noble, P. A., Tymowski, R. G., Fletcher, M., Morris, J. T., and Lewitus, A. J., 2003. Contrasting patterns of phytoplankton pigment composition in two salt marsh estuaries in Southeastern United States. *Applied Environmental Microbiology* 69: 4129–4143.

Nwaodua, E. C., Ortiz, J. D., and Griffith, E. M., 2014. Diffuse spectral reflectance of surficial sediments indicates sedimentary environments on the shelves of the Bering Sea and western Arctic. *Marine Geology* 355: 218–233.

Ortiz, J. D., Witter, D. L., Ali, K. A., Fela, N., Duff, M., and Mills, L., 2013. Evaluating multiple colour-producing agents in Case II waters from Lake Erie. *International Journal of Remote Sensing* 34(24): 8854–8880.

Robertson, A. L., Tedesco, L. L., Wilson, J., and Soyeux, E., 2009. Using partial least squares (PLS) method for estimating cyanobacterial pigments in eutrophic inland

waters. In W. G. Jackson (eds.), *Remote Sensing and Modeling of Ecosystems for Sustainability* 7454(8).

Rodriguez-Guzman, V. and Gilbes-Santaella, F., 2009. Using MODIS 250 m imagery to estimate total suspended sediment in a tropical open bay. *International Journal of Systems Applications, Engineering & Development* 3(1): 36–44.

Romero-Vivas, E., Von Borstel, F. D,. Perez-Estrada, C., Torres-Ariño, D., Villa-Medina, F. J., and Gutierrez J., 2015. On water remote monitoring robotic system for estimating patch coverage of *Anabaena* sp. filaments in shallow water. *Environmental Science: Processes and Impacts*. doi:10.1039/C5EM00097A.

Ryan, K. and Ali, K. A., 2016. Application of a partial least squares regression model to retrieve chlorophyll-*a* concentrations in coastal waters using hyper-spectral data. *Ocean Science Journal* 51(2):209–221.

Sathyendranath, S. and Platt, T., 1997. Analytical model of ocean color. *Applied Optics* 36(12): 2620–2629.

Schalles, J. F., 2006. Optical remote sensing techniques to estimate phytoplankton chlorophyll-*a* concentrations in coastal waters with varying suspended matter and CDOM concentrations. Ch. 3 In, Richardson, L. and E. LeDrew (eds.), *Remote Sensing of Aquatic Coastal Ecosystem Processes: Science and Management Applications*. Springer:27–79.

Soller, D. R and Mills, H. H., 1991. Surficial geology and geomorphology. In: J. W Horton and V.A Zullo (eds.), *The Geology of the Carolinas: Carolina Geological Society Fiftieth Anniversary Volume*. University of Tennessee Press, Knoxville, TN.

SCWRC, 1972. ACE framework study: Ashley-Combahee-Edisto River Basin. *South Carolina Water Resources Commission*, Columbia, SC.

Stapor, F. W., 1984. Sand transport at Edisto Beach, Colleton County, South Carolina. *South Carolina Marine Resources Center*. Technical Report No.60: 8.

Stumpf, R. P., 1988. Sediment transport in Chesapeake Bay during floods: Analysis using satellite surface observations. *Journal of Coastal Research* 4:1–15.

United States Environmental Protection Agency (USEPA), 2012. Oceans, Coasts and Estuaries. Retrieved 2015, from United States Environmental Protection Agency http://www3.epa.gov/region9/water/oce/coastalwaters.html.

Van Dolah, R. F., Jutte, P. C., Riekerk, G. H. M., Levisen, M. V., Crowe, S. E., Lewitus, A. J., Chestnut, D. E., McDermott, W., Bearden, D., and Fulton M. H., 2004. The condition of South Carolina's estuarine and coastal habitats during 2001–2002: *South Carolina Marine Resources Division*, Charleston, SC. Technical Report No.100: 70.

Vasilkov, A., and Kopelevich, O.,1982. Reasons for the appearance of the maximum near 700 nm in the radiance spectrum emitted by the ocean layer. *Oceanology* 22 (6): 697–701.

Witter, D. L., J. D. Ortiz, S. Palm, R. T. Heath, and Budd, J. W., 2009. Assessing the application of SeaWiFS ocean color algorithms to Lake Erie. *Journal of Great Lakes Research* 35: 361–370.

Yacobi Y. Z., Moses, M. J., Kaganovsky. S., Sulimani, B., Leavitt, B. C., and Gitelson, A. A., 2011. NIR-red reflectance-based algorithms for chlorophyll-*a* estimation in mesotrophic inland and coastal waters: Lake Kinneret case study. *Water Resources* 45:2428–2436.

Journal of South Carolina Water Resources, Volume 4, Issue 1, Pages 57–62, 2017

Drought and Water Shortages: South Carolina's Response Mechanisms, Vulnerabilities, and Needs

Ekaterina Altman[1], Kirsten Lackstrom[1], and Hope Mizzell[2]

AUTHORS: [1]Carolinas Integrated Sciences & Assessments (CISA), University of South Carolina, Columbia, SC, 29208, USA.
[2]State Climatology Office, SC Department of Natural Resources, 1000 Assembly Street, Columbia, SC, 29201, USA.

Abstract. The South Carolina Drought and Water Shortage Tabletop Exercise took place on September 27, 2017, at the South Carolina Emergency Operations Center in West Columbia, SC. The exercise gathered 80 participants, representing federal and state agencies, public water suppliers, county and municipal governments, industry, consulting companies, and nonprofit organizations. The purpose of the exercise was to review plans and procedures that govern state-, basin-, and local-level responses to drought and water shortages. Many of South Carolina's drought response mechanisms were updated by the 2000 Drought Response Act and Regulations, but a systematic effort has not been made to review or assess their effectiveness. Attendees walked through a series of exercise responses to gradually worsening drought scenarios and an activation of the Emergency Operations Plan. The event helped to identify strengths and weak points of the state's drought response and opportunities to proactively prepare for future droughts. The key needs discussed by participants included updated drought response *plans and procedures* to ensure a coordinated and timely response to droughts; greater *educational opportunities* to enhance agencies' familiarity with the Drought Response Program and their role in drought response and mitigation; more effective *communications* before, during, and after drought events, across agencies and with the public; and enhanced *data and information products* that can be used to build common understanding of drought risks, impacts, and vulnerabilities.

SOUTH CAROLINA DROUGHT RESPONSE

One goal of the tabletop exercise was to familiarize the participants with the legislation, regulations, plans, and procedures that recommend and require responses at different drought stages (Figure 1). The South Carolina Drought Response Act (S. C. Code Ann. §49-23-10 et. seq) and the supporting regulations (R.121-11.1–121-11.12, for §49-23-10 et seq., S. C. Code of Laws) formally establish and describe the responsibilities of the South Carolina Drought Response Committee (DRC), the state's major drought decision-making entity. The Drought Response Act also requires that all public water suppliers develop and implement local drought plans and ordinances.

In coordination with the South Carolina Department of Natural Resources (DNR) and State Climatology Office (SCO), the DRC monitors and evaluates drought-related data and information, consults with stakeholders about conditions and impacts, designates drought levels as defined by the Drought Response Act for affected counties, and disseminates drought status information to the public (R.121-11.8). South Carolina has four drought alert phases—incipient, moderate, severe, and extreme. The Drought Regulations detail the indicators and indices used to determine drought status. These include streamflow and groundwater levels, the Palmer Drought Severity Index, Crop Moisture Index, Standardized Precipitation Index, Keetch-Byram Drought Index, and United States Drought Monitor.

The DRC is composed of statewide and local members. State agency members include the Emergency Management Division (EMD), the Department of Health and Environmental Control, the Department of Agriculture, the Forestry Commission, and the Department of Natural Resources. Local members are organized according to the state's four Drought Management Areas (Figure 2) and represent counties, municipalities, public service districts, private water suppliers, agriculture, industry, domestic users, regional councils of government, commissions of public works, power generation facilities, special purpose districts, and soil and water conservation districts.

The DRC may recommend mandatory reduction or curtailment of nonessential water use when drought

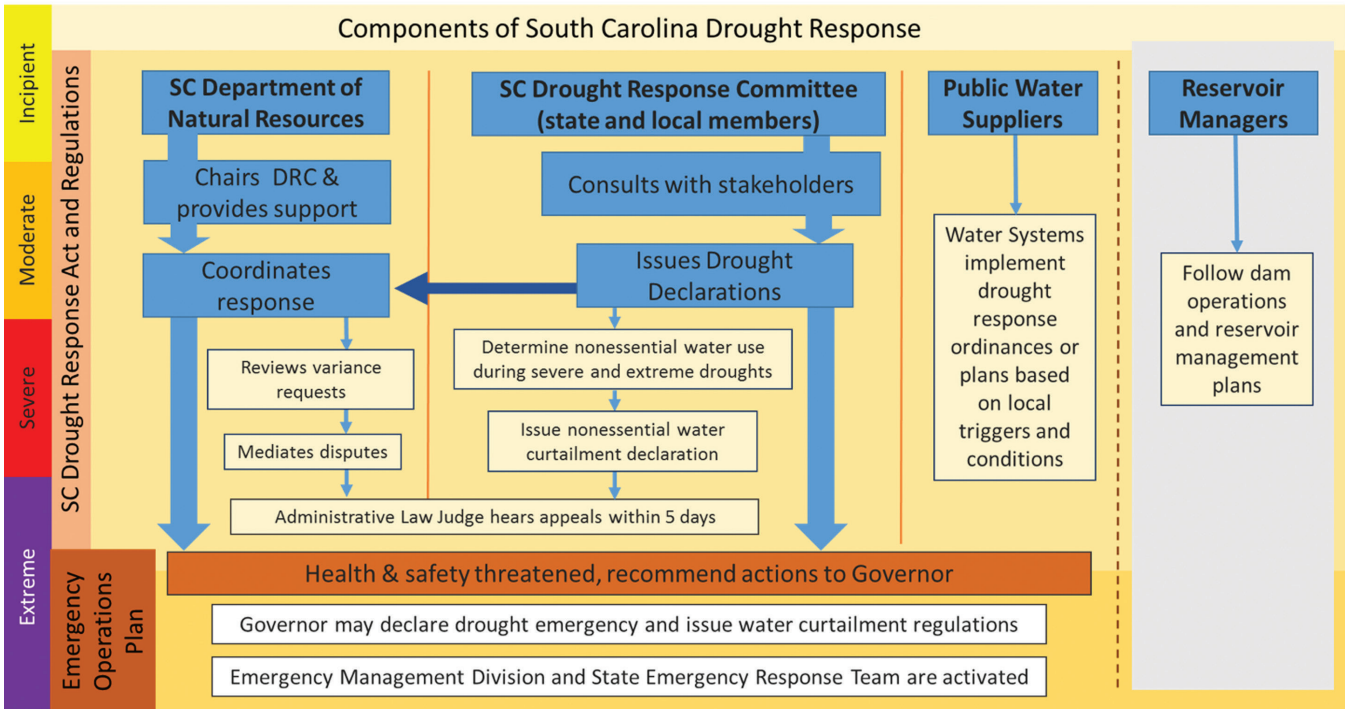

Figure 1. Components of South Carolina Drought Response and flowchart of responsibilities and actions

conditions escalate to severe or extreme drought (R.121-11.6). The DRC is also responsible for reviewing and determining which nonessential water uses should be curtailed. DNR is responsible for issuing and disseminating curtailment declarations, reviewing variance requests, and mediating disputes arising from competing demands for water.

The Emergency Operations Plan (EOP) (Appendix 10) may be activated when a drought management area, or a portion of a drought management area, is seriously threatened or impacted. Examples of such impacts are as follows: the risk of drinking water supply depletion; threats to public health, safety, and welfare; and the inability of local resources and actions to provide for citizens' safety. At this point, state-level actions and resources are necessary to provide relief from impacts.

The EMD maintains the EOP and leads multi-agency responses to hazard events. Upon an activation of the EOP, EMD and the State Emergency Response Team (SERT) assemble in the South Carolina Emergency Operations Center to coordinate the state's response.

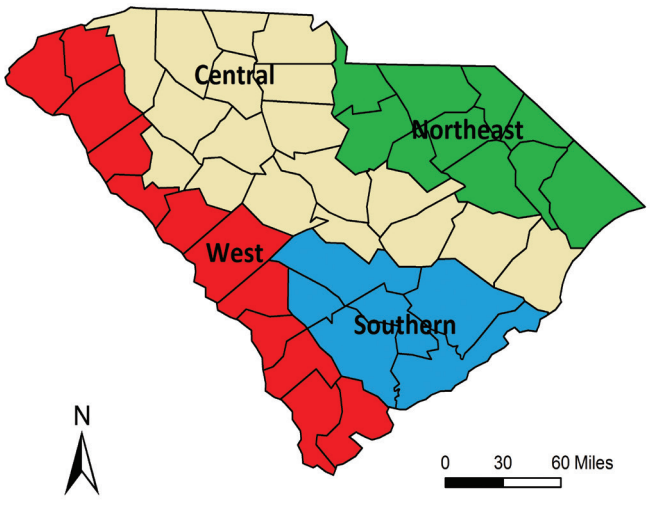

Figure 2. South Carolina Counties and Drought Management Areas

OVERVIEW OF THE EXERCISE

The state routinely exercises for hurricanes and other hazardous events but has never conducted an exercise for a drought or water shortage emergency. Over the last two decades, South Carolina has experienced several severe, statewide and regional droughts, highlighting the need for coordination across multiple agencies and organizations to manage water resources effectively (Collins et al., 2016; Schwab, 2013; Wilhite et al., 2014). Specific events occurred during 1998–2003, 2007–2009, and 2010–2013. The Upstate experienced extreme drought conditions during 2016–2017.[1]

While recent droughts have provided "opportunities" to implement the procedures as outlined in the State Drought Response Act and the accompanying regulations and local plans, a systematic effort has not been made to review and assess the effectiveness of response actions. Tabletop exercises are often used to test the implementation of plans, identify any shortcomings, train staff, and enhance the readiness of participating organizations (Whelton et al., 2006; Whitler and Stormont, 2011). The goal of this exercise

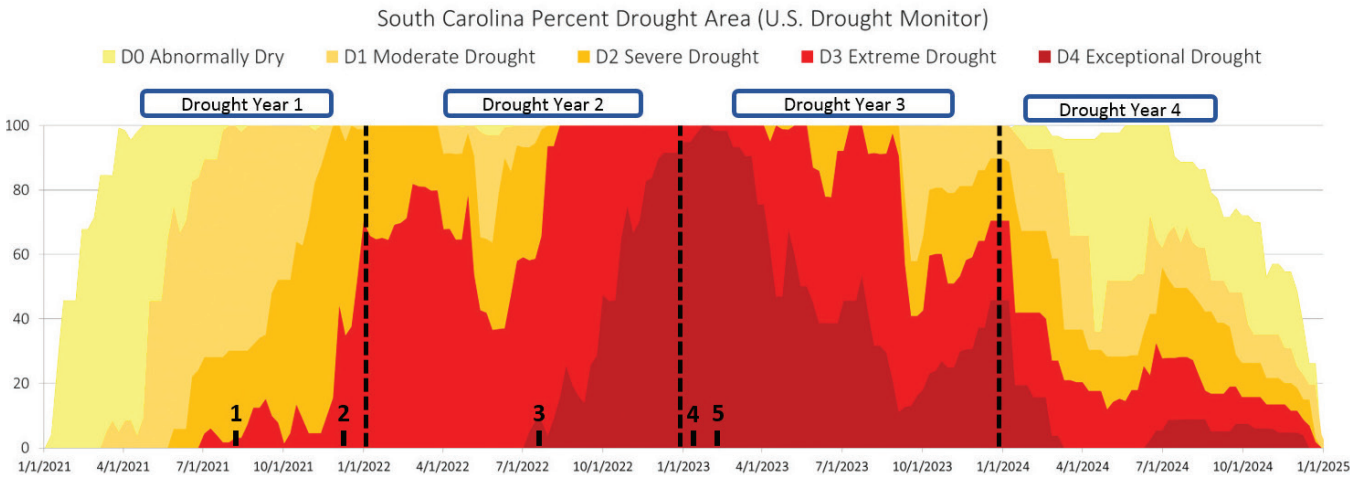

Figure 3. Drought timeline for the South Carolina Drought and Water Shortage Tabletop Exercise. The figure shows a hypothetical four-year drought, modeled after the United States Drought Monitor. The scenario time points are noted on the graph: 1—*Moderate Drought Statewide* (July–August 2021), 2—*Severe Drought Statewide* (December 2021), 3—*Extreme Drought Statewide* (July–August 2022), 4—*Extreme Drought Intensified* (January 2023), and 5—*Emergency Operations Plan is Activated* (February–April 2023).

was to generate ideas that will be used to enhance South Carolina's drought response and preparedness. The exercise provided an opportunity for water resource and emergency managers to discuss the "uncharted territory" of activating the EOP and responding to a water shortage emergency in the state.

Specific objectives included the following:

1. Identify and understand the strengths and constraints in the SC Drought Response Act, SC Drought Regulations, SC Emergency Operation Plan, and local drought plans and procedures.
2. Improve awareness of local, state, and federal players in South Carolina's drought response.
3. Identify key mission areas for each State Emergency Support Function (SERT).
4. Collect ideas and strategies for future exercises.

The exercise was divided into several segments. An introduction provided an overview of the relevant legislation and outlined the goals and objectives of the exercise. The attendees then walked through an intensifying multi-year drought scenario with five time points (Figure 3). For each time point, a set of maps, graphs, and other visualizations was presented to show drought conditions, impacts, and response.[2] Drought conditions were shown using drought indicators and indices described in the state's drought regulations. Figures showing worsening wildfire and hydrological impacts were similar to those typically presented at SC DRC meetings. Response actions were based on those outlined in South Carolina's Drought Response Act and Regulations, as well as in other plans operating in the state.[3] While South Carolina has never activated the EOP for drought, the scenarios were designed to plausibly exercise for these conditions and to evaluate key agency actions and functions in response to a water shortage emergency.

At Time Point 2, streamflow, groundwater, and lake levels were below normal levels, and water systems were beginning to request voluntary and mandatory water conservation from their customers. At Time Point 3, the SC Forestry Commission reported higher than normal fire activity, depletion of local firefighting resources, and the need for state resources to assist with fire suppression. At Time Point 4, impending water supply shortages threatened public health, safety, and welfare, necessitating the activation of the EOP at Time Point 5.

The participants were asked to consider questions designed specifically to reveal strengths and areas for improvement at each time point. Two recurring questions centered on communications and organizational resources and capacity to respond to drought. Table 1 summarizes the impacts, response actions, and discussion questions at each scenario time point. The final session ("hot wash") included a dedicated block of time for participants to review what they learned, provide feedback about the event, and recommend the next steps.

NEEDS AND NEXT STEPS IDENTIFIED BY PARTICIPANTS

The prevalence of formal plans to guide decisions and actions contributes to South Carolina's capacity to respond to drought events. However, having many different plans can make coordination difficult and hamper the development of consistent and clear public communications. This section summarizes the needs and recommendations for next steps as discussed by participants at the exercise.

Table 1. Impacts, response actions, and discussion questions for each time point in the multi-year drought scenario. Conditions and impacts are realistic representations based on historical records. Response actions are outlined in formal plans and legislation.

Example Impacts	Selected Response Actions	Main Discussion Questions
All Time Points and Drought Stages		
• What and how is your organization communicating with the public? • What would help your organization more effectively respond to and prepare for drought?		
Time Point 1: Moderate Drought Statewide (July–August 2021)		
• Declining water levels • Withering crops • Need for irrigation increases	• State agencies, local water systems, and reservoir managers monitor conditions • Voluntary water conservation measures are requested	• Does your organization have a plan for monitoring, responding to, and preparing for drought? • Are drought response plans and ordinances up to date and current?
Time Point 2: Severe Drought Statewide (December 2021)		
• Surface and groundwater levels continue to drop • Increasing number of wildfires • Poor grazing and agricultural conditions	• State agencies increase monitoring and communications • Affected sectors (agriculture, forestry, industry) request assistance • Water systems require water conservation	• How do inconsistencies at different levels (state, local, basin) affect drought response and communications? • Are local ordinances and plans consistent with other drought plans in neighboring areas?
Time Point 3: Extreme Drought Statewide (July–August 2022)		
• Widespread impacts to agriculture, forestry, water systems, and water-dependent businesses	• Forestry Commission requests that the Governor activate the National Guard to assist with fire suppression • Governor issues a press release requesting voluntary conservation • More water systems require water conservation	• How do inconsistencies at different levels (state, local, basin) affect drought response and communications? • Are local ordinances and plans consistent with other drought plans in neighboring areas?
Time Point 4: Extreme Drought Intensified (January 2023)		
•Safety, health, and welfare are threatened •Water systems report diminishing water supplies and water quality issues (for example, saltwater intrusion in coastal water supplies)	The Drought Response Committee: • Recommends state measures • Evaluates nonessential water uses for curtailment • Requests public statements from the governor's office regarding voluntary and/or mandatory water restrictions	• What resources, information, or additional capacity does the DRC need to assess non-essential water use and to curtail certain uses? • How will appeals to the administrative law judge affect the timeliness of conservation and response efforts? • When exactly, and for how long, will the Emergency Operations Plan and State Emergency Response Team (SERT) be activated?
Time Point 5: Emergency Operations Plan is Activated (February–April 2023)		
• Water systems and citizens are without or are losing access to water	• The State Emergency Response Team (SERT) is activated to lead the state-level response to the water shortage emergency	• Are the necessary resources, expertise, and capacity available? • What tasks or actions are not listed in the EOP, but should be included? • How will SC coordinate with other states?

PLANS AND PROCEDURES

It is important to update drought response legislation and procedures to ensure a better coordinated and timely response to drought. The current Drought Response Act, regulations, and guidance for local plans were established in 2000. Many local plans have not been revised since the early 2000s. Although the Emergency Operations Plan is regularly reviewed and updated by EMD, many participants had limited knowledge of the EOP Drought Response Plan prior to the exercise. It was clear that at least a partial activation of the EOP and involvement of the governor's office at earlier stages of drought would be beneficial. The exercise also highlighted the need to reexamine the DRC structure and membership, fill vacancies, and streamline the process for appointing new members.

COMMUNICATIONS

Improved information sharing across agencies and with the public will help South Carolina to better prepare for and respond to drought events and potential emergencies. This would include the development of clear and consistent messages for the public about drought conditions and coordination across different agencies to enhance current communication processes. For example, earlier involvement of the EMD Public Information Officer could help to ensure that the content, timing, and coordination of messages are efficient and appropriate at different stages of drought.

EDUCATION AND AWARENESS

The need for greater awareness of drought and drought impacts, as well as the plans and procedures that guide drought response, was prevalent across different agencies and audiences. Many SERT members noted that their agencies lacked familiarity with the Drought Response Program and were uncertain about their specific role(s) and responsibilities for drought response. As many of these agencies have not typically been involved in drought response and planning, additional training or resources would be beneficial for this group. More generally, participants noted a need for greater public awareness of drought, the effects of drought on different resources and communities, and the water conservation actions to take during drought.

DATA AND INFORMATION

Fulfilling the need to identify, collect, and update information could enhance drought response and planning. This includes new resources and tools being developed by agencies such as the National Weather Service to assess and forecast drought, weather, and climate events, as well as using and expanding existing networks to monitor conditions (e.g., the Community Collaborative Rain, Hail & Snow Network [CoCoRaHS]).[4] Other types of information (e.g., water system connections, water demand, and the economic effects of drought) would help build a common understanding of drought risks and vulnerabilities across different communities, sectors, and regions of the state.

RECOMMENDED NEXT STEPS

Participants voiced support for future exercises that would take place on the regional or watershed level and delve deeper into local vulnerabilities and response actions. The exercise helped to identify and provide momentum for actions that could be implemented in the near term. Next steps include following up with the governor's office to update the DRC membership, developing education and training modules for emergency managers and others to learn more about drought, and working with water suppliers to review local plans and ordinances. The participants recommended more substantial changes to legislation, regulations, and policies, but these will be more difficult to achieve. One important issue to consider is the need to balance the benefits of local flexibility in responding to drought with the need to develop more consistent messaging and response actions during severe events. In addition, recent efforts to allocate more resources and funding to the State's Drought Response Program have been unsuccessful. The state currently lacks a full-time, dedicated drought response coordinator, a position that could lead many of the efforts recommended at the exercise.

CONCLUSIONS

As the first such event in South Carolina (and one of only a few conducted across the country), this tabletop exercise provided an important opportunity to identify the strengths of South Carolina's drought response and areas to improve. Feedback from the participants indicated the importance, relevance, and value of the event to improve drought preparedness in the state. Attendees learned about important drought issues, increased their awareness about roles and responsibilities in drought response, and expressed a willingness to work together in future exercises and efforts. Follow-up activities to the tabletop exercise are expected to contribute toward the goal of proactively preparing the state for future extreme droughts before these events escalate into emergencies. A well-prepared state will be more resilient to climate extremes and variability in the future.

ACKNOWLEDGEMENTS

The authors express their thanks to the other planning team members for their efforts in organizing and conducting the tabletop exercise: Amanda Farris (Carolinas Integrated Sciences & Assessments, University of South Carolina), Robert Burton and Marshall Sykes (South Carolina Emergency

Management Division), and Jeff Allen and Dawn White (South Carolina Water Resources Center, Clemson University).

The authors thank Scott Harder (South Carolina Department of Natural Resources) and Darryl Jones (South Carolina Forestry Commission) for their assistance with the development of graphics and information for the drought scenario.

The authors also acknowledge the EMD leadership and staff for participating and providing the Emergency Operations Center for the exercise.

Funding for CISA's involvement in this project comes from the National Oceanic and Atmospheric Administration's (NOAA) Climate Program Office (Grant Nos. NA11OAR4310148 and NA16OAR4310163).

LITERATURE CITED

Collins, K., J. Hannaford, M. Svoboda, C. Knutson, N. Wall, T. Bernadt, N. Crossman, I. Overton, M. Acreman, S. Bachmair, and K. Stahl. 2016. Stakeholder coinquiries on drought impacts, monitoring, and early warning systems. *Bulletin of American Meteorological Society* 97(11): 217–220.

Schwab, J. C., ed. 2013. *Planning and Drought*. Chicago, IL: American Planning Association.

Whelton, A. J., P. K. Wisniewski, S. States, S. E. Birkmire, and M. K. Brown. 2006. Lessons learned from drinking water disaster and terrorism exercises. *Journal of the American Water Works Association* 98(8): 63–73.

Whitler, J. and C. Stormont, 2011. Lessons learned from WARN tabletop exercises. *Journal of American Water Works Association* 103(12): 24–27.

Wilhite, D. A., M. V. K. Sivakumar, and R. Pulwarty. 2014. Managing drought risk in a changing climate: The role of national drought policy. *Weather and Climate Extremes* 3: 4–13.

NOTES

1. Several resources were used to identify past droughts: South Carolina Drought Response Committee reports (http://www.dnr.sc.gov/climate/sco/Drought/drought_press_release.php), the United States Drought Monitor map archive (http://droughtmonitor.unl.edu/Maps/MapArchive.aspx), and *Carolinas Precipitation Patterns & Probabilities*, An Atlas of Hydroclimate Extremes (http://www.cisa.sc.edu/atlas/index.html).
2. The planning team consulted materials developed by the University of Nebraska for the North Platte Natural Resources District Invitational Drought Tournament (http://droughtthira.unl.edu/index.php).
3. Exercise materials and additional information are available on the websites of the State Climatology Office (http://www.dnr.sc.gov/climate/sco/) and CISA (http://www.cisa.sc.edu/projects__drought-response.html).
4. CoCoRaHS (https://www.cocorahs.org/) is a national network of citizen scientists who record daily precipitation observations. By increasing the density of local data, this network serves an important role in drought and rainfall monitoring in South Carolina.

SAVE THE DATE!

2018 South Carolina Water Resources Conference

October 17-18, 2018

Columbia Metropolitan Convention Center

http://www.scwaterconference.org

2018 Planning Committee

Chair

Jeffery S. Allen, Clemson University South Carolina Water Resources Center

Committee Members

Black & Veatch, *Robert Osborne*

Charleston Water System, *Jane Byrne*

Clemson University Center for Watershed Excellence, *Cal Sawyer*

Clemson University Environmental Engineering & Earth Sciences, *David Ladner*

Clemson University Plant and Environmental Sciences, *Sarah White*

Clemson University SC Water Resources Center, *Lori Dickes*

Coastal Carolina University, *Susan Libes*

College of Charleston, *Timothy J. Callahan*

NOAA Hollings Marine Laboratory, *Anne Blair*

Resource Environmental Solutions, LLC, *Rheta Geddings DiNovo*

Santee Cooper, *Jesse Cannon*

SC Department of Health and Environmental Control- Bureau of Water, *David Graves, Heather Preston*

SC Department of Natural Resources, *Brooke Czwartacki, Scott Harder*

South Carolina Sea Grant Consortium, *M. Richard DeVoe*

The Nature Conservancy- South Carolina, *Eric Krueger*

University of South Carolina School of the Earth, Ocean and Environment, *Gwendelyn Geidel*

University of South Carolina Arnold School of Public Health / Baruch Institute, *Dwayne Porter*

USDA Forest Service, *Devendra Amatya*

US Army Corps of Engineers, *Colton Bowles*

US Geological Survey, *Eric Strom*

South Carolina Water Resources Conference

2016 Major Contributors

CLEMSON
PUBLIC SERVICE AND AGRICULTURE

santee cooper®

DUKE ENERGY®

Greenville Water

Charleston Water System

ANDERSON REGIONAL JOINT WATER SYSTEM

dhec
Healthy People. Healthy Communities.

SOUTH CAROLINA DEPARTMENT OF NATURAL RESOURCES
DNR

YSI
a xylem brand

synTerra